

Parametric study of Finite Volume Solver for Dilute Gas-Droplet Flows with Evaporation

By
Pankaj Kumar
Roll No. ME11M11
M.Tech II Yr.-Thermofluids

A Thesis Submitted
in Partial Fulfillment of the Requirements
for the Degree of
Master of Technology

Department Of Mechanical Engineering
Indian Institute Of Technology Hyderabad



JULY 2013

Declaration

I declare that this written submission represents my ideas in my own words, and where ideas and words of others have been included, I have adequately cited and referenced the original sources. I also declare that I have adhered to all principles of academic honesty and integrity and have not misinterpreted or fabricated or falsified any idea/data/fact/source in my submission. I understand that any violation of the above will be a cause for disciplinary action by the Institute and can also evoke penal action from the sources that have thus not been properly cited, or from whom proper permission has not been taken when needed.

Pankaj Kumar

(Signature)

PANKAJ KUMAR

(Student Name)

ME11M11

(Roll No.)

Approval Sheet

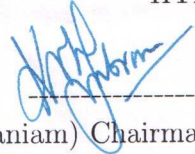
This thesis entitled "Parametric study of Finite Volume Solver for Dilute Gas Droplet flows with Evaporation" by Pankaj Kumar is approved for the degree of Master of Technology from IIT Hyderabad.



(Dr. K. Venkatasubbaiah) Examiner
Dept. of Mechanical Engg.
IITH



(Prof. Vinayak Eswaran) Adviser
Dept. of Mechanical Engg.
IITH



(Prof. Kolluru V.L. Subramaniam) Chairman
Dept. of Civil Engg.
IITH

Acknowledgements

I express my sincere gratitude to my thesis adviser Prof. Vinayak Eswaran for his valuable guidance, timely suggestions and constant encouragement. His interest and confidence in me has helped immensely for the successful completion of this work. I am thankful to Narendra Gajbiye for guiding me through the basics of Anupravaha solver and constantly helping and clearing my doubts. I am also grateful to Praveen Throvagunta for helping me with the code.

I would also like to express my sincere gratitude to Dr. Raja Banerjee, Assistant Professor, Dept. of Mechanical Engineering, IIT Hyderabad for lending me books which enabled me to gain more understanding. A special note of thanks to my classmates Mudassar, Nikhil for inspiring me by doing their best always. I would also like to thank all my friends in IIT Hyderabad for making my stay at IIT Hyderabad, memorable and enjoyable.

I would like to make a special mention of the excellent computational facilities provided by Professor Eswaran. I would also like to thank the staff and fellow students in CAE lab for creating a conducive environment to work in.

Finally, I would like to thank my family for their constant support and encouragement. Their faith in me has enabled me to do my best.

Pankaj Kumar

To my family ...

Abstract

An algorithm previously implemented (Mrunalini 2012) for dilute gas-droplet flows with evaporation in a general purpose CFD solver, *IITK-DAE ANUPRAVAHA SOLVER* was thoroughly tested with different test-cases in this thesis.

In the current study, the evaporation length of droplets introduced into a channel flow has been studied. The parameters influencing the problem are the gas Reynolds number Re_g , the droplet Reynolds number Re_d , and the Jacob number Ja . The Re_g in most practical flows is too high for laminar computations so here was fixed at a dummy value of 100 (it can be argued that the results are quite insensitive to this value). The parametric study of the relationship of the evaporation length dependence on the Jacob number Ja and the droplet Reynolds number was then attempted.

Contents

Declaration	i
Approval Sheet	ii
Acknowledgements	iii
Abstract	v
List of Figures	x
List of Tables	xiii
Nomenclature	xvi
1 Introduction	1
1.1 IITK-DAE Anupravaha Solver	3
1.2 Gas Droplet Flows with Evaporation	4
1.3 Literature survey	4
1.4 Solution Methods	6
1.4.1 The Eulerian-Lagrangian Approach	7
1.4.2 The Eulerian-Eulerian Approach	7
1.4.3 Two Fluid Model	8
1.5 Previous Work	9
1.6 Objectives of the Present Work	9

1.7	Thesis Organization	9
2	Governing Equations and Assumptions	10
2.1	Assumptions	10
2.2	The Governing Equations	11
2.2.1	Gas-Phase	11
2.2.2	Droplet-Phase	12
2.3	Non dimensionlized form of the equation :	13
2.4	Solution form of the governing equations :	15
2.4.1	Gas-Phase	15
2.4.2	Droplet-Phase	17
2.5	Boundary Conditions	18
2.5.1	At Solid Boundaries	18
2.5.2	Inlet	19
2.5.3	Outlet	19
2.6	Evaporation Model for Single Component Droplets	20
2.6.1	Classical D^2 -Law	20
2.6.2	Mathematical Formulation	22
2.6.3	Calculation of Steady-State Evaporation Rates	24
2.6.4	Evaporation Constant	25
2.7	Unsteady-State Analysis	25
2.7.1	Calculation of drop surface temperature	26
2.8	Drop analysis	27
2.9	Convective effects on evaporation	27
2.10	Property Evaluation	29
3	Discretization Procedure and Solution Algorithm	30
3.1	Description of the Finite Volume Method	30

3.2	Grid Generation	31
3.3	CGNS file format	31
3.4	Integral Form of Governing Equations	32
3.5	Description of the Finite-Volume Method	33
3.6	Discretization Procedure	33
3.6.1	Discretization of the General Convection-Diffusion Equation	33
3.7	The Discretized Equations	35
3.7.1	Gas-Phase	35
3.7.2	Droplet-Phase	37
3.8	The Solution Algorithm	38
3.9	Summary of the Algorithm	44
3.10	Implementation of the Algorithm	45
3.10.1	Limiter for Θ_d equation	45
3.10.2	Enforcing gas-phase and droplet-phase velocity equality	46
3.10.3	Enforcing T_d is constant after heat-up period	46
4	Results and Discussion	47
4.1	Gas-Droplet Flow Through 2-D Channel	47
4.1.1	Computational Domain and Property Values	48
4.1.2	Gas-droplet channel flow with dummy $Re = 100$ and $Ja = 3.071$	49
4.1.3	Gas-droplet channel flow with dummy $Re = 100$ and $Ja = 2.784$	55
4.1.4	Gas-droplet channel flow with dummy $Re = 100$ and $Ja = 0.5$	60
4.1.5	Gas-droplet channel flow with dummy $Re = 100$ and $Ja = 3.071$	65
4.1.6	Gas-droplet channel flow with dummy $Re = 100$ and $Ja = 2.784$	70
4.1.7	Gas-droplet channel flow with dummy $Re = 100$ and $Ja = 0.5$	75
4.1.8	Gas-droplet channel flow with dummy $Re = 200$ and $Ja = 3.071$	80
4.1.9	Gas-droplet channel flow with dummy $Re = 200$ and $Ja = 2.784$	85

4.1.10 Gas-droplet channel flow with dummy $Re = 200$ and $Ja = 0.5$.	90
4.1.11 Gas-droplet channel flow with dummy $Re = 100$ and $Ja = 3.071$	95
4.1.12 Gas-droplet channel flow with dummy $Re = 100$ and $Ja = 2.784$	95
4.1.13 Gas-droplet channel flow with dummy $Re = 100$ and $Ja = 0.5$.	103
4.1.14 Closure	108
5 Conclusion and Scope of the Future Work	109
A Appendix	112
A.1 Properties of fluids used	112
A.1.1 Properties of Air	112
A.1.2 Properties of n-heptane	112
A.1.3 Physical properties of Hexane ([24])	114
References	115

List of Figures

2.1	Variation of temperature and gas concentration during droplet evaporation (Faeth) [11]	
2.2	Burning rate curves for n-Heptane	22
4.1	The Computational Domain for 2D-Channel Gas-Droplet Flow Problem	48
4.2	Case 1: Gas-droplet channel flow with $u_{gi} = 1.0$ and $u_{di} = 1.0$ (a) Variation of droplet-	
4.3	Case 1: Gas-droplet channel flow with $u_{gi} = 1.0$ and $u_{di} = 1.0$.(a) Variation of droplet-	
4.4	Case 1: Gas-droplet channel flow with $u_{gi} = 2.0$ and $u_{di} = 2.0$ (a) Variation of droplet-	
4.5	Case 1: Gas-droplet channel flow with $u_{gi} = 2.0$ and $u_{di} = 2.0$.(a) Variation of droplet-	
4.6	Case 1: Gas-droplet channel flow with $u_{gi} = 2.0$ and $u_{di} = 1.0$. (a) Variation of droplet-	
4.7	Case 1: Gas-droplet channel flow with $u_{gi} = 2.0$ and $u_{di} = 1.0$. (a) Variation of droplet-	
4.8	Case 1: Gas-droplet channel flow with $u_{gi} = 1.0$ and $u_{di} = 2.0$. (a) Variation of droplet-	
4.9	Case 1: Gas-droplet channel flow with $u_{gi} = 1.0$ and $u_{di} = 2.0$. (a) Variation of droplet-	
4.10	Case 2:Gas-droplet channel flow with $u_{gi} = 1.0$ and $u_{di} = 1.0$.(a) Variation of droplet-p	
4.11	Case 2:Gas-droplet channel flow with $u_{gi} = 1.0$ and $u_{di} = 1.0$.(a) Variation of droplet-c	
4.12	Case 2:Gas-droplet channel flow with $u_{gi} = 2.0$ and $u_{di} = 2.0$. (a) Variation of droplet-	
4.13	Case 2: Gas-droplet channel flow with $u_{gi} = 2.0$ and $u_{di} = 2.0$. (a) Variation of droplet-	
4.14	Case 2: Gas-droplet channel flow with $u_{gi} = 2.0$ and $u_{di} = 1.0$. (a) Variation of droplet-	
4.15	Case 1: Gas-droplet channel flow with $u_{gi} = 2.0$ and $u_{di} = 1.0$. (a) Variation of droplet-	
4.16	Case 2: Gas-droplet channel flow with $u_{gi} = 1.0$ and $u_{di} = 2.0$. (a) Variation of droplet-	
4.17	Case 2: Gas-droplet channel flow with $u_{gi} = 1.0$ and $u_{di} = 2.0$. (a) Variation of droplet-	
4.18	Case 3:Gas-droplet channel flow with $u_{gi} = 1.0$ and $u_{di} = 1.0$. (a) Variation of droplet-	

- 4.46 Case 6: Gas-droplet channel flow with $u_{gi} = 2.0$ and $u_{di} = 1.0$. (a) Variation of droplet
- 4.47 Case 6: Gas-droplet channel flow with $u_{gi} = 2.0$ and $u_{di} = 1.0$. (a) Variation of droplet
- 4.48 Case 6: Gas-droplet channel flow with $u_{gi} = 1.0$ and $u_{di} = 2.0$. (a) Variation of droplet
- 4.49 Case 6: Gas-droplet channel flow with $u_{gi} = 1.0$ and $u_{di} = 2.0$. (a) Variation of droplet
- 4.50 Case 7: Gas-droplet channel flow with $u_{gi} = 1.0$ and $u_{di} = 1.0$. (a) Variation of droplet
- 4.51 Case 7: Gas-droplet channel flow with $u_{gi} = 1.0$ and $u_{di} = 1.0$. (a) Variation of droplet
- 4.52 Case 7: Gas-droplet channel flow with $u_{gi} = 2.0$ and $u_{di} = 2.0$. (a) Variation of droplet
- 4.53 Case 7: Gas-droplet channel flow with $u_{gi} = 2.0$ and $u_{di} = 2.0$. (a) Variation of droplet
- 4.54 Case 7: Gas-droplet channel flow with $u_{gi} = 2.0$ and $u_{di} = 1.0$. (a) Variation of droplet
- 4.55 Case 7: Gas-droplet channel flow with $u_{gi} = 2.0$ and $u_{di} = 1.0$. (a) Variation of droplet
- 4.56 Case 7: Gas-droplet channel flow with $u_{gi} = 1.0$ and $u_{di} = 2.0$. (a) Variation of droplet
- 4.57 Case 7: Gas-droplet channel flow with $u_{gi} = 1.0$ and $u_{di} = 2.0$. (a) Variation of droplet
- 4.58 Case 8: Gas-droplet channel flow with $u_{gi} = 1.0$ and $u_{di} = 1.0$. (a) Variation of droplet
- 4.59 Case 8: Gas-droplet channel flow with $u_{gi} = 1.0$ and $u_{di} = 1.0$. (a) Variation of droplet
- 4.60 Case 8: Gas-droplet channel flow with $u_{gi} = 2.0$ and $u_{di} = 2.0$. (a) Variation of droplet
- 4.61 Case 8: Gas-droplet channel flow with $u_{gi} = 2.0$ and $u_{di} = 2.0$. (a) Variation of droplet
- 4.62 Case 8: Gas-droplet channel flow with $u_{gi} = 2.0$ and $u_{di} = 1.0$. (a) Variation of droplet
- 4.63 Case 8: Gas-droplet channel flow with $u_{gi} = 2.0$ and $u_{di} = 1.0$. (a) Variation of droplet
- 4.64 Case 8: Gas-droplet channel flow with $u_{gi} = 1.0$ and $u_{di} = 2.0$. (a) Variation of droplet
- 4.65 Case 8: Gas-droplet channel flow with $u_{gi} = 1.0$ and $u_{di} = 2.0$. (a) Variation of droplet
- 4.66 Case 9: Gas-droplet channel flow with $u_{gi} = 1.0$ and $u_{di} = 1.0$. (a) Variation of droplet
- 4.67 Case 9: Gas-droplet channel flow with $u_{gi} = 1.0$ and $u_{di} = 1.0$. (a) Variation of droplet
- 4.68 Case 9: Gas-droplet channel flow with $u_{gi} = 2.0$ and $u_{di} = 2.0$. (a) Variation of droplet
- 4.69 Case 9: Gas-droplet channel flow with $u_{gi} = 2.0$ and $u_{di} = 2.0$. (a) Variation of droplet
- 4.70 Case 9: Gas-droplet channel flow with $u_{gi} = 2.0$ and $u_{di} = 1.0$. (a) Variation of droplet
- 4.71 Case 9: Gas-droplet channel flow with $u_{gi} = 2.0$ and $u_{di} = 1.0$. (a) Variation of droplet
- 4.72 Case 9: Gas-droplet channel flow with $u_{gi} = 1.0$ and $u_{di} = 2.0$. (a) Variation of droplet

- 4.73 Case 9: Gas-droplet channel flow with $u_{gi} = 1.0$ and $u_{di} = 2.0$. (a) Variation of droplet-di
- 4.74 Case 10: Gas-droplet channel flow with $u_{gi} = 1.0$ and $u_{di} = 1.0$. (a) Variation of droplet-p
- 4.75 Case 10: Gas-droplet channel flow with $u_{gi} = 1.0$ and $u_{di} = 1.0$. (a) Variation of droplet-d
- 4.76 Case 10: Gas-droplet channel flow with $u_{gi} = 1.0$ and $u_{di} = 2.0$. (a) Variation of droplet-p
- 4.77 Case 10: Gas-droplet channel flow with $u_{gi} = 1.0$ and $u_{di} = 2.0$. (a) Variation of droplet-d
- 4.78 Case 11: Gas-droplet channel flow with $u_{gi} = 1.0$ and $u_{di} = 1.0$. (a) Variation of droplet-p
- 4.79 Case 11: Gas-droplet channel flow with $u_{gi} = 1.0$ and $u_{di} = 1.0$.(a) Variation of droplet-di
- 4.80 Case 11: Gas-droplet channel flow with $u_{gi} = 2.0$ and $u_{di} = 2.0$. (a) Variation of droplet-p
- 4.81 Case 11: Gas-droplet channel flow with $u_{gi} = 2.0$ and $u_{di} = 2.0$. (a) Variation of droplet-d
- 4.82 Case 11: Gas-droplet channel flow with $u_{gi} = 2.0$ and $u_{di} = 1.0$. (a) Variation of droplet-p
- 4.83 Case 11: Gas-droplet channel flow with $u_{gi} = 2.0$ and $u_{di} = 1.0$.(a) Variation of droplet-di
- 4.84 Case 11: Gas-droplet channel flow with $u_{gi} = 1.0$ and $u_{di} = 2.0$. (a) Variation of droplet-p
- 4.85 Case 11: Gas-droplet channel flow with $u_{gi} = 1.0$ and $u_{di} = 2.0$. (a) Variation of droplet-d
- 4.86 Case 12:Gas-droplet channel flow with $u_{gi} = 1.0$ and $u_{di} = 1.0$. (a) Variation of droplet-ph
- 4.87 Case 12:Gas-droplet channel flow with $u_{gi} = 1.0$ and $u_{di} = 1.0$.(a) Variation of droplet-dia
- 4.88 Case 12:Gas-droplet channel flow with $u_{gi} = 2.0$ and $u_{di} = 2.0$. (a) Variation of droplet-ph
- 4.89 Case 12: Gas-droplet channel flow with $u_{gi} = 2.0$ and $u_{di} = 2.0$.(a) Variation of droplet-di
- 4.90 Case 12:Gas-droplet channel flow with $u_{gi} = 2.0$ and $u_{di} = 1.0$. (a) Variation of droplet-ph
- 4.91 Case 12 : Gas-droplet channel flow with $u_{gi} = 2.0$ and $u_{di} = 1.0$. (a) Variation of droplet-
- 4.92 Case 12: Gas-droplet channel flow with $u_{gi} = 1.0$ and $u_{di} = 2.0$. (a) Variation of droplet-p
- 4.93 Case 12: Gas-droplet channel flow with $u_{gi} = 1.0$ and $u_{di} = 2.0$. (a) Variation of droplet-d

List of Tables

4.1	Property values of fluids used	49
4.2	Case 1: Inlet conditions	50
4.3	Case 2: Inlet conditions	55
4.4	Case 3: Inlet conditions	60
4.5	Case 4: Inlet conditions	65
4.6	Case 5: Inlet conditions	70
4.7	Case 6: Inlet conditions	75
4.8	Case 7: Inlet conditions	80
4.9	Case 8: Inlet conditions	85
4.10	Case 9: Inlet conditions	90
4.11	Case 10: Inlet conditions	95
4.12	Case 11: Inlet conditions	98
4.13	Case 12: Inlet conditions	103

Nomenclature

u_g, v_g, w_g	Gas-phase velocity components (m/s)
u_d, v_d, w_d	Droplet-phase velocity components (m/s)
P	Pressure (N/m^2)
ρ_g	Density of gas-phase (kg/m^3)
μ	Molecular viscosity of gas-phase ($kg/m \cdot s$)
ν	Kinematic viscosity of gas-phase (m^2/s)
ρ_d	Material Density of droplet-phase (kg/m^3)
ϑ_d	Volume fraction of droplet-phase
Θ_d	Normalized volume fraction of droplet-phase
C_d	Drag coefficient
τ	Shear stress (N/m^2)
τ_w	Wall shear stress (N/m^2)
ΔV_p	Volume of the cell with centroid P
S	Surface area vector
F_{gf}	Volume flux gas-phase at face f
F_{df}	Volume flux droplet-phase at face f
F_{Mgf}	Momentum flux gas-phase at face f
F_{Mdf}	Momentum flux droplet-phase at face f
$F_{d\phi f}$	Diffusion flux of variable ϕ
Re	Flow Reynolds number
Re_d	Droplet Reynolds number
d_d	Particle diameter
\mathbf{f}_d	Drag force per unit volume (N/m^3)
β	Exchange coefficient for interphase drag
n	Number density of droplet-phase ($1/m^3$)
\dot{m}_v	Evaporation rate for a single droplet (kg/s)
g_x, g_y, g_z	Components of acceleration due to gravity (m/s^2)
C_{pc}	Specific heat at constant pressure of pure gas ($J/kg K$)
C_{pg}	Specific heat at constant pressure of gas-phase ($J/kg K$)
C_{vd}	Specific heat at constant pressure of evaporated fuel vapour ($J/kg K$)
C_{ld}	Specific heat for liquid droplet ($J/kg K$)
L	Latent heat of vaporization of liquid drop (J/kg)
k_g	Thermal conductivity of gas-phase ($W/m K$)
k_c	Thermal conductivity of pure gas ($W/m K$)
k_v	Thermal conductivity of evaporated fuel vapour ($W/m K$)
T_g	Gas-phase temperature (K)

T_d	Droplet-phase temperature (K)
T_s	Droplet surface temperature (K)
α	Thermal diffusivity for gas-phase ($\equiv \frac{k}{\rho C_p}$) (m^2/s)
D	Diffusion coefficient of fuel vapour in gas (m^2/s)
λ_{st}	Steady-state evaporation rate (mm^2/s)
R	Universal gas constant ($J/kmol K$)
Y_F	Fuel mass fraction
Y_{F_s}	Fuel mass fraction at the droplet surface
Y_{F_∞}	Fuel mass fraction at free stream
B_M	Spalding mass transfer number
B_T	Spalding heat transfer number
M_A	Molecular weight of gas ($kg/kmole$)
M_F	Molecular weight of fuel ($kg/kmole$)
h	Heat transfer coefficient ($W/m^2 K$)
Q	Heat transfer from gas to a single drop (J/s)
Q_e	Heat used in vaporization of fuel (J/s)
Nu	Nusselt number
Pr	Prandtl number ($\equiv \frac{\nu}{\alpha}$)
Sc	Schmidt number ($\equiv \frac{\nu}{D}$)
Le	Lewis number ($\equiv \frac{\alpha}{D}$)

Chapter 1

Introduction

Many natural processes like formation and motion of rain drops, sand dunes formation etc., and industrial processes like flows in boilers and evaporators, heat exchangers, internal combustion engines etc., involve the interaction between matter existing in different states. The interaction between the various phases or states of matter may be in terms of mass and/or momentum and/or energy transfer. Such flows are termed as Multi-phase flows. Multi-phase flows can be quite complex and may involve various phases interacting simultaneously.

The simplest of all multi-phase flows are *two-phase* flows. In this work, mathematical modeling of two-phase flows involving gas and evaporating liquid droplets is attempted considering certain assumptions. The development of accurate mathematical models of two-phase flows is important for optimum design and control of various industrial systems. Mathematical modeling of two-phase flows poses several challenges as the problem involves rapidly changing and/or moving interfaces and continuous interaction between the phases which affect the behavior of each of the interacting phases. In this work, we numerically solve dilute dispersed two-phase flows using the three fundamental principles that govern any fluid flow: (i) mass conservation, (ii) momentum conservation and (iii) energy conservation. A brief introduction to two-phase flows is given below.

Two phase flows, in general, can be characterized both by the combination of interacting phases and also by the interface structures. Classification based on the state of the constituents of the flow is as follows:

1. Gas-Solid flows (Particle laden flows, fluidized beds)

2. Gas-Liquid flows (Bubbly flows, slug flows, gas-droplet flows)
3. Liquid-Solid flows (Slurry flows, sediment transport)
4. Immiscible-liquid flows

The second classification, based on the geometry of the interface between the interacting phases is as follows:

1. Separated flow/Free surface flows in which the two phases are separated by a distinct interface.
2. Dispersed flows in which both the phases are thoroughly mixed with each other.
3. Transitional/Mixed flow where the transition from separated to dispersed flows occurs.

Dispersed flows are further divided into three regimes by considering the phase of dispersion as follows:

1. Bubbly flows
2. Droplet or mist flows
3. Particle flows

This thesis involves numerical modeling of *dilute dispersed gas-droplet* flows involving gas and evaporating liquid droplets. *Dilute gas-particle* flows are considered as a special case of gas-droplet flows without evaporation. Droplets/Particles are called as the *disperse* phase and the fluid in which the droplets move is called as *continuous* phase.

Mrunalini (2012) developed an algorithm for dilute-disperse gas droplet flow and tested it. In this thesis, we thoroughly validate the algorithm and attempt a new problem of parametrising the evaporation length for droplets of n-heptane with initial diameter in the range 100-200 microns with initial temperature at either saturation (371.4K) or room temperature(300 K). The problem is non-dimensionalized and there are three relevant non-dimensional parameters: the gas Reynolds number Re_g , the droplet Reynolds number Re_d and the Jacob number Ja , which is the ratio of sensible to latent heat and which governs the thermodynamics of phase change. The results of this study would be relevant to engineering practice in that it gives the distance of

evaporation of the droplet under the given conditions.

However, not all parameters of the practical problems can be simulated by numerical computations. The gas Reynolds number in most practical problems will be very high ($> 10^5$) and so in the turbulent range. The current code is not capable of turbulent simulations. The strategy used in this thesis is as follows : we simulate the correct droplet Reynolds number and Jacob number, but use a low dummy value (=100) for gas Reynolds number. The argument in favor of this strategy is as follows : Re_d and Ja are the most important parameters, the first determines the convection coefficient of the evaporation and the second influences the thermodynamics involved. Re_g on the other hand determines mainly the laminar-turbulent transition. Given that the code cannot do turbulent calculation, the current simulations can be taken as laminar approximations of the full turbulent problem.

1.1 IITK-DAE Anupravaha Solver

IITK-DAE Anupravaha Solver is a multi-block finite volume based solver capable of solving Navier-Stokes, energy and other scalar equations for solving flow and heat transfer problems of engineering applications. It uses non-orthogonal hexahedral structured grids and is coded using ‘C’ programming language. Anupravaha solver can be used on 2D, 2D Axis-symmetric and 3D structured grids. This solver is written using CGNS(CFD General Notation System) format and hence reads grids in CGNS format, solves the required equations and generates results in CGNS files which can be read and displayed by any post-processing software. The solver uses dynamic memory allocation and user choices for grid, equations, variables, boundary conditions, type of algorithm, type of time-stepping schemes, type of convective schemes etc., are made directly using the compiled code. There is also a provision for incorporating user-defined functions for various physical properties. A variable density approach has been completely integrated in the solver. The following modules are available in the solver

1. Conjugate Heat Transfer module
2. Various Turbulence models
3. Solidification and Melting module
4. Combustion module

5. Two-Phase module
6. Flow field coupled with Electric Field
7. Liquid Metal Magneto-Hydro Dynamics
8. Radiation

1.2 Gas Droplet Flows with Evaporation

Gas droplet flows are encountered in many engineering applications like IC engines, gas turbine systems, heat exchangers etc.. Gas-droplet flows may be dilute or dense. In dense gas droplet flow, the interaction between the droplets is of prime importance. Therefore, phenomena such as droplet-collision, droplet break-up, the effect of adjacent drop on transport rate etc., have to be modeled in dense gas-droplet flows. This involves a three-way coupling for modeling the effect of droplets on gas, the effect of gas on droplets and the effect of neighboring droplets on each other. On the other hand, dilute gas-droplet flow does not require the consideration of droplet-droplet interaction. In such a case, depending on the droplet concentration, a one-way or two-way coupling would suffice.

A one-way coupling indicates that the droplets are affected by the fluid flow, but not vice-versa; in two-way coupling the two phases influence each other. It follows therefore that for very low particle concentrations a one-way coupling is sometimes enough to model the interactions, whereas for somewhat denser flows a two-way coupling must be considered. The governing equations for a two-phase flows are considerably more complex than for single phase flows due to this reason. In this work, a two-way coupling is employed to take into account the mass, momentum and energy transfer between the droplet and the surrounding gas.

1.3 Literature survey

The problem of two-phase flows involving particles or droplets in a gas stream has garnered a lot of attention from researchers owing to their practical applications. Considerable amount of work has been done in this subject from the early 1950s. The fundamental concepts of two-phase flows, its classification and solution strategies are

discussed in detail in the book by Ishii-Hibiki [22]. In the early years of research, motion of particles/droplets in a gas stream and the evaporation characteristics have been addressed independently. Numerical approaches for solving the motion of particles using Eulerian-Lagrangian model have been extensively discussed by Loth [15]. An extensive review on the various modelling approaches for droplet vaporization is given by Sazhin et al. [33].

Gas-droplet flows with evaporation involve simultaneous heat and mass transfer. The physics of the mass and heat transfer involved in gas-droplet flows is explained in detail in the book by Koichi Asano [3]. The governing equations used for both the phases in two-continua formulation is given in book by Sirignano [35]. Previous research on two-fluid modeling is reported by Crowe et al. [5], Darwish [7] and Guo et al. [18]. The parameters used in the study such as volume fraction, number density are described in detail, with various averaging procedures, in Crowe et al. [5]. The evaporation model used in this work is based on the Spalding model analyzed extensively by Chin and Lefebvre. [4]

The simplest model for droplet evaporation was first suggested by Maxwell in 1877 [16]. According to this model, the rate of evaporation is controlled exclusively by the diffusion process. His model ignores the effect of the convective flow of the mixture of gas and fuel vapor away from the surface of the droplet. The classical d^2 -law of evaporation is formulated by Godsave [17] and Spalding [36] for a single isolated droplet evaporating in a quiescent environment. To take into account the effect of the convective flow of the surrounding gas, which enhances the heat and mass transfer between the droplet and the gas phase, many researchers have given correction factors for the basic models. In a comprehensive theoretical and experimental study, Frossling [14] first showed that effects of convection on heat and mass transfer rates could be accommodated by a correction factor that is a function of the Reynolds number and the Schmidt (or Prandtl) number. This correlation was later modified by Ranz and Marshall [30]. Later, Faeth [11] analyzed the available data on convective effects and proposed a synthesized correlation. The present study uses the correlation given by Ranz and Marshall [30].

The evaporation model used in the present study is essentially the classical model of Spalding [36]. The model used is described in the book by Lefebvre [23]. In the present study, the ‘rapid mixing model’ for the liquid droplet described in Faeth [11] is used.

This simplifies the analysis by assuming infinite conductivity of the liquid. However, this may lead to small error in the solution. For the liquid droplet phase analysis, Abramzon et al.[1] used effective conductivity model. Expressions for the variation of properties of gases and liquids used in this study are taken from Perry [28] and Reid [31]. Hubbard et al. [19] studied the effect of transient and variable properties on drop evaporation rate, and showed that the ‘1/3’ rule worked well as a mixing rule used. In the present evaporation model this rule is used for the calculation of the properties at droplet surface based on average temperature and composition.

In the literature, there are many experimental studies dealing with droplet evaporation. However, there are only few studies that come to the basic and ideal case of a single droplet evaporation in a quiescent or convective environment. A large number of studies consider multi-component droplets in turbulent evaporating sprays, jets with different classes of droplets where each class refers to a group of droplets of same diameters having their own volume fraction, mass flow rates. Therefore we compare our results with experimental results of Downing [8], Ranz and Marshall [30] and the numerical results of Chin and Lefebvre [4], Kolaitis [20] and Miller et al. [24]. For the study of laminar gas-droplet flows in one of the cases we have assumed the initial droplet temperature is the saturation temperature, to simplify the analysis as discussed in Mongia et al.[25] and Elghobashi et al.[10].

1.4 Solution Methods

Models for two-phase flows can be categorized into two different groups. In the first group, there are models that track the interface between the two phases. These are ideal for separated flows. In the second group, there are models where the exact position of the interface is not followed specifically. Dispersed flows are usually modeled using models from this second group. The number of interfaces between the two phases in dispersed flow is too high for interface tracking methods to be suitable, at least with today’s computing capacity. To model this type of flows, another strategy is employed in which the dispersed phase is assumed to be composed of spherical particles/droplets/bubbles. This assumption negates the need for interface tracking. Based on this strategy, there are two approaches commonly used for modeling gas-disperse phase flows: Eulerian-Eulerian approach and the Eulerian-Lagrangian approach.

1.4.1 The Eulerian-Lagrangian Approach

The general idea in this approach is to follow each particle/droplet/bubble of the flow as they advect in the continuous phase. The carrier phase is treated as a continuum and is calculated in an Eulerian reference frame, while particles/droplets/bubbles of the disperse phase are tracked using a Lagrangian approach. In this approach, the inter-phase transfer terms are calculated for the disperse phase while tracking the particles/droplets/bubbles using Lagrangian framework and these are then used in the Eulerian form of the equations of the continuous phase. This kind of iterative solution of carrier and disperse phases inevitably requires strong relaxation of inter-phase source terms for improving the convergence behaviour. Hence, Eulerian-Lagrangian approach works well for few particles/droplets/bubbles but becomes computationally expensive for modeling a large number of particles/droplets/bubbles unless each tracked entity is assumed to be a proxy for many actual particles/droplets/bubbles. Eulerian-Lagrangian approach for simulating evaporating gas-droplet flows has been extensively applied by Salman et al. [32].

1.4.2 The Eulerian-Eulerian Approach

Another approach to model dispersed flows is to treat both the phases as a continuum. This is generally referred to as Eulerian-Eulerian approach or two-fluid model, first discussed by Ishii [22]. In this case local instantaneous equation of mass, momentum and energy balance for both the phases are derived along with source terms for interaction between the phases. A very important concept in the Eulerian-Eulerian approach is that of *volume-fraction* or volume concentration which is defined in the Section 1.4.3.

The following modeling approaches are used within the purview of the Eulerian-Eulerian method based on the interaction between the two phases:

1. **Homogeneous Equilibrium Model:** In this model, flow is analyzed by treating it as an idealized ‘mixture’ fluid whose properties are determined based on the properties of its constituents and their proportions.
2. **Drift Flux Model:** Drift flux model is similar to the homogeneous equilibrium model but it takes into account for the ‘slip’ i.e., the differential motion between the phases, and so additional terms appear in the equations. The drift flux model and the homogeneous models are sometimes referred to as mixture models. They are simpler than the two-fluid model described below.

3. **Two Fluid Model:** In the two fluid model both the phases have their own velocity and temperature field equations and separate properties. The interaction between the two phases is taken care of by including exchange coefficients. This is the method adopted in this work¹. Details are given in section 1.4.3. One drawback of this approach is implementation of exchange coefficients.

1.4.3 Two Fluid Model

In the present work, an Eulerian-Eulerian two-fluid model is used to simulate two-phase flows. The phases are treated as inter-penetrating continua and mass, momentum and energy equations are solved to obtain the velocity and temperature fields separately for the phases. Each dependent variable at any specific point is an instantaneous average value over a neighbourhood of that point that includes both phases. Therefore, properties of both carrier phase and disperse phase exist at a point, regardless of whether that point is actually in the carrier phase or in the disperse phase at that instant.

Hereafter, we will refer to the carrier phase as gas and disperse phase as liquid, although the formulation is general and will work for liquid (carrier phase)-solid (disperse phase) flows as well. This method is a two-continua approach since both a continuum of gas properties and a continuum of liquid properties are defined. Details of the governing equations are given in section 2.2.

We define the volume fraction of any phase ‘ p ’ as the ratio of the volume occupied by that phase to the total volume in a small region around the point under consideration. Mathematically, we can write

$$\vartheta_p = \lim_{\Delta V \rightarrow 0} \frac{\Delta V_p}{\Delta V}$$

Here ϑ_p denotes the volume fraction of phase ‘ p ’, and ΔV_p is the volume occupied by that phase in the neighbourhood of the point of interest, whereas ΔV is the total volume occupied by the two phases in the neighborhood of the point. Defined in this way, ϑ becomes a function, with a value at each point. In the Eulerian-Eulerian framework ϑ is assumed to be a continuous variable and often transport equations are solved for it.

¹It must be noted that the detailed flow field *within* droplets are not obtained using this method. Rather, the average momentum of droplets are computed.

According to the conservation principle, the summation of the volume fractions must be unity, $\vartheta_g + \vartheta_d = 1$ where, ϑ_g is the volume fraction of the gas phase and ϑ_d is the volume fraction of the droplet phase. Another important parameter, number density is defined as the number of particles/droplets per unit volume, we can write

$$n = \lim_{\Delta V \rightarrow 0} \frac{\Delta N}{\Delta V}$$

also

$$n = \frac{6\vartheta_d}{\pi d_d^3} \quad (1.1)$$

where n denotes the number density of the disperse phase, and ΔN is the number of particles/droplets in unit volume and d_d is diameter of the particles/droplets (which are assumed to be spheres of the same size).

1.5 Previous Work

Dilute gas-particle flows and dilute gas-droplet flows problems were incorporated in IITK-DAE Anupravaha Solver by Mrunalini B. in 2012. This thesis uses the same formulation and the same computer program for the simulations presented here.

1.6 Objectives of the Present Work

1. To validate the solver by comparing the results with those obtained using analytical solutions, numerical solutions and experimental solutions.
2. To modify the equation by non dimensionlizing it and to implement in the solver
3. To study parametric behaviour of the non dimensionlized equation.

1.7 Thesis Organization

The thesis is organized in the following way. Chapter 2 deals with the assumptions, governing equations and boundary conditions. Chapter 3 includes the discretization procedure and the solution algorithm. Chapter 4 presents the results.

Chapter 2

Governing Equations and Assumptions

The formulation presented here is the same as followed by Mrunalini (2012).

2.1 Assumptions

An Eulerian two-fluid model is employed in the present study employing two-way coupling between the two phases, using governing equations derived based on the following assumptions:

1. The spray is assumed to be *dilute* ($\vartheta_a < 0.1\%$) . Under this assumption droplet collisions are ignored and the effect of adjacent drops on drop transport rates are neglected. Also viscous stresses, and temperature and pressure variation *within* the dispersed phase are neglected.
2. At each location of the flow field, droplet-phase and gas -phase co-exist and inter-penetrate with each other, each having its own velocity and temperature.
3. The flow around the droplet is assumed to be quasi-steady, that means the flow immediately adjusts to the local boundary conditions. This allows the use of drag coefficient formulations to represent the inter-phase forces on the droplets.
4. The droplets are assumed to be spherical and mono-sized.
5. The radial velocity of the liquid surface due to the evaporation of the liquid is neglected.

6. Effects of drag and forced convection are represented by empirical relations.
7. It is assumed that the only significant inter-phase force is due to drag. This is largely true for droplet-to-gas density ratios $(\rho_d/\rho_g) > 600$.
8. During the evaporation process, droplets do not break-up; chemical reaction is also neglected.
9. The gas phase Lewis number is assumed to be unity. This assumption implies that thermal diffusivity and molecular diffusivity are equal hence enabling us to use gas-phase properties while calculating the evaporation rate of a droplet without the need to find the molecular diffusivity of the droplets in the gas phase.

2.2 The Governing Equations

2.2.1 Gas-Phase

The governing equations for the gas phase are the Navier-Stokes equations, energy equation and mass fraction equation with extra source terms that reflects the contribution of the droplet phase on the gas phase. In cartesian coordinates, the equations are as below. All symbols are explained at the end of this sub-section.

Continuity: A source term for mass transfer due to evaporation is incorporated in the continuity equation. The continuity equation is as follows

$$\frac{\partial \vartheta_g \rho_g}{\partial t} + \frac{\partial \vartheta_g \rho_g U_{g,j}}{\partial x_j} = n \dot{m}_v \quad (2.1)$$

Writing in vector notation, it is

$$\frac{\partial \vartheta_g \rho_g}{\partial t} + \nabla \cdot (\vartheta_g \rho_g \mathbf{u}_g) = n \dot{m}_v \quad (2.2)$$

Momentum: Apart from the drag force between the dispersed and the continuous phase, momentum transfer also occurs due to evaporation.

$$\frac{\partial (\vartheta_g \rho_g U_{g,i})}{\partial t} + \frac{\partial (\vartheta_g \rho_g U_{g,i} U_{g,j})}{\partial x_j} = \frac{\partial}{\partial x_i} \left(\frac{\vartheta_g \mu_g \partial U_{g,i}}{\partial x_j} \right) - \vartheta_g \frac{\partial P}{\partial x_i} + \vartheta_g \rho_g g_i + n \dot{m}_v U_{d,i} - \vartheta_d f_{d,i} \quad (2.3)$$

Writing in vector notation,

$$\frac{\partial (\vartheta_g \rho_g \mathbf{u}_g)}{\partial t} + \nabla \cdot (\vartheta_g \rho_g \mathbf{u}_g \mathbf{u}_g) = \nabla \cdot (\mu_g \vartheta_g \nabla \mathbf{u}_g) - \vartheta_g \nabla P + \vartheta_g \rho_g \mathbf{g} + n \dot{m}_v \mathbf{u}_d - \vartheta_d \mathbf{f}_d \quad (2.4)$$

Energy: Evaporation process differs from other mass transfer in the fact that energy is also transferred simultaneously with mass. The heat transfer from the continuous phase to the dispersed phase should hence be considered while computing the temperature of the continuous phase.

$$\frac{\partial (\vartheta_g \rho_g C_{pg} T_g)}{\partial t} + \frac{\partial (\vartheta_g \rho_g C_{pg} T_g U_{g,j})}{\partial x_j} = \frac{\partial}{\partial x_i} (\vartheta_g k_g \frac{\partial T_g}{\partial x_j}) + n \dot{m}_v C_{vd} T_d - n Q \quad (2.5)$$

Writing in vector notation, it is

$$\frac{\partial (\vartheta_g \rho_g C_{pg} T_g)}{\partial t} + \nabla \cdot (\vartheta_g \rho_g C_{pg} T_g \mathbf{u}_g) = \nabla \cdot (\vartheta_g k_g \nabla T_g) + n \dot{m}_v C_{vd} T_d - n Q \quad (2.6)$$

Species Mass Fraction: As evaporation from the droplets is also considered, it is assumed that the evaporated vapour is of a different species (say, fuel) than the ambient gas. Therefore, an equation for the species Y_F is also solved:

$$\frac{\partial (\vartheta_g \rho_g Y_F)}{\partial t} + \frac{\partial (\vartheta_g \rho_g Y_F U_{g,j})}{\partial x_j} = \frac{\partial}{\partial x_i} (\vartheta_g \rho_g D \frac{\partial Y_F}{\partial x_j}) + n \dot{m}_v \quad (2.7)$$

Writing in Vector notation,

$$\frac{\partial (\vartheta_g \rho_g Y_F)}{\partial t} + \nabla \cdot (\vartheta_g \rho_g Y_F \mathbf{u}_g) = \nabla \cdot (\vartheta_g \rho_g D \nabla Y_F) + n \dot{m}_v \quad (2.8)$$

where ρ_g is the density of the gas phase, \mathbf{u}_g and T_g are velocities and temperature of the gas phase respectively. The subscripts g and d refer to the gas and droplet phases respectively. Y_F is the evaporated fuel mass fraction, μ is viscosity, C_{pg} is the specific heat at constant pressure, k_g is thermal conductivity of the gas phase, \mathbf{g} is acceleration due to gravity. \dot{m}_v is the evaporation rate for a single droplet, n is the number density of droplets per unit volume of flow, C_{vd} is the specific heat of the *vapour* phase of the liquid in the droplet, T_d is droplet temperature, D is the diffusion coefficient of fuel vapour in gas and Q is heat transfer from the gas to a single drop, \mathbf{f}_d the drag force acting on the droplet per unit volume. This is described in next section, 2.2.2.

2.2.2 Droplet-Phase

The governing equations for the droplet phase are derived as follows:

Continuity: due to evaporation, some amount of mass is transferred from the droplet phase to the gas phase. It is accounted by incorporating a negative source term in the continuity equation of the droplet phase.

$$\frac{\partial (\rho_d \vartheta_d)}{\partial t} + \frac{\partial (\rho_d \vartheta_d U_{d,i})}{\partial x_i} = -n \dot{m}_v \quad (2.9)$$

Writing in vector notation,

$$\frac{\partial (\rho_d \vartheta_d)}{\partial t} + \nabla \cdot (\rho_d \vartheta_d \mathbf{u}_d) = -n \dot{m}_v \quad (2.10)$$

Momentum: An equal and opposite amount of momentum is exchanged from the gas phase to the droplet phase so that the total momentum of the system remains constant.

$$\frac{\partial \rho_d \vartheta_d U_{di}}{\partial t} + \frac{\partial (\rho_d \vartheta_d U_{di} U_{dj})}{\partial x_i} = -\vartheta_d \frac{\partial P}{\partial x_i} + \vartheta_d \rho_d g_i - n \dot{m}_v U_{di} + \vartheta_d f_{di} \quad (2.11)$$

Writing in Vector notation,

$$\frac{\partial \rho_d \vartheta_d \mathbf{u}_d}{\partial t} + \nabla \cdot (\rho_d \vartheta_d \mathbf{u}_d \mathbf{u}_d) = -\vartheta_d \nabla P + \vartheta_d \rho_d \mathbf{g} - n \dot{m}_v \mathbf{u}_d + \vartheta_d \mathbf{f}_d \quad (2.12)$$

where ϑ_d is the volume fraction, ρ_d is the material density of the droplet phase and \mathbf{u}_d is local velocity of the droplets. The term $(\vartheta_d \mathbf{f}_d)$ in equations 2.4 and 2.12 is the drag force acting on the droplet phase per unit volume and is given by (Kolev [21]):

$$\mathbf{f}_d = \rho_g \frac{1}{\left(\frac{4}{3} \pi \left\{\frac{d_d}{2}\right\}^3\right)} \frac{1}{2} C_d |\mathbf{u}_g - \mathbf{u}_d| (\mathbf{u}_g - \mathbf{u}_d) \left(\frac{\pi}{4} d_d^2\right) = \beta (\mathbf{u}_g - \mathbf{u}_d)$$

where d_d is the diameter of the droplets and C_d is the drag coefficient which is given by (Kolev [21]):

$$C_d = \begin{cases} \frac{24}{Re_d} & \text{if } Re_d \leq 1 \\ \frac{24}{Re_d} (1 + 0.15 Re_d^{0.687}) & \text{if } 1 \leq Re_d \leq 1000 \end{cases}$$

where Re_d is the *droplet Reynolds number*, defined as (Miller et al. [24])

$$Re_d = \frac{\rho_g |\mathbf{u}_g - \mathbf{u}_d| d_d}{\mu_g}$$

Energy:

$$\frac{\partial [\rho_d \vartheta_d C_{ld} T_d]}{\partial t} + \nabla \cdot (\rho_d \vartheta_d C_{ld} T_d \mathbf{u}_d) = -n \dot{m}_v C_{ld} T_d - n \dot{m}_v L + n Q \quad (2.13)$$

where T_d is droplet temperature and L is the latent heat of vaporization of the liquid droplet at the droplet temperature.

2.3 Non dimensionlized form of the equation :

Non Dimensionalizing variables are

1. Length L

2. Free Stream velocity u_0
3. Free strem viscosity μ_0
4. Free stream specific heat C_{po}
5. Pressure P_0
6. Free stream air density ρ_0
7. Reference temperature difference $(T_w - T_{in})$
8. Free Stream thermal conductivity K_o
9. Diffusion constant D_o
10. Droplet diameter d_0

The dimensionless quantity are defined by a star as the superscript. thus

1. $\nabla^* = \nabla L$
2. $u_g^* = \frac{u_g}{u_0}$
3. $\tau = \frac{t u_0}{L}$
4. $n^* = L^3 n$
5. $\rho_g^* = \frac{\rho_g}{\rho_0}$
6. $\rho_d^* = \frac{\rho_d}{\rho_{do}}$
7. $P^* = \frac{1}{\rho_0} \frac{P}{u_0^2}$
8. $\dot{m}^* = \frac{\dot{m}}{\rho_0 L^2 u_0}$
9. $\mu_g^* = \frac{\mu_g}{\mu_0}$
10. $T^* = \frac{T - T_{in}}{T_w - T_{in}}$
11. $C_p^* = \frac{C_p}{C_{po}}$
12. $C_l^* = \frac{C_l}{C_{lo}}$
13. $Q^* = \frac{Q}{\rho_0 L^2 u_0 C_{po} (T_w - T_{in})}$

$$14. D^* = \frac{D}{L u_0}$$

$$15. d^* = \frac{d}{L}$$

$$Re = \frac{\rho_0 u_0 L}{\mu_0}$$

$$Pr = \frac{\mu_0 C_{p_0}}{K_o}$$

$$Ja = \frac{C_{l_0} (T_w - T_{in})}{L}$$

2.4 Solution form of the governing equations :

2.4.1 Gas-Phase

Continuity:

The continuity equation for the gas phase, Eqn. (2.2) may be written as: Since $\vartheta_g = 1 - \vartheta_d \simeq 1$, we take it out of the derivatives and get,

$$\frac{\partial \rho_g}{\partial t} + \nabla \cdot (\rho_g \mathbf{u}_g) = \frac{1}{\vartheta_g} n \dot{m}_v \quad (2.14)$$

or,

$$\frac{D \rho_g}{Dt} + \rho_g \nabla \cdot \mathbf{u}_g = \frac{1}{\vartheta_g} n \dot{m}_v \quad (2.15)$$

Non Dimensionized form of the eqn :-

$$\frac{\partial \rho_g^*}{\partial \tau} + \nabla \cdot (\rho_g^* \mathbf{u}_g^*) = \frac{1}{\vartheta_g} n^* \dot{m}_v^* \quad (2.16)$$

Momentum:

momentum Eqn. (2.4) can be simplified further as,

$$\begin{aligned} \frac{\partial \mathbf{u}_g}{\partial t} + \nabla \cdot (\mathbf{u}_g \mathbf{u}_g) - \frac{1}{\rho_g} [\nabla \cdot (\mu_g \nabla \mathbf{u}_g)] = & -\frac{1}{\rho_g} \nabla P + \mathbf{g} - \frac{1}{\vartheta_g \rho_g} [n \dot{m}_v \mathbf{u}_g] \\ & + \frac{1}{\vartheta_g \rho_g} [n \dot{m}_v \mathbf{u}_d] - \frac{\vartheta_d}{\vartheta_g \rho_g} \mathbf{f}_d + \mathbf{u}_g [\nabla \cdot \mathbf{u}_g] \end{aligned} \quad (2.17)$$

Non Dimensionized form of Momentum equation :-

$$\begin{aligned} \frac{\partial \mathbf{u}_g^*}{\partial t} + \nabla^* \cdot (\mathbf{u}_g^* \mathbf{u}_g^*) - \frac{1}{Re \rho_g^*} [\nabla^* \cdot (\mu_g^* \nabla^* \mathbf{u}_g^*)] = & -\frac{1}{\rho_g^*} \nabla^* P^* + \frac{L \mathbf{g}}{u_0^2} - \frac{1}{\vartheta_g \rho_g^*} [n^* \dot{m}_v^* \mathbf{u}_g^*] \\ & + \frac{1}{\vartheta_g \rho_g^*} [n^* \dot{m}_v^* \mathbf{u}_d^*] - \frac{\vartheta_d}{\vartheta_g \rho_g^*} \mathbf{f}_d^* + \mathbf{u}_g^* [\nabla^* \cdot \mathbf{u}_g^*] \end{aligned} \quad (2.18)$$

$$\mathbf{f}_d = \rho_g \frac{1}{\left(\frac{4}{3}\pi\left\{\frac{d_d}{2}\right\}^3\right)} \frac{1}{2} C_d |\mathbf{u}_g - \mathbf{u}_d| (\mathbf{u}_g - \mathbf{u}_d) \left(\frac{\pi}{4} d_d^2\right) = \beta (\mathbf{u}_g - \mathbf{u}_d)$$

where d_d is the diameter of the droplets and C_d is the drag coefficient

$$\mathbf{f}_d^* = \frac{3\rho_g^*}{4 d_d^*} C_d |u_g^* - u_d^*| (u_g^* - u_d^*)$$

where d_d is the diameter of the droplets and C_d is the drag coefficient

Energy:

The energy equation of carrier phase Eqn. (2.6) can be further simplified as,

$$\begin{aligned} \frac{\partial (C_{pg} T_g)}{\partial t} + \nabla \cdot (C_{pg} T_g \mathbf{u}_g) &= \frac{1}{\rho_g} [\nabla \cdot (k_g \nabla T_g)] + \frac{1}{\vartheta_g \rho_g} [n \dot{m}_v C_{vd} T_d] \\ &\quad - \frac{1}{\vartheta_g \rho_g} [n \dot{m}_v C_{pg} T_g] - \frac{n Q}{\vartheta_g \rho_g} + C_{pg} T_g [\nabla \cdot \mathbf{u}_g] \end{aligned} \quad (2.19)$$

Non Dimensionized form of Energy equation :-

$$\begin{aligned} \frac{\partial (C_{pg}^* T_g^*)}{\partial \tau} + \nabla \cdot (C_{pg}^* T_g^* \mathbf{u}_g^*) &= \frac{1}{Re Pr \rho_g^*} [\nabla \cdot (k_g^* \nabla T_g^*)] + \frac{1}{\vartheta_g \rho_g^*} [n^* \dot{m}_v^* C_{vd}^* T_d^*] \\ &\quad - \frac{1}{\vartheta_g \rho_g^*} [n^* \dot{m}_v^* C_{pg}^* T_g^*] - \frac{n^* Q^*}{\vartheta_g \rho_g^*} + C_{pg}^* T_g^* [\nabla \cdot \mathbf{u}_g^*] \\ &\quad + \frac{1}{\vartheta_g \rho_g^* (T_w - T_{in})} [n^* \dot{m}_v^* C_{vd}^* T_{in}] - \frac{1}{(T_w - T_{in}) \vartheta_g \rho_g^*} [n^* \dot{m}_v^* C_{pg}^* T_{in}] \end{aligned} \quad (2.20)$$

gas phase specific heat C_{pg} and thermal conductivity k_g are computed by mixing laws as a mass fraction average of pure species specific heat and thermal conductivity as follows,

$$C_{pg}^* = \frac{Y_F C_{vd}}{C_{p0}} + \frac{(1 - Y_F) C_{pc}}{C_{p0}} \quad \text{and} \quad k_g^* = \frac{Y_F k_{vd}}{k_0} + \frac{(1 - Y_F) k_c}{k_0} \quad (2.21)$$

where C_{pc} and k_c are the specific heat and thermal conductivity for pure gas respectively, while the subscripts vd refer to the corresponding qualities for the evaporated vapour from the droplets.

Species Mass Fraction:

$$\frac{\partial (Y_F)}{\partial t} + \nabla \cdot (Y_F \mathbf{u}_g) = \frac{1}{\rho_g} \nabla \cdot (\rho_g D \nabla Y_F) + \frac{1}{\vartheta_g \rho_g} n \dot{m}_v (1 - Y_F) + Y_F [\nabla \cdot \mathbf{u}_g] \quad (2.22)$$

Non Dimensionized form of the equation :-

$$\frac{\partial (Y_F)}{\partial \tau} + \nabla^* \cdot (Y_F \mathbf{u}_g^*) = \frac{1}{\rho_g^*} \nabla^* \cdot (\rho_g^* D^* \nabla^* Y_F) + \frac{1}{\vartheta_g \rho_g^*} n \dot{m}_v^* (1 - Y_F) + Y_F [\nabla^* \cdot \mathbf{u}_g^*] \quad (2.23)$$

2.4.2 Droplet-Phase

Continuity:

The continuity equation for the droplet phase is written as,

$$\frac{\partial (\rho_d \vartheta_d)}{\partial t} + \nabla \cdot (\rho_d \vartheta_d \mathbf{u}_d) = -n \dot{m}_v \quad (2.24)$$

For dilute two-phase flows, $\vartheta_d < 0.1\%$. Hence, for computational ease, we normalize the volume fraction equation by considering the initial volume fraction as ϑ_0 and define the normalized volume fraction of the dispersed phase as Θ_d .

$$\Theta_d \equiv \frac{\vartheta_d}{\vartheta_0}$$

Writing Eq(2.9) in vector notation, we get

$$\frac{\partial (\rho_d \Theta_d \vartheta_0)}{\partial t} + \nabla \cdot (\rho_d \Theta_d \vartheta_0 \mathbf{u}_d) = -n \dot{m}_v \quad (2.25)$$

On simplifying it further we get,

$$\frac{d \Theta_d}{dt} + \nabla \cdot (\Theta_d \mathbf{u}_d) = -\frac{n \dot{m}_v}{\rho_d \vartheta_0} \quad (2.26)$$

Non Dimensionized form of the equation :-

$$\frac{d \Theta_d}{d\tau} + \nabla^* \cdot (\Theta_d \mathbf{u}_d^*) = -\frac{n^* \dot{m}_v^*}{\rho_d^* \vartheta_0} \quad (2.27)$$

Momentum:The droplet phase momentum equation, Eqn. (2.11) can be simplified as follows:

$$\frac{\partial \mathbf{u}_d}{\partial t} + \nabla \cdot (\mathbf{u}_d \mathbf{u}_d) = -\frac{1}{\rho_d} \nabla P + \mathbf{g} + \frac{1}{\rho_d} \mathbf{f}_d + \mathbf{u}_g [\nabla \cdot \mathbf{u}_g] \quad (2.28)$$

Substituting Eqn. (2.9), the momentum equation can be simplified as

$$\frac{\partial U_{d,i}}{\partial t} + U_{d,j} \frac{\partial (U_{d,i})}{\partial x_j} = -\frac{1}{\rho_d} \frac{\partial P}{\partial x_i} + g_i + \frac{1}{\rho_d} f_{di} \quad (2.29)$$

Writing in vector form,

$$\frac{\partial \mathbf{u}_d}{\partial t} + \nabla \cdot (\mathbf{u}_d \mathbf{u}_d) = -\frac{1}{\rho_d} \nabla P + \mathbf{g} + \frac{1}{\rho_d} \mathbf{f}_d + \mathbf{u}_d [\nabla \cdot \mathbf{u}_d] \quad (2.30)$$

Non Dimensionized form of the equation :-

$$\frac{\partial \mathbf{u}_d^*}{\partial \tau} + \nabla^* \cdot (\mathbf{u}_d^* \mathbf{u}_d^*) = -\frac{1}{2\rho_d^*} \nabla^* P^* + \frac{L\mathbf{g}}{u_0^2} + \frac{1}{\rho_d^*} \mathbf{f}_d^* + \mathbf{u}_d^* [\nabla^* \cdot \mathbf{u}_d^*] \quad (2.31)$$

Energy:

$$\frac{\partial C_{ld} T_d}{\partial t} + \nabla \cdot (C_{ld} T_d \mathbf{u}_d) = -\frac{n\dot{m}_v \mathbb{L}}{\rho_d \vartheta_d} + \frac{nQ}{\rho_d \vartheta_d} + C_{ld} T_d [\nabla \cdot \mathbf{u}_d] \quad (2.32)$$

Non Dimensionized form of the equation :-

$$\frac{\partial C_{ld}^* T_d^*}{\partial \tau} + \nabla^* \cdot (C_{ld}^* T_d^* \mathbf{u}_d^*) = -\frac{n^* \dot{m}_v^*}{Ja \rho_d^* \vartheta_d} + \frac{n^* Q^*}{\rho_d^* \vartheta_d} + C_{ld}^* T_d^* [\nabla^* \cdot \mathbf{u}_d^*] \quad (2.33)$$

2.5 Boundary Conditions

2.5.1 At Solid Boundaries

At solid boundaries a no-slip condition is specified for the gas phase. Hence at the solid boundaries,

$$u_g = 0, \quad v_g = 0, \quad w_g = 0.$$

so,

$$u_g^* = 0, \quad v_g^* = 0, \quad w_g^* = 0.$$

For pressure, it is usual to specify a homogeneous Neumann boundary condition, that is

$$\frac{\partial P}{\partial n} = 0$$

So,

$$\frac{\partial P^*}{\partial n} = 0$$

where n is the coordinate normal to the wall.

For the droplet phase a free-slip boundary condition is assumed at the wall. Hence we have

$$u_{d,n} = 0$$

$$\frac{\partial u_{d,t}}{\partial n} = 0$$

So,

$$\begin{aligned} u_{d,n}^* &= 0 \\ \frac{\partial u_{d,t}^*}{\partial n} &= 0 \end{aligned}$$

where n , t is the wall normal and tangential component of velocity, respectively. For volume fraction, fuel mass fraction and droplet temperature a homogeneous Neumann boundary condition is specified at the walls.

$$\frac{\partial \phi}{\partial n} = 0$$

So,

$$\frac{\partial \phi^*}{\partial n} = 0$$

where ϕ^* is ϑ_d , Y_F and T_d^* .

2.5.2 Inlet

At the inlet, all variables other than pressure are specified using Dirichlet condition:

$$\phi = \phi_{in}$$

So,

$$\phi = \phi_{in}^*$$

where ϕ is any variable except pressure. The boundary condition for pressure is once again assumed to be of homogeneous Neumann type,

$$\frac{\partial P}{\partial n} = 0$$

So,

$$\frac{\partial P^*}{\partial n} = 0$$

2.5.3 Outlet

At the outlet a homogeneous Neumann condition is assumed for all flow variables except pressure.

$$\frac{\partial \phi}{\partial n} = 0$$

So,

$$\frac{\partial \phi^*}{\partial n} = 0$$

where ϕ^* is any variable except pressure. For pressure, any constant value may be specified, because it is only the pressure gradient that is important, and not the absolute pressure. It is convenient to specify a homogeneous Dirichlet condition for pressure at the outlet.

$$P = 0$$

So,

$$P^* = 0$$

2.6 Evaporation Model for Single Component Droplets

2.6.1 Classical D^2 -Law

The classical D^2 -law was formulated in the 1950s by Godsave [17] and Spalding [36]. It was derived for an isolated, pure-component droplet burning in a quiescent, oxidizing environment. This evaporation model is based on the following assumptions:

1. The drop is spherical.
2. The fuel is a pure liquid having a well-defined boiling point.
3. Radiation heat transfer is negligible.

It has since then been termed the D^2 -law, because it predicts that the square of the droplet diameter decreases linearly with time. The model can be used both for the combustion and for the evaporation of a droplet. This model is explained in detail in [23].

A sketch of the droplet evaporation process is provided in Fig. 2.1, for the hypothetical case where a single-component drop is suddenly introduced into a gas at elevated temperature. At typical injection temperatures, the fuel vapour concentration at liquid surface is low which leads to negligible mass diffusion from the drop. Under these conditions, the droplet behaves like any cold body placed in a hot environment and

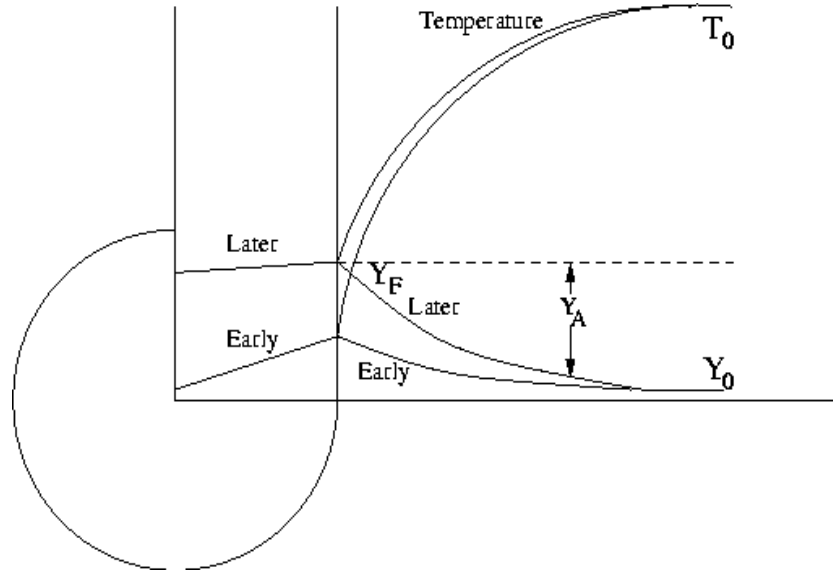


Figure 2.1: Variation of temperature and gas concentration during droplet evaporation (Faeth) [11].

utilizes the heat received to increase its temperature. In general, temperature is not uniform within the droplet but is lower at the center of the drop, with maximum liquid temperature at the surface. Initially, almost all of the heat supplied to the drop serves to raise its temperature. As the liquid temperature rises, the fuel vapour formed at the liquid surface has two effects i.e., an increasing portion of the energy reaching the drop surface is utilized for providing the heat of vaporization of the evaporating fuel, and the outward flow of the fuel vapour reduces the heat transfer to the droplet. This slows the rate of increase of the liquid surface temperature and therefore, later in the process, the temperature becomes relatively uniform in the droplet. Eventually, a stage is reached where all the heat reaching the surface is utilized for the heat of vaporization and the droplet stabilizes at a temperature called the “wet bulb temperature”. The droplet attains its steady-state and the drop diameter diminishes with time according to the relationship ([36],[17])

$$d_0^2 - d^2 = \lambda_{st}t \quad (2.34)$$

Burning rate curves are shown in Fig. 2.2 for n-Heptane which for the studied case has $\lambda_{st} = 0.30 \text{ mm}^2/\text{s}$.

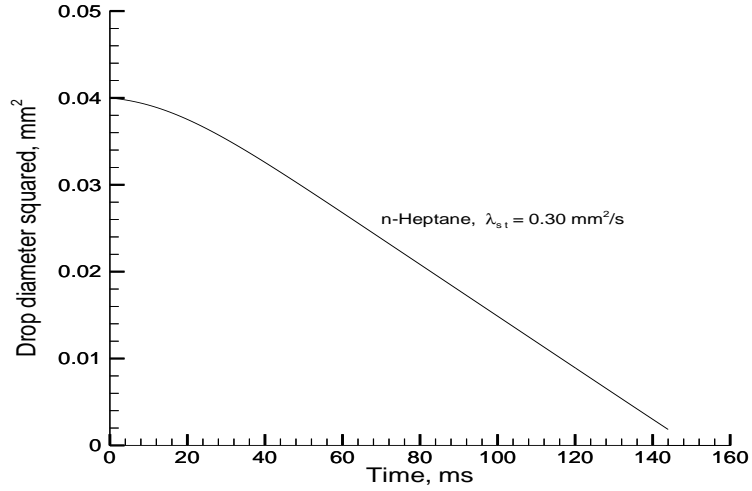


Figure 2.2: Burning rate curves for n-Heptane

2.6.2 Mathematical Formulation

Evaporation process is characterized by simultaneous mass and heat transfer. A measure of the mass transfer rate from the droplet to the surrounding gas and heat transfer rate from the ambient gas to the drop is hence required to analyze the rate of evaporation of the droplets. We use two parameters, mass transfer number (B_M) and heat transfer number (B_T) to quantitatively measure mass and heat transfer rates.

Mass transfer number

An expression for the mass transfer number, B_M and hence, the rate of evaporation of a single spherical fuel drop, \dot{m}_v is derived by neglecting thermal diffusion and assuming that the driving force for species diffusion is a concentration gradient in the direction of the diffusion path, the following expression is obtained for an evaporating drop [23]:

$$\frac{dY_F}{dr} = -\frac{RT}{D_c P} (\dot{m}_v Y_A) \quad (2.35)$$

Y_F = fuel mass fraction

Y_A = air mass fraction

\dot{m}_v = mass rate of diffusion per unit area

D_c = diffusion coefficient

P = gas pressure

r = radius ($r = 0$ at center of drop and $r = r_s$ at drop surface)

From continuity considerations, the mass rate of diffusion at the drop surface, \dot{m}_{v_s} is given by

$$\dot{m}_{v_s} 4\pi r_s^2 = \dot{m}_v 4\pi r^2$$

Applying the following boundary conditions

$$\begin{array}{lll} r = r_s; & T = T_s; & Y_F = Y_{F_s} \\ r = \infty; & T = T_\infty; & Y_F = Y_{F_\infty} = 0 \end{array}$$

and integrating Eqn. 2.35 between $r = r_s$ and $r = \infty$ gives the mass transfer rate as

$$\dot{m}_v = 2\pi d_d \rho D_c \ln(1 - Y_{F_s}) \quad (2.36)$$

Assuming the Lewis number ($Le \equiv \frac{\alpha}{D}$) is equal to unity, the quantity ρD_c can be replaced by $(k/C_p)_g$, where k and C_p are the mean thermal conductivity and specific heat, respectively.

Defining

$$B_M = \frac{Y_{F_s} - Y_{F_\infty}}{(1 - Y_{F_s})} \quad (2.37)$$

Now substituting B_M in Eq. 2.36 gives [23]

$$\dot{m}_v = 2\pi d_d \left(\frac{k}{C_p} \right)_g \ln(1 + B_M) \quad (2.38)$$

This is the basic equation for the evaporation rate of a fuel drop of diameter d_d . Its accuracy is very much dependent on the choice of the values of k_g and C_{pg} . The reference temperature and composition for the evaluation of the average properties will be discussed later in this chapter.

Heat transfer number

Similar to the above analysis but based on the convective and conductive heat fluxes across a thin shell surrounding the evaporating drop, lead to the following expression for heat transfer number [36]:

$$B_T = \frac{C_{pg}(T_\infty - T_s)}{L} \quad (2.39)$$

where L is the latent heat of vaporization of fuel at droplet surface temperature T_s .

The number B_T denotes the ratio of the available enthalpy in the surrounding gas to the heat required to evaporate the fuel. In this case the rate of evaporation, for Lewis number of unity, is obtained as

$$\dot{m}_v = 2\pi d_d \left(\frac{k}{C_p} \right)_g \ln(1 + B_T) \quad (2.40)$$

Under the steady-state condition $B_M = B_T$ and either Eq. 2.38 or Eq. 2.40 may be used to calculate the rate of evaporation. The advantage of Eq. 2.38 is that it applies under all conditions, including the transient state of droplet heat-up, whereas Eq. 2.40 can only be used for steady-state evaporation. However, Eq.2.40 is usually easier to evaluate, since the magnitudes of various terms are either contained in the data of the problem or readily available in the literature. This is particularly true when the ambient gas temperature is significantly higher than the fuel surface temperature T_s , then T_s can be replaced by the boiling temperature of the fuel with little loss in accuracy.

2.6.3 Calculation of Steady-State Evaporation Rates

The stage in the drop evaporation process when the drop surface has attained its wet-bulb temperature is called as steady-state. At steady state, all the heat reaching the drop surface is utilized in providing the latent heat of evaporation. Hence, at steady-state $B_M = B_T$ which leads to the relation between Y_{F_s} and T_s as.

$$\frac{Y_{F_s}}{(1 - Y_{F_s})} = \frac{C_{pg}(T_\infty - T_s)}{L} \quad (2.41)$$

The fuel vapour mass fraction at the droplet surface is calculated by taking the partial pressure weighted average of molecular weights,

$$Y_{F_s} = \left[1 + \left(\frac{P}{P_{F_s}} - 1 \right) \frac{M_A}{M_F} \right]^{-1} \quad (2.42)$$

where,

P_{F_s} = fuel vapour pressure at the drop surface

P = ambient pressure (sum of fuel vapour pressure and air partial pressure at the drop surface)

M_A = molecular weight of air

M_F = molecular weight of fuel

The quantitative values of P , M_A , M_F , and T_∞ are usually known for any problem. Fuel vapour pressure is a function of T_S and can be easily obtained using the following modified form of Clausius-Clapeyron equation for organic fuels [23]

$$P_{F_S} = \exp\left(a - \frac{b}{T_s - 43}\right) \text{ kPa} \quad (2.43)$$

Eqns. 2.41 and 2.43 form a set of equations for the two unknowns Y_{F_S} and T_S . Having obtained these values, the mass evaporation rate for the drop can be calculated from equation 2.38 or 2.40.

2.6.4 Evaporation Constant

It has been shown earlier that during the steady-state period of an evaporating drop its diameter at any instant may be related to its initial diameter by an expression

$$d_0^2 - d^2 = \lambda_{st} t \quad (2.44)$$

where λ is the evaporation constant as defined by Godsave [17]. and is rewritten as

$$\lambda_{st} = \frac{d(d_d)^2}{dt} = 2 d_d \frac{d(d_d)}{dt} \quad (2.45)$$

The value of λ_{st} may be used to determine the steady-state transfer number $B = B_M = B_T$. From Eq. 2.45 it can be shown that

$$\dot{m}_v = \frac{dm_v}{dt} = \frac{d}{dt} \left\{ \rho_d \frac{4\pi}{3} \frac{d_d^3}{8} \right\} = \frac{\pi}{4} \rho_d d_d \lambda_{st} \quad (2.46)$$

Equating 2.38 and 2.46 gives

$$\lambda_{st} = \frac{8 k_g \ln(1 + B)}{C_{pg} \rho_d} \quad (2.47)$$

2.7 Unsteady-State Analysis

Even before the drop reaches its wet-bulb temperature, a very small amount of evaporation takes place owing to the diffusion of fuel vapors at the drop surface. This can be seen from Fig. 2.2 showing the relationship between droplet diameter squared and time. During most of the evaporation period, the slope of d_d^2/t is seen to be constant but at the start it is almost zero. The slope then gradually increases with time until the droplet attains its wet-bulb temperature, after which it remains constant throughout its lifetime.

For the purpose of analysis, the vaporization process is divided into the transient or unsteady state and the steady state. The magnitude of the unsteady portion depends on many parameters such as properties of fuel, ambient pressure and temperature and initial temperature of the drop.

2.7.1 Calculation of drop surface temperature

If the rate of heat transfer to a drop per unit surface area per unit time is denoted by q , then

$$\dot{q} = \frac{\dot{m}_v L}{\pi d_d^2} \quad (2.48)$$

Substituting for \dot{m}_v gives

$$\dot{q} = \frac{2(k/C_p)_g L \ln(1 + B_M)}{d_d} \quad (2.49)$$

A quasi-steady gas phase is assumed in which the boundary layer around the drop has the same characteristics as a steady boundary layer for the same conditions of drop size, velocity, surface temperature and ambient temperature. Nusselt number is then given by [23]

$$Nu = \frac{h d_d}{k_g} = \frac{\dot{q} d_d}{k_g(T_\infty - T_s)}$$

On substituting Eqn. (2.49) we have,

$$Nu = 2L \frac{\ln(1 + B_M)}{C_{pg}} = 2 \frac{\ln(1 + B_M)}{B_M} = 2 \frac{\ln(1 + B_M)}{B_M} \quad (2.50)$$

The heat transferred from the gas to the drop is then given by

$$\dot{Q} = \pi d_d^2 \dot{q} \quad (2.51)$$

or

$$\dot{Q} = 2 \pi d_d k_g (T_\infty - T_s) \frac{\ln(1 + B_M)}{B_M} \quad (2.52)$$

Now the heat used in vaporization of the fuel is

$$\dot{Q}_e = \dot{m}_v L = 2 \pi d_d (k/C_p)_g L \ln(1 + B_M) \quad (2.53)$$

The heat available for the heating up the drop is hence the difference between \dot{Q} and \dot{Q}_e

$$\dot{Q} - \dot{Q}_e = 2 \pi d_d k_g \ln(1 + B_T) \left(\frac{T_\infty - T_s}{B_M} - \frac{L}{C_{pg}} \right) \quad (2.54)$$

or

$$\dot{Q} - \dot{Q}_e = \dot{m}_v L \left(\frac{B_T}{B_M} - 1 \right) \quad (2.55)$$

It should be noted in Eq. 2.55 that when $B_T = B_M$ the value of $Q - Q_e$ becomes zero, denoting the end of the heat-up period. Now the rate of change of the drop surface temperature is given by

$$\frac{dT_s}{dt} = \frac{\dot{Q} - \dot{Q}_e}{C_{ld} m} = \frac{\dot{m}_v L}{C_{ld} m} \left(\frac{B_T}{B_M} - 1 \right) \quad (2.56)$$

where $m = \text{drop mass} = (\pi/6) \rho_F d_d^3$. The Eulerian form of the above equation, Eqn. (2.13) is used in the present study which has been discussed earlier in this chapter. Since, uniform temperature model is being considered for droplet phase, $T_d = T_s$. Also, the rate of change of diameter of droplet may be given by combining equations 2.45 and 2.47,

$$\frac{dd_d}{dt} = \frac{4k_g \ln(1 + B_M)}{C_{pg} \rho_d d_d} \quad (2.57)$$

Eqns (2.56) and (2.57) give the change of droplet surface temperature T_s and diameter d_d during the transient period. However, they can be used even after steady-state is reached then $T_s = T_{sat}$, as $B_M = B_T$, while Eqn (2.56) continues to give correct values for the change in diameter (as in Eqns 2.45-2.47) according to the D^2 model.

2.8 Drop analysis

Transport processes within the drop are treated in different ways by different models such as the thin skin model, uniform temperature model, uniform state model. In this study we will use the uniform temperature model also known as ‘rapid mixing limit’ or ‘infinite conductivity model’ which postulates infinite thermal diffusivity and assumes that the temperature within the droplet is spatially uniform although time varying. We also assume that the species concentration is uniform within the drop.

2.9 Convective effects on evaporation

For drop evaporation under quiescent conditions, the principal mode of heat transfer is conduction. But if relative motion exists between the droplet and the surrounding fluid, the rate of evaporation is enhanced. The gas-phase convective environment has a considerable impact on the droplet evaporation process, as both the heat and the

mass transfer process between the phases are enhanced by relative motion between them. In order to consider these phenomena, mass flux and energy transfer rates are corrected by implementing semi-empirical correlations for the calculation of both mass and heat transfer numbers. One of the first reliable correlations was given by Frossling [14]. He showed that the effect of convection on heat and mass transfer rates could be accommodated by a correction factor that is a function of Reynolds number and either Schmidt or Prandtl number. This correction factor has been later modified by Ranz and Marshall [30].

The correction factor when the diffusion rates are controlling the evaporation rate is

$$1 + 0.3 Re_d^{0.5} Sc_g^{0.33} \quad (2.58)$$

And when the heat transfer rates are controlling the evaporation rate,

$$1 + 0.3 Re_d^{0.5} Pr_g^{0.33} \quad (2.59)$$

Combining equations 2.38 and 2.59 yields the following equation for the rate of fuel evaporation under convective environment:

$$\dot{m}_v = 2\pi d_d \left(\frac{k}{C_p} \right)_g \ln(1 + B_M) (1 + 0.3 Re_d^{0.5} Pr_g^{0.33}) \quad (2.60)$$

This equation gives the instantaneous rate of evaporation for a drop of diameter d_d . As described earlier heat transfer rates between the phases are also enhanced under convective environment. So the expression for rate of heat transferred from the gas to the drop Q (Eqn. 2.52) and the heat used in vaporization of the fuel Q_e (Eqn. 2.53) can also be modified using the correction factor as follows,

$$Q = 2\pi d_d k_g (T_\infty - T_s) \frac{\ln(1 + B_M)}{B_M} (1 + 0.3 Re_d^{0.5} Pr_g^{0.33}) \quad (2.61)$$

and

$$Q_e = \dot{m}_v L = 2\pi d_d \left(\frac{k}{C_p} \right)_g L \ln(1 + B_M) (1 + 0.3 Re_d^{0.5} Pr_g^{0.33}) \quad (2.62)$$

In the above expressions Re_d is the droplet Reynolds number. The definition of droplet Reynolds number is based on the relative velocity between the droplet and the surrounding gas, on the free stream density and the average gas film viscosity. Generally, most evaporation processes occur due to the temperature difference between the droplet phase and gas phase. So, in all such cases, heat transfer controls the evaporation process and Eqns. (2.60) through (2.62) are appropriate. If however, mass transfer is the controlling mechanism we replace Pr_g by Schmidt number Sc_g in these equations.

2.10 Property Evaluation

The evaporation model given by Spalding [36] is based on the assumption that the Lewis number within the gas phase is unity. From the definition of the Lewis number, $Le \equiv \alpha/D_c$, it can be seen that $\alpha = D_c$ for the present case, where $\alpha = k/(\rho C_p)$ is the thermal diffusivity. This implies that the rate of heat and mass transfer are of the same magnitude. This assumption provides simplification and as a consequence, the number of properties which has to be evaluated in order to solve the problem is reduced. This is true only for the steady-state analysis. The properties such as density and thermal conductivity of the evaporated liquid has to be evaluated at some mean film temperature and composition. In the literature several schemes have been proposed but many authors found that the scheme which they called the ‘1/3 rule’ worked best. The rule used the following reference states for temperature and composition, designated with the subscript r:

$$T_r = T_S + \frac{T_\infty - T_S}{3} \quad (2.63)$$

$$Y_{F_r} = Y_{F_S} + \frac{Y_{F_\infty} - Y_{F_S}}{3} \quad (2.64)$$

where Y_F is mass fraction of the fuel vapour. Subscripts s and ∞ refer to the surface and ambient conditions. If the fuel concentration at an infinite distance from the droplet is assumed to be zero, Eqn. (2.64) becomes

$$Y_{F_r} = \frac{2}{3} Y_{F_S} \quad (2.65)$$

$$Y_{A_r} = 1 - Y_{F_r} = 1 - \frac{2}{3} Y_{F_S} \quad (2.66)$$

where Y_{A_r} is the reference mass fraction of air. The above equations are used in this study to calculate the reference values of the physical properties of the vapour-gas mixture that constitutes the environment of the evaporating drop. This means that the reference state is closer to the droplet surface than the mean film value. For example, the reference specific heat and thermal conductivity is obtained as,

$$C_{pg} = Y_{A_r} (C_{pA} \text{ at } T_r) + Y_{F_r} (C_{pv} \text{ at } T_r) \quad (2.67)$$

$$k_g = Y_{A_r} (k_A \text{ at } T_r) + Y_{F_r} (k_v \text{ at } T_r) \quad (2.68)$$

Chapter 3

Discretization Procedure and Solution Algorithm

The formulation presented here is the same as followed by Mrunalini (2012).

3.1 Description of the Finite Volume Method

The Finite Volume method for solving the incompressible Navier Stokes equations has become very popular in recent years because of the following advantages

1. It is easy to implement on non-orthogonal curvilinear grids.
2. The solution can be obtained in the actual physical domain without transforming the governing equations.
3. It is easy to implement the boundary conditions.

When the primitive variable (e.g.velocity and pressure) approach is used, special treatment for pressure is required in the solution algorithm because the pressure does not have its own governing equation for incompressible flow. The continuity equation, having no explicit link to the pressure, is just an additional constraint on the velocity field that must be satisfied together with the momentum equations. It is an appropriate manipulation of that constraint which leads to an equation for the pressure.

In the present study, the Navier Stokes and Energy equations have been solved using the finite volume method. We have used non-staggered (collocated) grid arrangement,

where the dependent variables are calculated at the centroid of the finite volume. But this arrangement can produce non-physical oscillations in the pressure field, the so-called checker-board pressure distribution. When central differencing is used to represent both the pressure gradient term in the momentum equations and the cell-face velocity in the continuity equation, it then happens that the velocities depend on pressure at alternate nodes and not on adjacent ones and the pressure too depends on velocities at alternate nodes. This behavior is called velocity-pressure decoupling, Patankar [27].

To avoid this decoupling, the momentum interpolation method, first proposed by Rhie and Chow [29] has been used. In this approach, the cell-face velocity in the continuity equations are evaluated by linearly interpolating the so-called “mass” velocities computed without the pressure terms in the discretized equations while directly evaluating the pressure gradient using values at the adjacent cell centers. This results in a strong velocity-pressure coupling. The pressure gradient terms, appearing in the momentum equations, are still represented by central difference approximation.

3.2 Grid Generation

Grids used in this thesis are generated using *ANSYS ICEMCFD* software. The grids used in this thesis are structured grids with quadrilateral nodes. *ANSYS ICEMCFD* is a grid generation system combining various technologies such as computer aided geometric design, computational geometry and computer graphics, structured and unstructured grid generation algorithms. Grids generated in *ANSYS ICEMCFD* are saved in Version 2.4 CGNS format.

3.3 CGNS file format

CGNS (CFD General Notation System) originated in 1994 as a joint effort between Boeing and NASA, and has since grown to include many other contributing organizations worldwide. It is an effort to standardize CFD input and output, include grid (both structured and unstructured), flow solution, connectivity, boundary conditions (BCs), and auxiliary information. CGNS is also extensible, and allows for file-stamping and user-inserted-commenting. It employs ADF (Advanced Data Format), a system which reads a binary files that are portable across computer platforms. CGNS also

includes a second layer of software known as the mid-level library, or API (Application Programming Interface), which eases the implementation of CGNS into existing codes.

A CGNS file is an entity that is organized (inside the file itself) into a set of *nodes* in a tree-like structure, in much the same way as directories are organized in the UNIX environment. The top-most node is referred to as the *root node*. Each node below the root node is defined by both a name and a label, and may or may not contain information data. Each node can also be a *parent* to one or more *child* nodes.

CGNS files are binary files and they cannot be viewed by user with standard UNIX ASCII- editing tools. The utility ADF was created to allow users to easily view CGNS files. For more detailed information, readers are suggested to see the CGNS website www.cgns.org (especially the User's Guide Section).

In the present work, CGNS version 2.4 file-format is used to store grids and flow solution. Post processing is done by *Tecplot 360*, which is also a CGNS compatible software.

3.4 Integral Form of Governing Equations

The three-dimensional Navier-Stokes equations can be expressed in the following general convection-diffusion-source integral form:

$$\frac{\partial}{\partial t} \int_V \rho dV + \int_S \rho \mathbf{u} \cdot \mathbf{dS} = 0 \quad (3.1)$$

$$\frac{\partial}{\partial t} \int_V \rho \phi dV + \int_S [\rho \mathbf{u} \phi - \Gamma_\phi \nabla \phi] \cdot \mathbf{dS} = \int_V S_\phi dV \quad (3.2)$$

where ρ represents the fluid density, \mathbf{u} is the fluid velocity, Γ_ϕ is the diffusion coefficient for the quantity ϕ (viscosity in case of momentum equations), ϕ stands for any vector component or scalar quantity, S_ϕ is the volumetric source term. If ϕ is other than velocity *i.e* temperature, scalar *etc.* then density (ρ) should be replaced by $(\rho C_p)_\phi$.

In this formulation we work with **Cartesian components** of velocity. So ϕ can be the three Cartesian component of velocity u, v, w as well as any scalar *e.g.*, temperature, species concentration, which needs to be determined.

3.5 Description of the Finite-Volume Method

We will now discuss the finite volume method applied to a general 3-D geometry. The entire solution domain is initially divided into zones and then zones are subdivided into a number of finite volumes defined by the coordinates of their eight vertices read from the CGNS grid file. We have used the collocated grid arrangement where all the dependent variables are defined at the centroid of the cell. The FVM method used in this work is explained in detail in BARC Report [9].

3.6 Discretization Procedure

The discretization of the transport equations is performed using the finite volume approach. All the transport equation can be represented in the following general form,

$$\frac{\partial}{\partial t} \int_V \rho \phi dV + \int_S [\rho \mathbf{u} \phi - \Gamma_\phi \nabla \phi] \cdot \mathbf{dS} = \int_V S_\phi dV \quad (3.3)$$

which consists of the rate of change of ϕ , convection diffusion fluxes and the source term. The rate of change and source terms are integrated over the cell volume, whereas the convection and diffusion terms sum fluxes through the CV faces.

3.6.1 Discretization of the General Convection-Diffusion Equation

(a) Rate of change: In the discretization of the unsteady term it has been assumed that the value of the dependent variable at the centroid is the average over the entire control volume. Thus

$$\frac{\partial}{\partial t} \int_V \rho \phi dV \approx \frac{(\rho \phi V)_P^{n+1} - (\rho \phi V)_P^n}{\Delta t} \approx V_P \frac{(\rho \phi)_P^{n+1} - (\rho \phi)_P^n}{\Delta t} \quad (3.4)$$

where V_P is the volume of the cell.

(b) Convection fluxes: The approximation of the surface integral over convection flux of variable ϕ has been done in the following way,

$$\int_S \rho \mathbf{u} \phi \cdot \mathbf{dS} \approx \sum_j \rho_j \phi_j (\mathbf{u} \cdot \mathbf{S})_j = \sum F_j \phi_j \quad (3.5)$$

where ϕ_j is the value of ϕ at the center of the face j . In this work, the value of the ϕ_j is evaluated using upwind scheme or Center difference scheme(CDS).

The upwind scheme is based on the assumption that the convected cell face value is equal to that at the upstream cell along the same coordinate direction. Thus, the value ϕ_e at the east face is assigned the value ϕ_P if $u_e \geq 0$, *i.e.*, the flux F_e is positive, and the value ϕ_E if $u_e < 0$, *i.e.*, the flux F_e is negative. This can be conveniently summarized as

$$F_e \phi_e = \phi_P [|F_e, 0|] - \phi_E [| -F_e, 0|] \quad (3.6)$$

Here $[|p, q|]$ denotes the maximum of p and q . Similar expression can be written for the rest of the faces.

While using CDS, the value of ϕ_j is evaluated using center difference linear interpolation from the neighboring nodal values.

$$F_e \phi_e = F_e \left(\frac{V_E}{V_E + V_P} \phi_P + \frac{V_P}{V_E + V_P} \phi_E \right) \quad (3.7)$$

(c) Diffusion fluxes: The surface integral over diffusion flux of variable ϕ can be approximated as

$$\int_S \Gamma_\phi \nabla \phi \cdot \mathbf{dS} \approx \sum_{j=e,w,n,s,t,b} (\Gamma_\phi \nabla \phi \cdot \mathbf{S})_j = \sum_j -F_j^d \quad (3.8)$$

For east face we can write,

$$F_e^d = -\Gamma_\phi \left(\alpha_1 \frac{\phi_E - \phi_P}{\Delta x^1} + \alpha_2 \frac{\phi_{se} - \phi_{ne}}{\Delta x^2} + \alpha_3 \frac{\phi_{te} - \phi_{be}}{\Delta x^3} \right) \quad (3.9)$$

Calculation of $\alpha_1, \alpha_2, \alpha_3$, the edge center values appearing in cross derivative diffusion flux, special treatment of diffusion fluxes of corner cells and computation of spatial derivatives at cell-center of a non-orthogonal grid is elaborated in Barc Report [9].

(d) Source: The source term is integrated over the cell volume as follows:

$$\int_V S_\phi dV \approx (S_\phi)_p V_P \quad (3.10)$$

In the momentum equations, the pressure term is a source term, while in species transport equations chemical reaction could be a source term.

(e) Pressure Term: Its discretization is same as that of the ordinary diffusion flux and is given by

$$-\int_{V_P} \nabla p \mathbf{n}_i dV \approx -(\nabla p \cdot \mathbf{n}_i)_P V_P \quad (3.11)$$

where \mathbf{n}_i is the unit vector in the direction of the velocity component, u_i . However, the Gauss divergence theorem can be used to convert the volume integral to a surface integral which can be discretized as

$$-\int_S p n_i d\mathbf{S} \approx -\sum_j p_j S_{ij} \quad (3.12)$$

p_j is the pressure at the j^{th} face center and S_{ij} is the i^{th} direction component of the surface vector for face j .

3.7 The Discretized Equations

3.7.1 Gas-Phase

We now present the discretized versions of the equations discussed in the previous chapter. **Continuity:**

The discretized form of Eqn. (2.14) is:

$$\Delta V_p \frac{\rho_g^{n+1} - \rho_g^n}{\Delta t} + \sum_f \rho_{gf}^{n+1} F_{gf}^{n+1} = \frac{1}{\vartheta_g^{n+1}} \Delta V_p (n \dot{m}_v)^n \quad (3.13)$$

Momentum:

The discretized form of Eqn. (2.18) is:

$$\begin{aligned} \Delta V_p \frac{u_g^{n+1} - u_g^n}{\Delta t} + \sum_f u_{gf}^m F_{gf}^m + \frac{1}{\rho_g^n} \sum_f F_{duf}^{n+1} + \frac{\Delta V_p}{\vartheta_g^n \rho_g^n} A^n u_g^{n+1} = \\ \frac{-1}{\rho_g^n} \sum_f P_f^{n+1} S_{fx} + \Delta V_p g_x \\ + \frac{\Delta V_p}{\vartheta_g^n \rho_g^n} (A^n u_d^n - \vartheta_d^n f_{dx}^n) + u_g^n \sum_f F_{gf}^m \end{aligned} \quad (3.14)$$

$$\begin{aligned} \Delta V_p \frac{v_g^{n+1} - v_g^n}{\Delta t} + \sum_f v_{gf}^m F_{gf}^m + \frac{1}{\rho_g^n} \sum_f F_{dvf}^{n+1} + \frac{\Delta V_p}{\vartheta_g^n \rho_g^n} A^n v_g^{n+1} = \\ \frac{-1}{\rho_g^n} \sum_f P_f^{n+1} S_{fy} + \Delta V_p g_y \quad (3.15) \\ + \frac{\Delta V_p}{\vartheta_g^n \rho_g^n} (A^n v_d^n - \vartheta_d^n f_{dy}^n) + v_g^n \sum_f F_{gf}^m \end{aligned}$$

$$\begin{aligned} \Delta V_p \frac{w_g^{n+1} - w_g^n}{\Delta t} + \sum_f w_{gf}^m F_{gf}^m + \frac{1}{\rho_g^n} \sum_f F_{dwf}^{n+1} + \frac{\Delta V_p}{\vartheta_g^n \rho_g^n} A^n w_g^{n+1} = \\ \frac{-1}{\rho_g^n} \sum_f P_f^{n+1} S_{fz} + \Delta V_p g_z \quad (3.16) \\ + \frac{\Delta V_p}{\vartheta_g^n \rho_g^n} (A^n w_d^n - \vartheta_d^n f_{dz}^n) + w_g^n \sum_f F_{gf}^m \end{aligned}$$

Energy:

The discretized form of Eqn. (2.20) is:

$$\begin{aligned} \Delta V_p C_{pg} \frac{T_g^{n+1} - T_g^n}{\Delta t} + \sum_f C_{pgf} T_{gf}^{n+1} F_{gf}^{n+1} + \frac{1}{\rho_g^{n+1}} \sum_f F_{dTf}^{n+1} + \frac{\Delta V_p}{\vartheta_g^{n+1} \rho_g^{n+1}} A^n C_{pg} T_g^{n+1} \\ = \frac{\Delta V_p}{\vartheta_g^{n+1} \rho_g^{n+1}} A^n C_{vd} T_d^{n+1} - \frac{\Delta V_p}{\vartheta_g^{n+1} \rho_g^{n+1}} n^n Q^n + C_{pg} T_g^n \sum_f F_{gf}^{n+1} \quad (3.17) \end{aligned}$$

Fuel Mass Fraction:

The discretized form of Eqn. (2.23) is:

$$\begin{aligned} \Delta V_p \frac{Y_F^{n+1} - Y_F^n}{\Delta t} + \sum_f Y_F^{n+1} F_{gf}^{n+1} + \frac{1}{\rho_g^{n+1}} \sum_f F_{dYf}^{n+1} = -\frac{\Delta V_p}{\vartheta_g^{n+1} \rho_g^{n+1}} A^n Y_F^{n+1} \\ + Y_F^n \sum_f F_{gf}^{n+1} + \frac{\Delta V_p}{\vartheta_g^{n+1} \rho_g^{n+1}} A^n \quad (3.18) \end{aligned}$$

In the equations 3.14 through 3.16, $m = n + 1$ for a fully implicit method and $m = n$ for a semi-implicit method. In the above equations, ΔV_p is the volume of the Finite Volume cell, u_g, v_g, w_g are the components of the gas phase velocity, u_d, v_d, w_d are the components of the droplet phase velocity, g_x, g_y, g_z are the components of acceleration due to gravity in X, Y, and Z directions respectively, $A^n \equiv n^n \dot{m}_v^n$ and

$$F_{gf} \equiv \mathbf{u}_{gf} \cdot \mathbf{S}_f$$

is the volume flux for the fluid phase, whereas

$$F_{d\phi f} \equiv -\mu \nabla \phi_{gf} \cdot \mathbf{S}_f; \quad F_{dTf} \equiv -k_{gf} \nabla T_{gf} \cdot \mathbf{S}_f$$

and

$$F_{dYf} \equiv -(\rho_g D) \nabla Y_F \cdot \mathbf{S}_f$$

are the diffusion flux for the fluid (where $\phi = u, v, w$), diffusion flux for temperature and mass fraction respectively. Note that in the energy equation the value of C_{pg} is lagged by one time step.

3.7.2 Droplet-Phase

The discretized equations for the droplet phase are

Continuity:

The discretized form of Eqn. (2.27) is

$$\Delta V_p \left(\frac{\Theta_d^{n+1} - \Theta_d^n}{\Delta t} \right) + \sum_f \Theta_{df}^{n+1} F_{df}^{n+1} = -\frac{\Delta V_p}{\rho_d \vartheta_0} A^n \quad (3.19)$$

Momentum:

The discretized form of Eqn. (2.31) is

$$\begin{aligned} \Delta V_p \frac{u_d^{n+1} - u_d^n}{\Delta t} + \sum_f u_{df}^m F_{df}^m &= -\frac{1}{\rho_d^n} \sum_f P_f^{n+1} S_{fx} + \Delta V_p g_x \\ &+ \frac{\Delta V_p}{\rho_d^n} f_{dx}^n + u_d^n \sum_f F_{df}^m \end{aligned} \quad (3.20)$$

$$\begin{aligned} \Delta V_p \frac{v_d^{n+1} - v_d^n}{\Delta t} + \sum_f v_{df}^m F_{df}^m &= -\frac{1}{\rho_d^n} \sum_f P_f^{n+1} S_{fy} + \Delta V_p g_y \\ &+ \frac{\Delta V_p}{\rho_d^n} f_{dy}^n + v_d^n \sum_f F_{df}^m \end{aligned} \quad (3.21)$$

$$\begin{aligned} \Delta V_p \frac{w_d^{n+1} - w_d^n}{\Delta t} + \sum_f w_{df}^m F_{df}^m &= -\frac{1}{\rho_d^n} \sum_f P_f^{n+1} S_{fz} + \Delta V_p g_z \\ &+ \frac{\Delta V_p}{\rho_d^n} f_{dz}^n + w_d^n \sum_f F_{df}^m \end{aligned} \quad (3.22)$$

In the equations 3.20 through 3.22, $m = n + 1$ for a fully implicit method and $m = n$ for a semi-implicit method.

$$F_{df} \equiv \mathbf{u}_{df} \cdot \mathbf{S}_f$$

is the convective flux for the droplet phase.

Energy:

The discretized form of Eqn. (2.33) is

$$\begin{aligned} \Delta V_p C_{ld} \frac{T_d^{n+1} - T_d^n}{\Delta t} + C_{ld} \sum_f T_{gf}^{n+1} F_{df}^{n+1} = \frac{\Delta V_p}{\rho_d \vartheta_d^{n+1}} (n^n Q^n - A^n L) \\ + C_{ld} T_d^n \sum_f F_{df}^{n+1} \end{aligned} \quad (3.23)$$

3.8 The Solution Algorithm

We use a time-accurate time stepping method to solve the equations. The total evaporation rate per unit volume is represented by the parameter A and is given by

$$A^n = n^n \dot{m}_v^n \quad (3.24)$$

where, \dot{m}_v is the rate of evaporation for a single droplet and has to be found from the evaporation model as described earlier. The number density of droplets per unit volume, n , is found for each cell by using the previous time step values of ϑ_d and d_d as

$$n^n = \frac{6 \vartheta_d^n}{\pi d_d^{3^n}} \quad (3.25)$$

The diameter of the droplets are updated by using the previous time-step's normalized volume fraction values as follows,

$$d_d = d_0 (\Theta_d^n)^{1/3} \quad (3.26)$$

We then calculate the source term due to drag by calculating C_d and β for each cell and storing the final drag value \mathbf{f}_d^n .

We use a fully implicit scheme for solving the momentum equations for the gas phase. Hence the discretized momentum equations become

$$\begin{aligned} \Delta V_p \frac{u_g^{n+1} - u_g^n}{\Delta t} + \sum_f u_{gf}^{n+1} F_{gf}^{n+1} + \frac{1}{\rho_g^n} \sum_f F_{duf}^{n+1} + C_v \frac{\Delta V_p}{\vartheta_g^n \rho_g^n} A^n u_g^{n+1} = \\ -\frac{1}{\rho_g^n} \sum_f P_f^{n+1} S_{fx} + \Delta V_p g_x \\ + C_v \frac{\Delta V_p}{\vartheta_g^n \rho_g^n} (A^n u_d^n - \vartheta_d^n f_{dx}^n) + u_g^n \sum_f F_{gf}^{n+1} \end{aligned} \quad (3.27)$$

$$\begin{aligned} \Delta V_p \frac{v_g^{n+1} - v_g^n}{\Delta t} + \sum_f v_{gf}^{n+1} F_{gf}^{n+1} + \frac{1}{\rho_g^n} \sum_f F_{dvf}^{n+1} + C_v \frac{\Delta V_p}{\vartheta_g^n \rho_g^n} A^n v_g^{n+1} = \\ -\frac{1}{\rho_g^n} \sum_f P_f^{n+1} S_{fy} + \Delta V_p g_y \\ + C_v \frac{\Delta V_p}{\vartheta_g^n \rho_g^n} (A^n v_d^n - \vartheta_d^n f_{dy}^n) + v_g^n \sum_f F_{gf}^{n+1} \end{aligned} \quad (3.28)$$

$$\begin{aligned} \Delta V_p \frac{w_g^{n+1} - w_g^n}{\Delta t} + \sum_f w_{gf}^{n+1} F_{gf}^{n+1} + \frac{1}{\rho_g^n} \sum_f F_{dwf}^{n+1} + C_v \frac{\Delta V_p}{\vartheta_g^n \rho_g^n} A^n w_g^{n+1} = \\ -\frac{1}{\rho_g^n} \sum_f P_f^{n+1} S_{fz} + \Delta V_p g_z \\ + C_v \frac{\Delta V_p}{\vartheta_g^n \rho_g^n} (A^n w_d^n - \vartheta_d^n f_{dz}^n) + w_g^n \sum_f F_{gf}^{n+1} \end{aligned} \quad (3.29)$$

We follow a two-step procedure to obtain the gas phase velocity components. The first step has two major loops - an inner loop (*) and an outer loop (**). In the inner loop, we first ignore the pressure completely and solve the Eqns.(3.30) through (3.32) for the so-called ‘‘mass’’ velocities u_g^* , v_g^* and w_g^* . The equations for mass velocity are

$$\begin{aligned} \Delta V_p \frac{u_g^* - u_g^n}{\Delta t} + \sum_f u_{gf}^* F_{gf}^{**} + \frac{1}{\rho_g^n} \sum_f F_{duf}^* + C_v \frac{\Delta V_p}{\vartheta_g^n \rho_g^n} A^n u_g^* = \\ \Delta V_p g_x + C_v \frac{\Delta V_p}{\vartheta_g^n \rho_g^n} (A^n u_d^n - \vartheta_d^n f_{dx}^n) \\ + u_g^n \sum_f F_{gf}^{**} \end{aligned} \quad (3.30)$$

$$\begin{aligned} \Delta V_p \frac{v_g^* - v_g^n}{\Delta t} + \sum_f v_{gf}^* F_{gf}^{**} + \frac{1}{\rho_g^n} \sum_f F_{dvf}^* + C_v \frac{\Delta V_p}{\vartheta_g^n \rho_g^n} A^n v_g^* = \\ \Delta V_p g_y + C_v \frac{\Delta V_p}{\vartheta_g^n \rho_g^n} (A^n v_d^n - \vartheta_d^n f_{dy}^n) \\ + v_g^n \sum_f F_{gf}^{**} \end{aligned} \quad (3.31)$$

$$\begin{aligned} \Delta V_p \frac{w_g^* - w_g^n}{\Delta t} + \sum_f w_{gf}^* F_{gf}^{**} + \frac{1}{\rho_g^n} \sum_f F_{dwf}^* + C_v \frac{\Delta V_p}{\vartheta_g^n \rho_g^n} A^n w_g^* = \\ \Delta V_p g_z + C_v \frac{\Delta V_p}{\vartheta_g^n \rho_g^n} (A^n w_d^n - \vartheta_d^n f_{dz}^n) \\ + w_g^n \sum_f F_{gf}^{**} \end{aligned} \quad (3.32)$$

Eqns. (3.30) through (3.32) are iterated to convergence within the inner loop ¹. We use a superscript * for the diffusion term because the diffusion terms are calculated in terms of the mass velocities as they are being iterated in the inner loop. The superscript ** used in the convective flux F_{gf} which is evaluated in the outer loop of the first step, and is kept unchanged during the inner loop (*) iterations ².

We then follow the same procedure for the momentum equations of the droplet phase. Hence, we have the fully-implicit discretized momentum equations as

$$\begin{aligned} \Delta V_p \frac{u_d^{n+1} - u_d^n}{\Delta t} + \sum_f u_{df}^{n+1} F_{df}^{n+1} = -\frac{1}{\rho_d^n} \sum_f P_f^{n+1} S_{fx} + \Delta V_p g_x \\ + \frac{\Delta V_p}{\rho_d^n} f_{dx}^n + u_d^n \sum_f F_{df}^{n+1} \end{aligned} \quad (3.33)$$

$$\begin{aligned} \Delta V_p \frac{v_d^{n+1} - v_d^n}{\Delta t} + \sum_f v_{df}^{n+1} F_{df}^{n+1} = -\frac{1}{\rho_d^n} \sum_f P_f^{n+1} S_{fy} + \Delta V_p g_y \\ + \frac{\Delta V_p}{\rho_d^n} f_{dy}^n + v_d^n \sum_f F_{df}^{n+1} \end{aligned} \quad (3.34)$$

¹Actually, Eqns.(3.30) through (3.32) are calculated in three separate subloops within the inner loop.

²A single * indicated quantities that are computed using the inner loop of the first step, whereas the ** indicates quantities calculated in the outer loop.

$$\begin{aligned} \Delta V_p \frac{w_d^{n+1} - w_d^n}{\Delta t} + \sum_f w_{df}^{n+1} F_{df}^{n+1} &= -\frac{1}{\rho_d^n} \sum_f P_f^{n+1} S_{fz} + \Delta V_p g_z \\ &+ \frac{\Delta V_p}{\rho_d^n} f_{dz}^n + w_d^n \sum_f F_{df}^{n+1} \end{aligned} \quad (3.35)$$

The discretized equations for droplet “mass” velocities is as follow

$$\begin{aligned} \Delta V_p \frac{u_d^* - u_d^n}{\Delta t} + \sum_f u_{df}^* F_{df}^{**} &= \Delta V_p g_x \\ &+ \frac{\Delta V_p}{\rho_d^n} f_{dx}^n + u_d^n \sum_f F_{df}^{**} \end{aligned} \quad (3.36)$$

$$\begin{aligned} \Delta V_p \frac{v_d^* - v_d^n}{\Delta t} + \sum_f v_{df}^* F_{df}^{**} &= \Delta V_p g_y \\ &+ \frac{\Delta V_p}{\rho_d^n} f_{dy}^n + v_d^n \sum_f F_{df}^{**} \end{aligned} \quad (3.37)$$

$$\begin{aligned} \Delta V_p \frac{w_d^* - w_d^n}{\Delta t} + \sum_f w_{df}^* F_{df}^{**} &= \Delta V_p g_z \\ &+ \frac{\Delta V_p}{\rho_d^n} f_{dz}^n + w_d^n \sum_f F_{df}^{**} \end{aligned} \quad (3.38)$$

Eqns. (3.36) through (3.38) too are iterated to convergence in three separate sub-loops in the inner loop of the first step. During any pass through the droplet “mass” velocity loop, we hold the convective fluxes F_{df}^{**} fixed and iterate for the mass velocities. Once the gas and droplet “mass” velocities are obtained, we update the pressure and the fluxes in the outer loop and return to the inner loop and use the updated fluxes for the next pass. This continues until the fluxes F_{gf}^{**} and F_{df}^{**} converge in the outer loop, and henceforth, are taken as the final values, F_{gf}^{n+1} and F_{df}^{n+1} .

We now look into the outer loop calculations. Having obtained the tentative mass velocities we turn to the pressure Poisson equation. This is derived from the total mass conservation principle. By adding Eqn.(2.2) and Eqn.(2.10), we get

$$\frac{\partial \vartheta_g \rho_g}{\partial t} + \nabla \cdot (\vartheta_g \rho_g \mathbf{u}_g) + \frac{\partial \vartheta_d \rho_d}{\partial t} + \nabla \cdot (\vartheta_d \rho_d \mathbf{u}_d) = 0 \quad (3.39)$$

For steady state problems, the temporal derivative tends to zero. Hence, we can simplify Eqn.(3.39) as,

$$\nabla \cdot (\vartheta_g \rho_g \mathbf{u}_g) + \nabla \cdot (\vartheta_d \rho_d \mathbf{u}_d) = 0 \quad (3.40)$$

which is the continuity equation that should be applied at the (n+1)th time level. So, we get

$$\nabla \cdot (\vartheta_g \rho_g \mathbf{u}_g)^{n+1} + \nabla \cdot (\vartheta_d \rho_d \mathbf{u}_d)^{n+1} = 0 \quad (3.41)$$

By subtracting Eqn. (3.30) from Eqn. (3.27), Eqn. (3.31) from Eqn.(3.28) and Eqn. (3.32) from Eqn. (3.29)we get

$$\mathbf{u}_g^{n+1} - \mathbf{u}_g^* = -\frac{\Delta t}{\rho_g} \nabla P \quad (3.42)$$

Similar conclusion can be made for droplet phase as,

$$\mathbf{u}_d^{n+1} - \mathbf{u}_d^* = -\frac{\Delta t}{\rho_d} \nabla P \quad (3.43)$$

By multiplying Eqn.(3.42) and Eqn.(3.43) by $\rho_g \vartheta_g$ and $\rho_d \vartheta_d$ respectively and substituting in Eqn.(3.41), we get

$$\Delta t \nabla^2 P = \nabla \cdot (\vartheta_g \rho_g \mathbf{u}_g^*) + \nabla \cdot (\vartheta_d \rho_d \mathbf{u}_d^*) \quad (3.44)$$

In the above equation, we have used the principle $\vartheta_g + \vartheta_d = 1$. Discretization of Eqn.(3.44) leads to

$$\sum_f \nabla P_f^{**} \cdot \mathbf{S}_f = \frac{1}{\Delta t} \sum_f \rho_g^n \vartheta_g^n \mathbf{u}_{gf}^* \cdot \mathbf{S}_f + \frac{1}{\Delta t} \sum_f \rho_d^n \vartheta_d^n \mathbf{u}_{df}^* \cdot \mathbf{S}_f \quad (3.45)$$

We can define the fluxes on the R.H.S of Eqn. (3.45) as

$$F_{Mgf}^{**} [= (\vartheta_{gf}^n \rho_{gf}^n \mathbf{u}_{gf}^*) \cdot \mathbf{S}_f] = (\vartheta_{gf}^n \rho_{gf}^n) F_{gf}^{**} \quad (3.46)$$

$$F_{Mdf}^{**} [= (\vartheta_{df}^n \rho_{df}^n \mathbf{u}_{df}^*) \cdot \mathbf{S}_f] = (\vartheta_{df}^n \rho_{df}^n) F_{df}^{**} \quad (3.47)$$

Here the values of u_{gi}^* and u_{di}^* at the cell faces is obtained by a volume interpolation. The superscript ** is used for pressure because Eqn. (3.45) is now iterated to convergence in the outer loop of step one.

Having obtained the pressure field P^{**} from Eqn.(3.45) we update the fluxes F_{gf} and F_{df} using momentum interpolation

$$F_{gf}^{**} = \mathbf{u}_{gf}^* \cdot \mathbf{S}_f - \left(\frac{\Delta t}{\rho_g^n} \right) \nabla P_f^{**} \cdot \mathbf{S}_f \quad (3.48)$$

$$F_{df}^{**} = \mathbf{u}_{df}^* \cdot \mathbf{S}_f - \left(\frac{\Delta t}{\rho_d^n} \right) \nabla P_f^{**} \cdot \mathbf{S}_f \quad (3.49)$$

After updating the fluxes F_{gf}^{**} and F_{df}^{**} in the outer loop, we once again solve the inner loop for the “mass” velocities, followed by the pressure and update the fluxes. This cycle continues until the values of fluxes converge. At that point we accept that $F_{gf}^{n+1} = F_{gf}^{**}$, $F_{df}^{n+1} = F_{df}^{**}$ and $P^{n+1} = P^{**}$. We now iterate the full momentum Eqns.(3.27) through (3.29) and Eqns.(3.33) through (3.35) to convergence. This last part comprises step two of the two-step algorithm. We now have the \mathbf{u}_g^{n+1} and \mathbf{u}_d^{n+1} values.

Also in the second step, we next iterate to convergence the continuity equation of the droplet phase to obtain the normalized volume fraction using F_{df}^{n+1} obtained from the converged \mathbf{u}_{df}^{n+1} .

$$\Delta V_p \left(\frac{\Theta_d^{n+1} - \Theta_d^n}{\Delta t} \right) + \sum_f \Theta_{df}^{n+1} F_{df}^{n+1} = -C_v \frac{\Delta V_p}{\rho_d \vartheta_0} A^n \quad (3.50)$$

We next solve the continuity equation of gas phase for density using F_{gf}^{n+1} obtained from the converged \mathbf{u}_{gf}^{n+1} . The discretized form is iterated to convergence.

$$\Delta V_p \frac{\rho_g^{n+1} - \rho_g^n}{\Delta t} + \sum_f \rho_{gf}^{n+1} F_{gf}^{n+1} = C_v \frac{1}{(1 - \vartheta_d^{n+1})} \Delta V_p (n \dot{m}_v)^n \quad (3.51)$$

Next, we solve the droplet temperature equation by iterating

$$\begin{aligned} \Delta V_p C_{ld} \frac{T_d^{n+1} - T_d^n}{\Delta t} + C_{ld} \sum_f T_{df}^{n+1} F_{df}^{n+1} &= C_v \frac{\Delta V_p}{\rho_d \vartheta_d^{n+1}} (n^n Q^n - A^n L) \\ &+ C_{ld} T_d^n \sum_f F_{df}^{n+1} \end{aligned} \quad (3.52)$$

to convergence. We then solve the mass fraction equation and the energy equation of the gas phase.

$$\begin{aligned} \Delta V_p \frac{Y_F^{n+1} - Y_F^n}{\Delta t} + \sum_f Y_F^{n+1} F_{gf}^{n+1} + \frac{1}{\rho_g^{n+1}} \sum_f F_{dYf}^{n+1} \\ + C_v \frac{\Delta V_p}{\vartheta_g^{n+1} \rho_g^{n+1}} A^n Y_F^{n+1} = +Y_F^n \sum_f F_{gf}^{n+1} + C_v \frac{\Delta V_p}{\vartheta_g^{n+1} \rho_g^{n+1}} A^n \end{aligned} \quad (3.53)$$

$$\begin{aligned} \Delta V_p C_{pg} \frac{T_g^{n+1} - T_g^n}{\Delta t} + \sum_f C_{pgf} T_{gf}^{n+1} F_{gf}^{n+1} + \frac{1}{\rho_g^{n+1}} \sum_f F_{dTf}^{n+1} + \\ C_v \frac{\Delta V_p}{\vartheta_g^{n+1} \rho_g^{n+1}} A^n C_{vd} T_g^{n+1} = C_v \frac{\Delta V_p}{\vartheta_g^{n+1} \rho_g^{n+1}} A^n C_{vd} T_d^{n+1} \\ - C_v \frac{\Delta V_p}{\vartheta_g^{n+1} \rho_g^{n+1}} n^n Q^n + C_{pg} T_g^n \sum_f F_{gf}^{n+1} \end{aligned} \quad (3.54)$$

Note that the previous time step source term values are used in all the equations. The above steps are sequentially carried out at each time step. For all the equations of the droplet phase the convective terms are discretized by the first-order upwind scheme. This is specially helpful in avoiding negative or un-physical values of the volume fraction, however the inherent dissipation effects of the scheme reduces the sharp gradients in the solution.

3.9 Summary of the Algorithm

1. Initialize properties and fields for the carrier phase and the droplet phase, grids and other parameters.
2. Transfer $(n + 1)^{th}$ time level values to n^{th} time level for all the solvable variables as volume fraction, velocity, density, temperature for the gas phase and droplet phase, fuel mass fraction and pressure.
3. Compute and store all the source terms with the previous time step values. Compute and store diameter d_d by using the following relation:

$$d_d = d_0(\Theta_d)^{1/3}$$

4. Solve for the “mass” velocity for the gas phase and droplet phase separately by iterating Eqns.(3.30) through (3.32) and (3.36) through (3.38) respectively with previous time step source term values.
5. Compute momentum fluxes, F_{Mgf}^{**} and F_{Mdf}^{**} using Eqn.(3.46) and Eqn.(3.47).
6. Solve for the pressure P^{**} by iterating Eqn. (3.45) to convergence.
7. Compute volume fluxes F_{gf}^{**} and F_{df}^{**} using Eqns. (3.48) and (3.49).
8. Repeat steps 4 to 7 until the fluxes, F_{gf}^{**} and F_{df}^{**} converge.
9. Accept $P^{n+1} = P^{**}$, $F_{gf}^{n+1} = F_{gf}^{**}$ and $F_{df}^{n+1} = F_{df}^{**}$
10. Iterate the full momentum equations for gas phase Eqns.(3.27) through (3.29) and full momentum equations for droplet phase (3.33) through (3.35) to convergence separately to obtain \mathbf{u}_g^{n+1} and \mathbf{u}_d^{n+1} , respectively.

11. Solve the continuity equation of droplet phase Eqn.(3.50) for normalized volume fraction of droplet, Θ_d^{n+1} . The volume fraction of the droplet phase is found using the relation $\vartheta_d = \vartheta_0 * \Theta_d$. Volume fraction of gas phase is obtained by using the relation $\vartheta_g = 1 - \vartheta_d$.
12. Solve the continuity equation of gas Eqn.(3.51) for obtaining gas phase density, ρ_g^{n+1} .
13. Solve the energy equation for the droplet phase Eqn.(3.52) for droplet temperature T_d^{n+1} .
14. Solve the evaporated fuel vapour mass fraction Eqn.(3.53) to obtain Y_F^{n+1} .
15. Solve the gas-phase energy Eqn.(3.54) to obtain T_g^{n+1} .
16. If the stopping criterion for the time stepping is not met return to step 2 and repeat steps 2 through 15 for the next time step and march forward in time.

3.10 Implementation of the Algorithm

The following limiters have been implemented for the algorithm to give converged solution for smaller particle/droplet diameters.

3.10.1 Limiter for Θ_d equation

If for a cell $\Theta_d^n < \epsilon$ ($\sim 1e - 4$) we put $A^n = 0$ and $C_v = 0$. Otherwise, put $C_v = 1$ and compute and store A using n^{th} level variable values by the aforementioned relationship. The value of ϵ implies that we are not allowing the diameter of the droplet to fall below a certain value which depends on the droplet initial diameter and volume fraction. The value of C_v used in the equations becomes zero when the diameter of the droplet reaches this particular value. When $C_v = 0$, all the inter-phase mass, momentum and energy transfer terms go to zero resulting in only the convection of the smallest droplets by the gas.

3.10.2 Enforcing gas-phase and droplet-phase velocity equality

When very small particles/droplets are released in a moving gas stream, they acquire the velocity of the carrier-phase in a matter of few milli-seconds. We enforce this condition when the volume fraction of the droplet phase reduces to such a small value that the droplet diameter is only a few microns. Therefore, for a cell if $\Theta_d^n < \epsilon$ then we put $\mathbf{u}_d^n = \mathbf{u}_g^n$. This also enforces the condition that drag force, $\mathbf{f}_d^n = 0$ in those cells.

3.10.3 Enforcing T_d is constant after heat-up period

Once the temperature of the droplet reaches the saturation temperature (wet-bulb temperature), the heat provided to the droplet from the gas phase is utilized completely in providing the heat of vaporization. In other words, $\dot{Q} = \dot{Q}_e$ making the source term in Eqn.(2.13) zero. But, in actual numerical implementation, it is seen that there is a small difference in \dot{Q} and \dot{Q}_e , and Eqn.(2.13), the term $n\dot{Q} - n\dot{Q}_e$ is magnified by being divided by $\vartheta_d\rho_d$. This leads to convergence problems for the T_d equation. In order to overcome this problem, the source term in Eqn.(2.13) is made zero as soon as T_d reaches the saturation temperature. We check whether saturation temperature has reached by checking if $B_M - B_T \leq 0.0001$. If so, we enforce $\dot{Q} - \dot{Q}_e = 0$.

Chapter 4

Results and Discussion

In this chapter, we attempt a new problem of parametrising the evaporation length for droplets of n-heptane with initial diameter in the range 100-200 microns with initial temperature at either saturation (371.4K) or room temperature(300 K). The problem is non-dimensionlized and there are three relevent non-dimensional parameters: the gas Reynolds number Re_g , the droplet Reynolds number Re_d and the Jacob number Ja , which is the ratio of sensible to latent heat and which governs the thermodynamics of phase change. The results of this study would be relevent to engineeing practice in that it gives the distance of evaporation of the droplet under the given conditions.

However, not all parameters of the practical problems can be simulated by numerical computations. The gas Reynolds number in most practical problems will be very high ($> 10^5$) and so in the turbulent range. The current code is not capable of turbulent simulations. The starategy used in this thesis is as follows : we simulate the correct droplet Reynolds number and Jacob number, but use a low dummy value (=100) for gas Reynolds number. The argument in favor of this strategy is as follws : Re_d and Ja are the most important parameters, the first determines the convection coefficient of the evaporation and the second influences the thermodynamics involved. Re_g on the other hand determines mainly the laminar-turbulent transition. Given that the code cannot do turbulent calculation, the current simulations can be taken as laminar approximations of the full turbulent problem.

4.1 Gas-Droplet Flow Through 2-D Channel

Having validated the flow gas-droplet flow solver against basic cases and the evaporation model against available literature, we now attempt to solve few complete problems

of gas-droplet two-phase flows with evaporation. We consider different problems of gas droplet flows varying only in boundary conditions and deal with n-heptane liquid droplets moving in air in a channel having uniform velocity profiles at inlet for the gas-phase as well as for the droplet-phase. Each case has four problems, which are as follows:

Non Dimensionalized conditions				
Gas-phase inlet velocity, u_{gi}	1.0	2.0	2.0	1.0
Droplet-phase inlet velocity, u_{di}	1.0	2.0	1.0	2.0

Here we have two type of problems: For the first case, the inlet temperature of the droplets is taken to be at room temperature, and in the second case, the droplet inlet temperature is assumed to be equal to the saturation temperature. The latter assumption simplifies the problem as we need not consider the transient liquid droplet heating and the droplet temperature remains at saturation temperature throughout its lifetime.

4.1.1 Computational Domain and Property Values

The domain considered for all the cases, except fourth problem of each case, is shown in the Figure 4.1, where $H = 0.1 m$ and $L = 0.5 m$. The domain for fourth problem has dimension as $H = 0.5 m$ and $L = 2 m$. Expressions for the variation of properties for liquid and vapour phase of n-heptane fuel are given in Appendix. The property values of gas-phase (air) and droplet phase (n-heptane) which are common for all the cases are shown in Table 4.1.

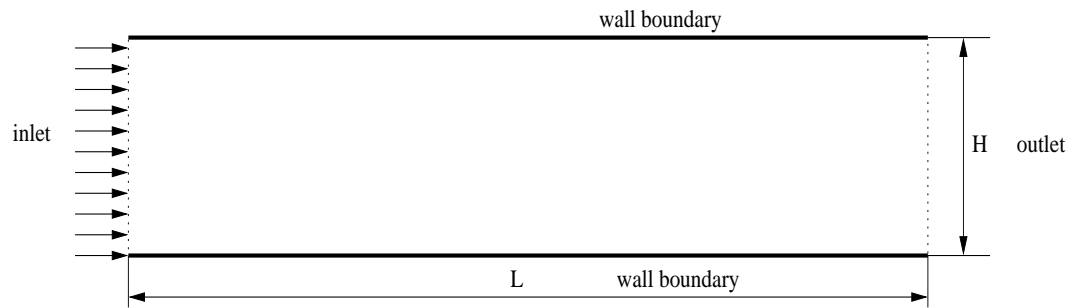


Figure 4.1: The Computational Domain for 2D-Channel Gas-Droplet Flow Problem

The variation of the droplet-phase volume fraction, droplet diameter and fuel mass fraction along the length of the channel is shown in Fig. 4.2 to Fig. 4.93. As expected

Table 4.1: Property values of fluids used

Property values	NonDimensionalized values	Actual values
Viscosity of gas(at $T = 500K$)	0.000125	$2.225 \times 10^{-5} \text{ N s/m}^2$
Liquid droplet density, ρ_d	1.0	684.0 kg/m^3
Specific heat of air, C_{pa}	1.0	1006.43 J/kg K
Specific heat of fuel vapour, C_{vd}	2.4553	2471.0 J/kg K
Specific heat of liquid droplet, C_{ld}	2.2048	2219.0 J/kg K
Thermal conductivity of air, k_a	1.0	0.0242 W/m K
Thermal conductivity of fuel vapour, k_v	0.5982	0.0128 W/m K
Latent heat of fuel, L		320096.0 J/kg
Mass diffusivity of vapour in gas, D		$2.26 \times 10^{-5} \text{ m}^2/\text{s}$

the gas-phase temperature drops off along the length of the channel due to heat transfer from the gas-phase to the droplets. Also the fuel mass fraction and the gas-phase density are seen to increase due to droplet evaporation.

4.1.2 Gas-droplet channel flow with dummy $Re = 100$ and $Ja = 3.071$

The inlet droplet non-dimensionalized temperature equal to 0 ($= 300K$). The non-dimensionalized saturation temperature of n-heptane, T_{sat} , is 0.16117 ($= 371.4 \text{ K}$) at atmospheric pressure. The inlet properties are given in Table. 4.2. At the wall, the homogeneous Neumann boundary condition is applied for gas-phase velocity. This condition means friction-less ('slip') walls (to avoid friction-work) and ensures a uniform flow profile in the channel. Since we have applied constant \mathbf{Ja} , therefore, we apply non-dimensionalized Dirichlet boundary condition of 1 ($= 773.0K$) at both the walls for droplet-phase temperature. Since, the droplet inlet temperature is lower than the saturation temperature, transient heating of the droplets takes place. The conditions are such that the droplets evaporate totally by the end of the channel.

It is also observed from the plots that evaporation length in second case is almost double compared to the first case as the residence time of droplets is less due to the increased speed, evaporation length in third case is almost similar to first case but

Table 4.2: Case 1: Inlet conditions

Inlet non dimensiontionalized conditions	
Gas-phase inlet temperature, T_{gi}	1(=773.0 K)
Droplet-phase inlet temperature, T_{di}	0(=300.0 K)
Inlet fuel mass fraction, M_{Fo}	0.0
Gas-phase inlet density, ρ_{gi}	1(=1.225 kg/m ³)
Droplet-phase inlet volume fraction, ϑ_{do}	0.0005
Droplet inlet diameter, d_{do}	200

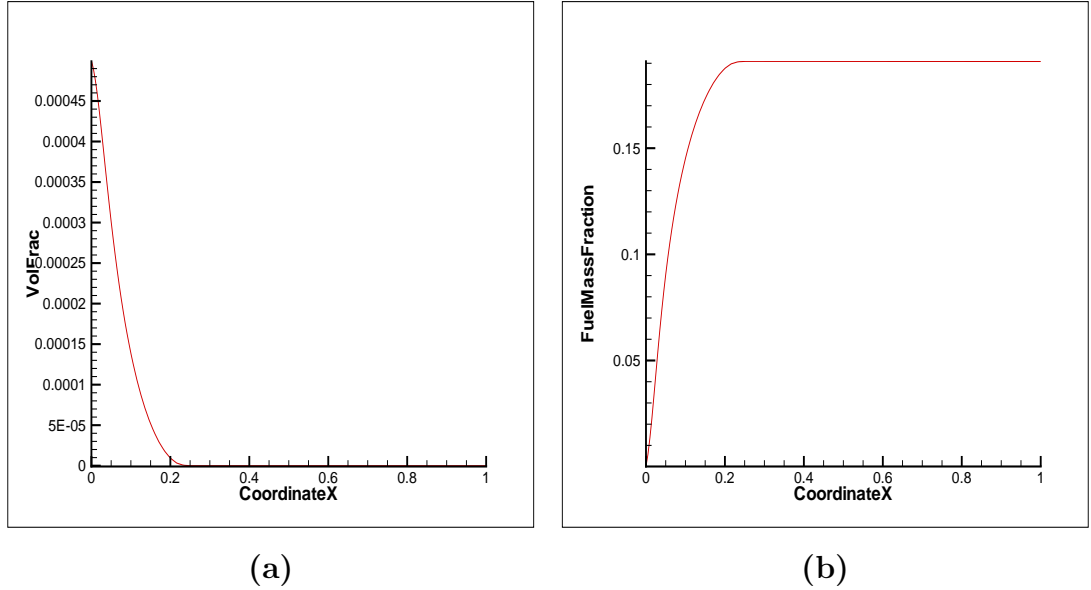


Figure 4.2: Case 1: Gas-droplet channel flow with $u_{gi} = 1.0$ and $u_{di} = 1.0$ (a) Variation of droplet-phase volume fraction, ϑ_d along the channel (b) Variation of evaporated fuel mass fraction, M_F along the channel

residence time of droplets is less and evaporation length is less and residence time of droplets in fourth case is more as compared to all above three cases.

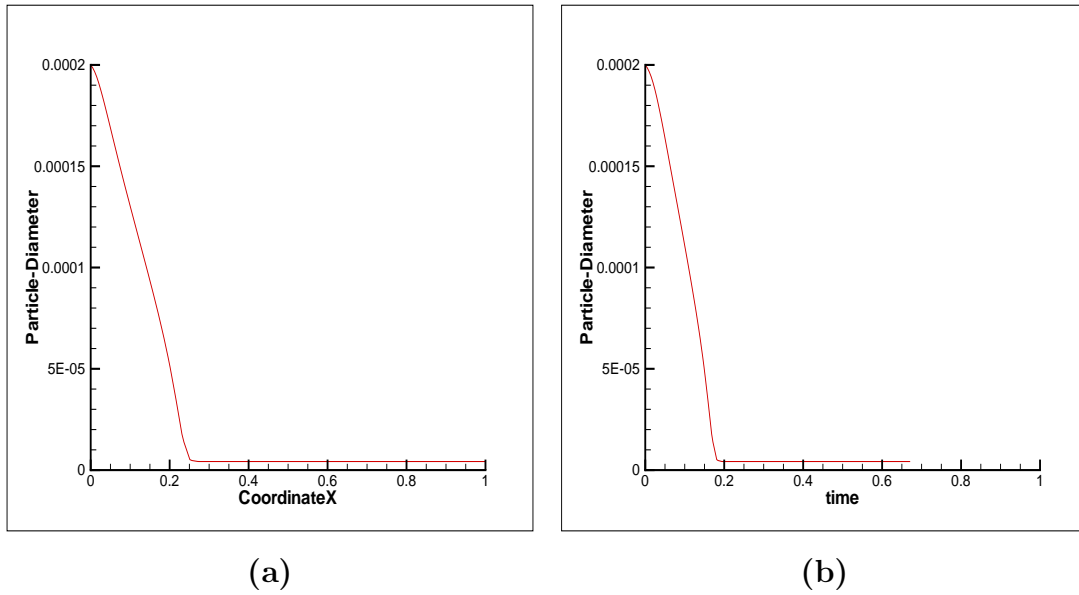


Figure 4.3: Case 1: Gas-droplet channel flow with $u_{gi} = 1.0$ and $u_{di} = 1.0$. (a) Variation of droplet-diameter, d_d along the channel (b) Variation of droplet-diameter, d_d , with time

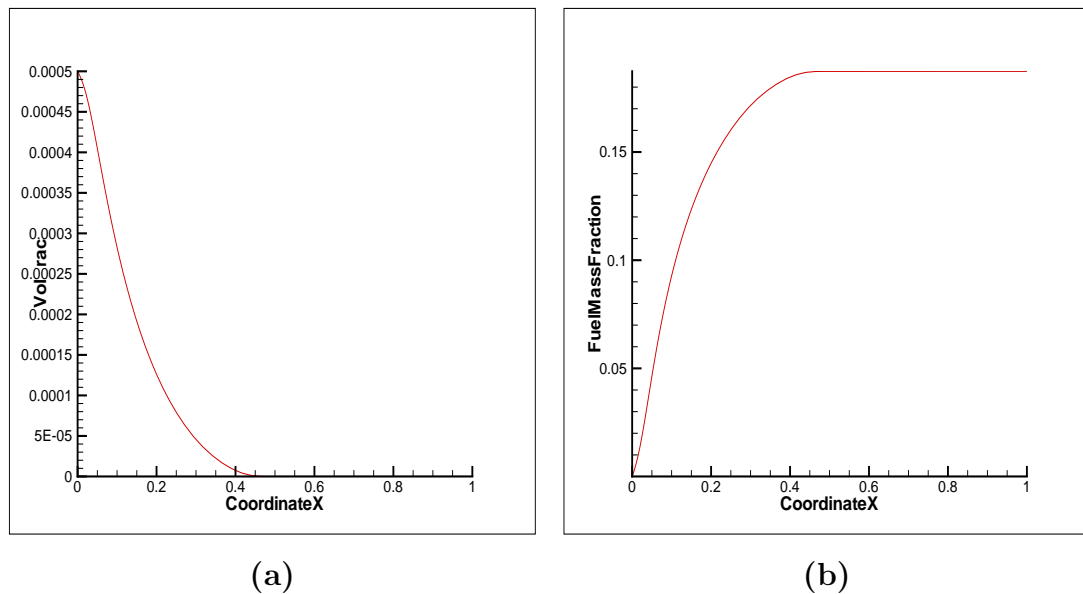


Figure 4.4: Case 1: Gas-droplet channel flow with $u_{gi} = 2.0$ and $u_{di} = 2.0$ (a) Variation of droplet-phase volume fraction, ϑ_d along the channel (b) Variation of evaporated fuel mass fraction, M_F along the channel

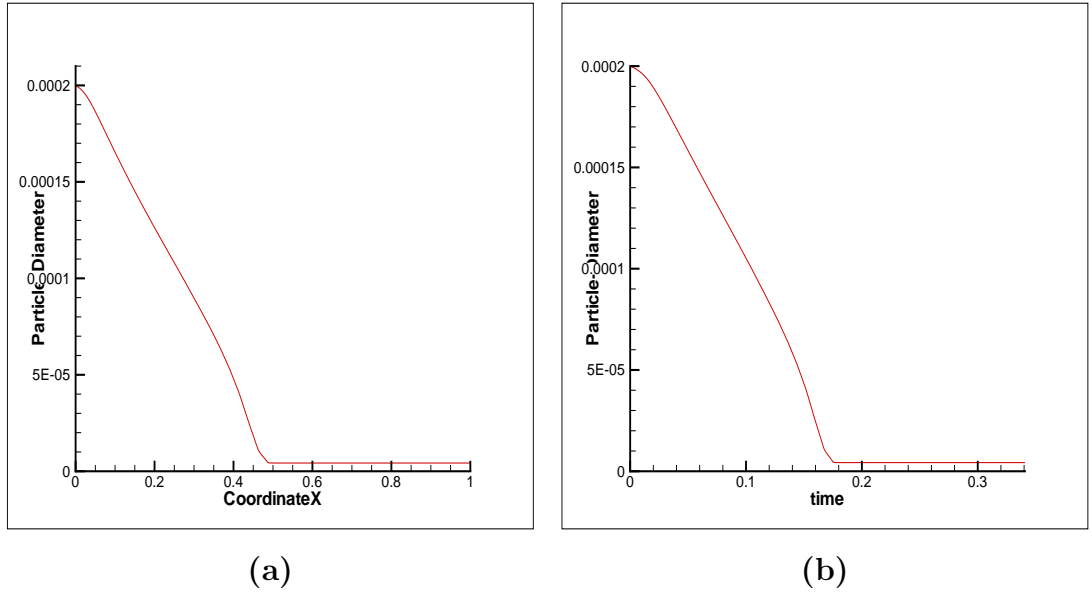


Figure 4.5: Case 1: Gas-droplet channel flow with $u_{gi} = 2.0$ and $u_{di} = 2.0$. (a) Variation of droplet-diameter, d_d along the channel (b) Variation of droplet-diameter, d_d , with time

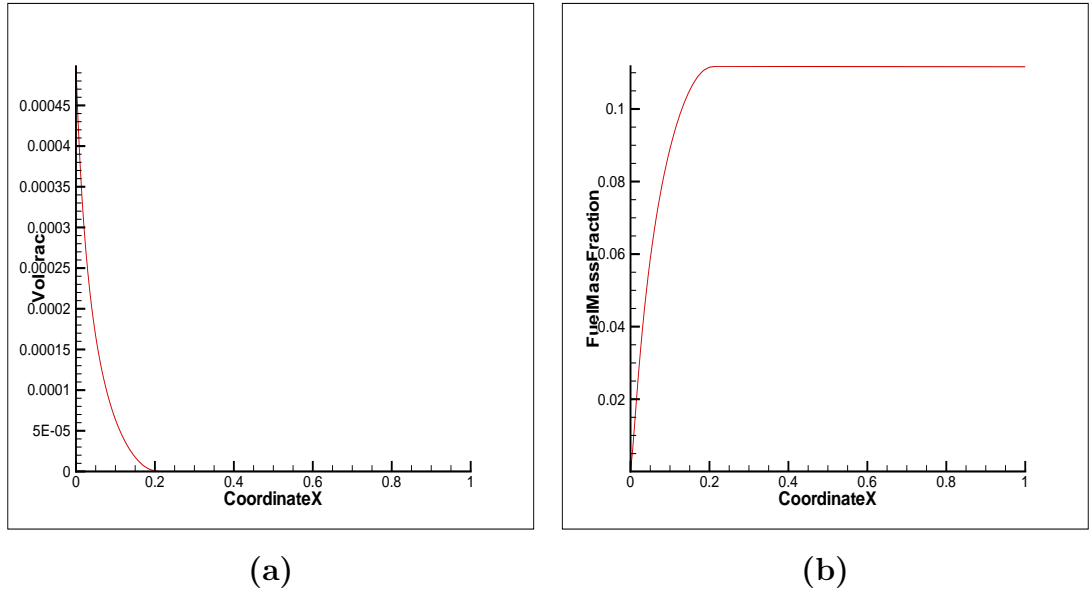


Figure 4.6: Case 1: Gas-droplet channel flow with $u_{gi} = 2.0$ and $u_{di} = 1.0$. (a) Variation of droplet-phase volume fraction, ϑ_d along the channel (b) Variation of evaporated fuel mass fraction, M_F along the channel

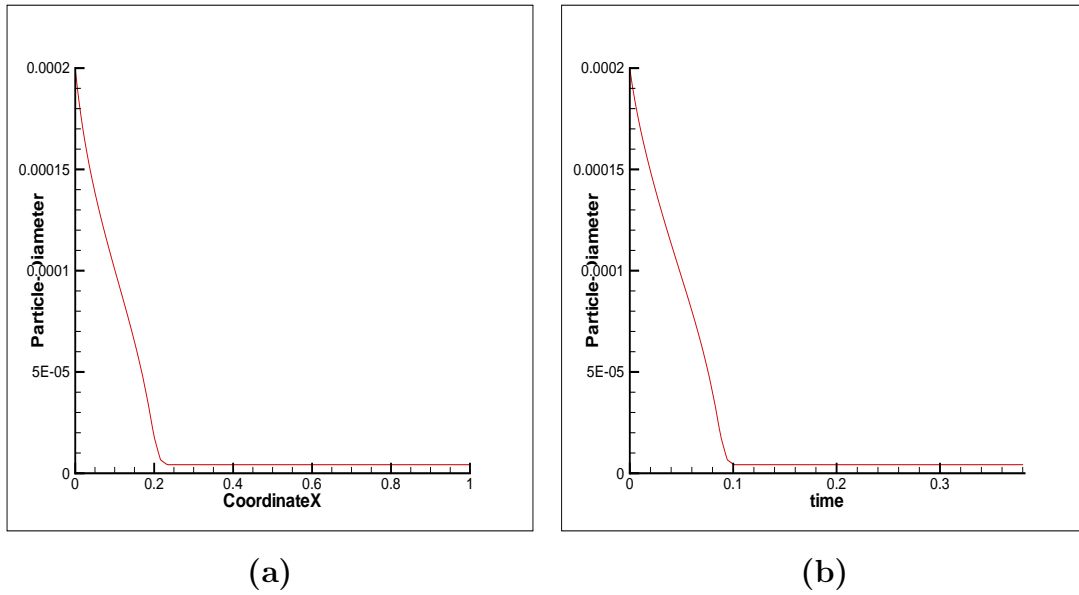


Figure 4.7: Case 1: Gas-droplet channel flow with $u_{gi} = 2.0$ and $u_{di} = 1.0$. (a) Variation of droplet-diameter, d_d along the channel (b) Variation of droplet-diameter, d_d , with time

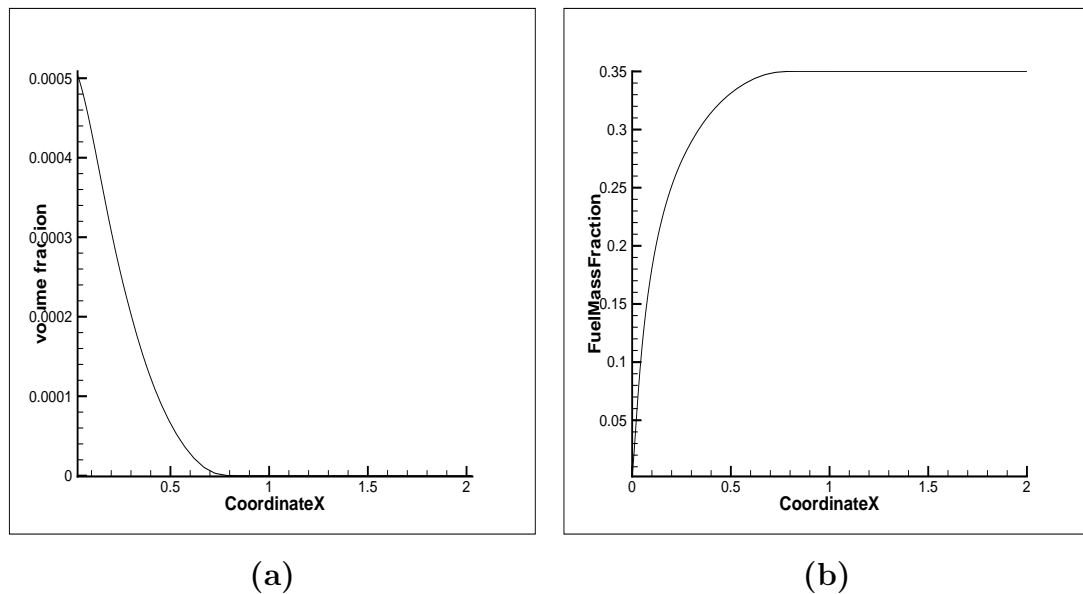


Figure 4.8: Case 1: Gas-droplet channel flow with $u_{gi} = 1.0$ and $u_{di} = 2.0$. (a) Variation of droplet-phase volume fraction, ϑ_d along the channel (b) Variation of evaporated fuel mass fraction, M_F along the channel

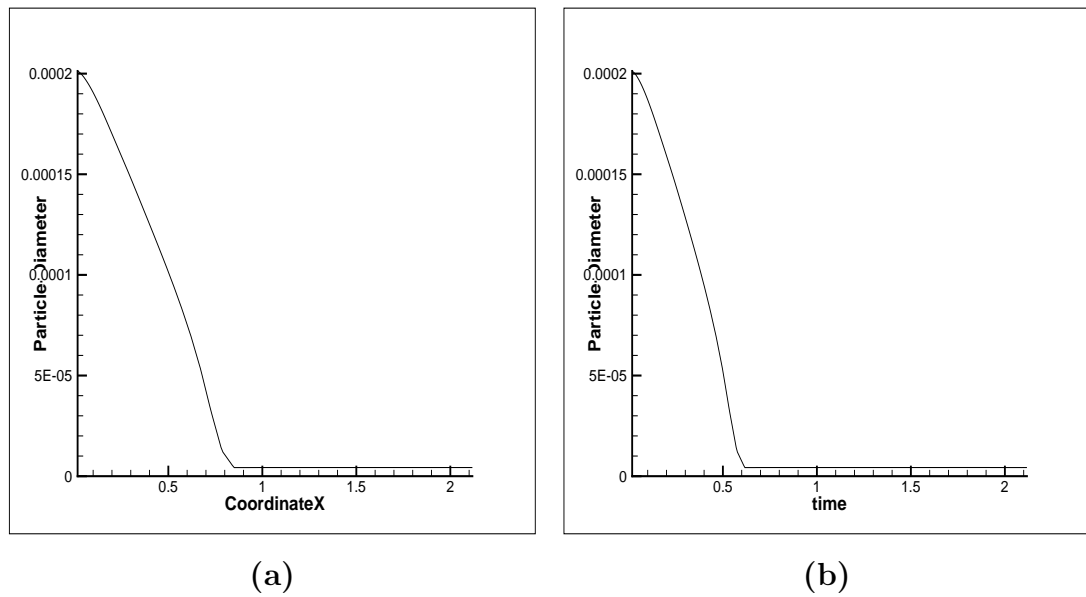


Figure 4.9: Case 1: Gas-droplet channel flow with $u_{gi} = 1.0$ and $u_{di} = 2.0$. (a) Variation of droplet-diameter, d_d along the channel (b) Variation of droplet-diameter, d_d , with time

4.1.3 Gas-droplet channel flow with dummy $Re = 100$ and $Ja = 2.784$

The inlet non-dimensionalized droplet temperature equal to 0 ($= 371.4\text{K}$). The non-dimensionalized saturation temperature of n-heptane, T_{sat} , is 0 ($= 371.4\text{ K}$) at atmospheric pressure. The inlet properties are given in Table. 4.3. At the wall, the homogeneous Neumann boundary condition is applied for gas-phase velocity and the gas-phase temperature. The latter condition means an insulated boundary condition is applied for temperature while the former implies friction-less ('slip') walls (to avoid friction-work) and ensures a uniform flow profile in the channel. Since we have applied constant \mathbf{Ja} , therefore, we apply non-dimensionalized Dirichlet boundary condition of 1 ($= 773.0\text{K}$) at both the walls for droplet-phase temperature. Since, the droplet inlet temperature is equal to the saturation temperature, no transient heating of the droplets takes place and the droplet temperature remains constant at its inlet value while the droplets evaporate due to heating. The conditions are such that the droplets evaporate totally by the end of the channel.

Table 4.3: Case 2: Inlet conditions

Inlet non dimensionlized conditions	
Gas-phase inlet temperature, T_{gi}	1($=773.0\text{ K}$)
Droplet-phase inlet temperature, T_{di}	0($=371.4\text{ K}$)
Inlet fuel mass fraction, M_{F_o}	0.0
Gas-phase inlet density, ρ_{gi}	1($=1.225\text{ kg}/\text{m}^3$)
Droplet-phase inlet volume fraction, ϑ_{do}	0.0005
Droplet inlet diameter, d_{do}	200

It is observed that evaporation length is less compared to previous case as the droplet inlet temperature is equal to the saturation temperature, no transient heating of the droplets is taking place.

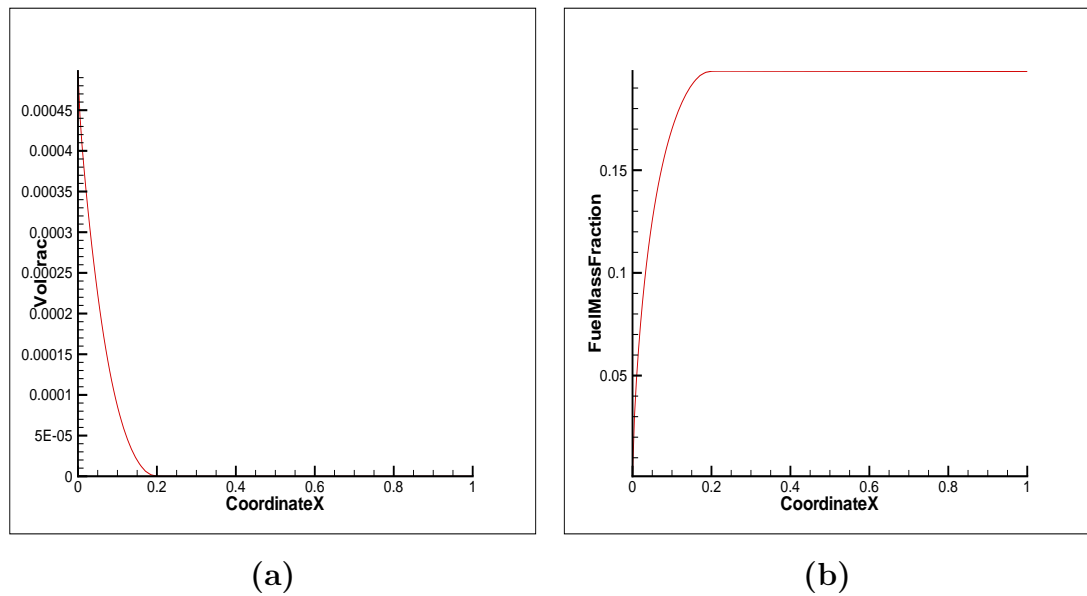


Figure 4.10: Case 2: Gas-droplet channel flow with $u_{gi} = 1.0$ and $u_{di} = 1.0$. (a) Variation of droplet-phase volume fraction, ϑ_d along the channel (b) Variation of evaporated fuel mass fraction, M_F along the channel

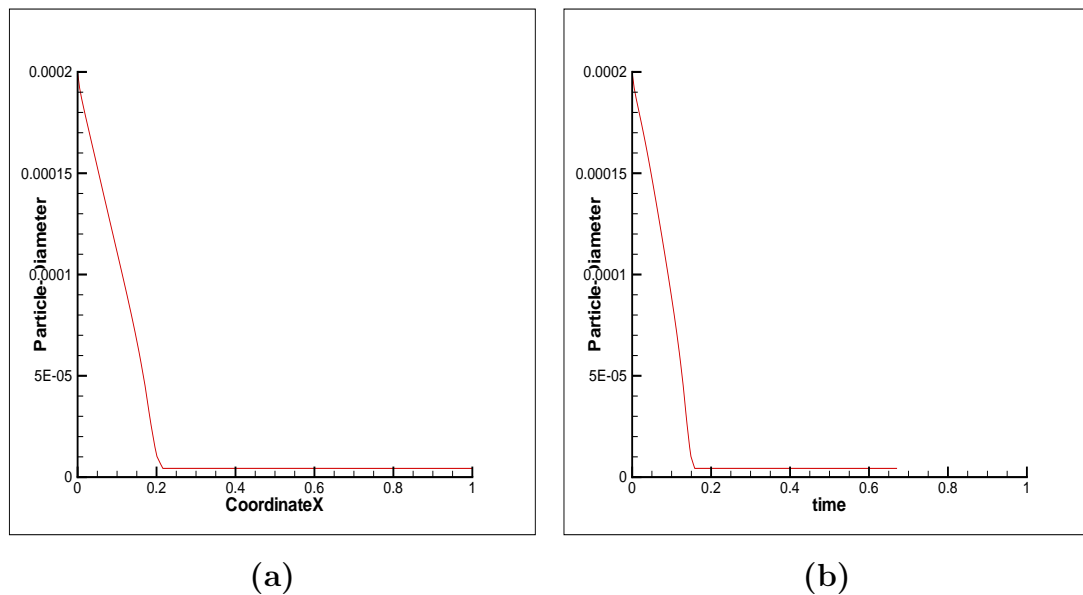


Figure 4.11: Case 2: Gas-droplet channel flow with $u_{gi} = 1.0$ and $u_{di} = 1.0$. (a) Variation of droplet-diameter, d_d along the channel (b) Variation of droplet-diameter, d_d , with time

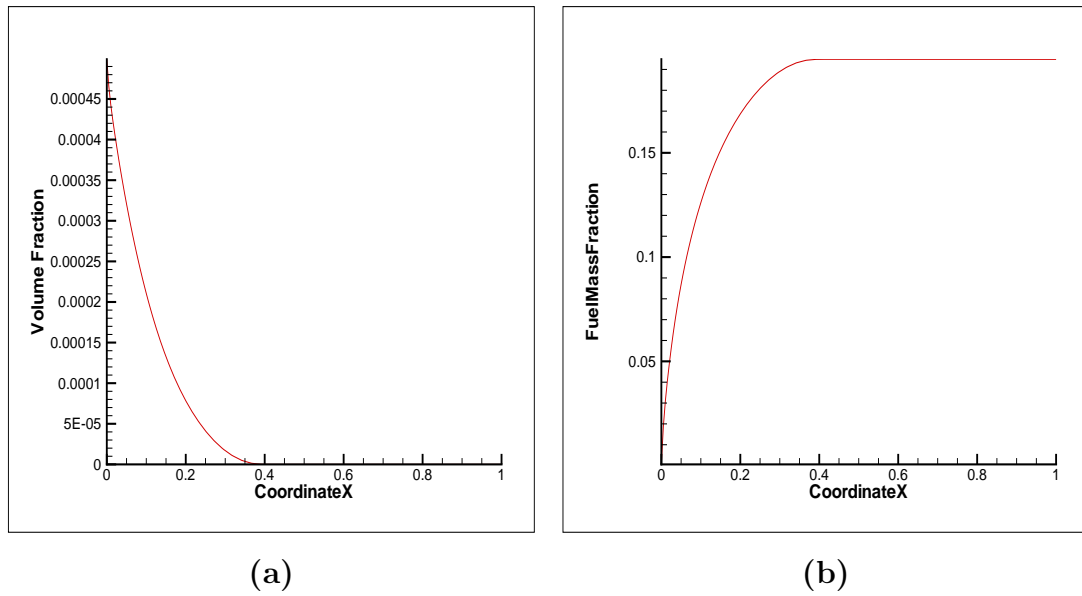


Figure 4.12: Case 2: Gas-droplet channel flow with $u_{gi} = 2.0$ and $u_{di} = 2.0$. (a) Variation of droplet-phase volume fraction, ϑ_d along the channel (b) Variation of evaporated fuel mass fraction, M_F along the channel

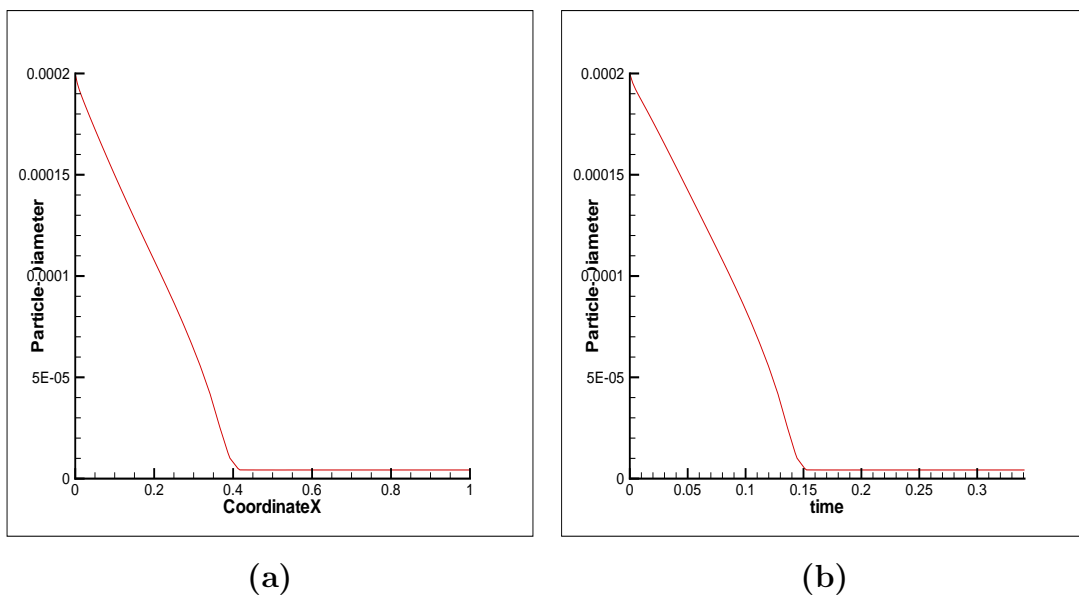


Figure 4.13: Case 2: Gas-droplet channel flow with $u_{gi} = 2.0$ and $u_{di} = 2.0$. (a) Variation of droplet-diameter, d_d along the channel (b) Variation of droplet-diameter, d_d , with time

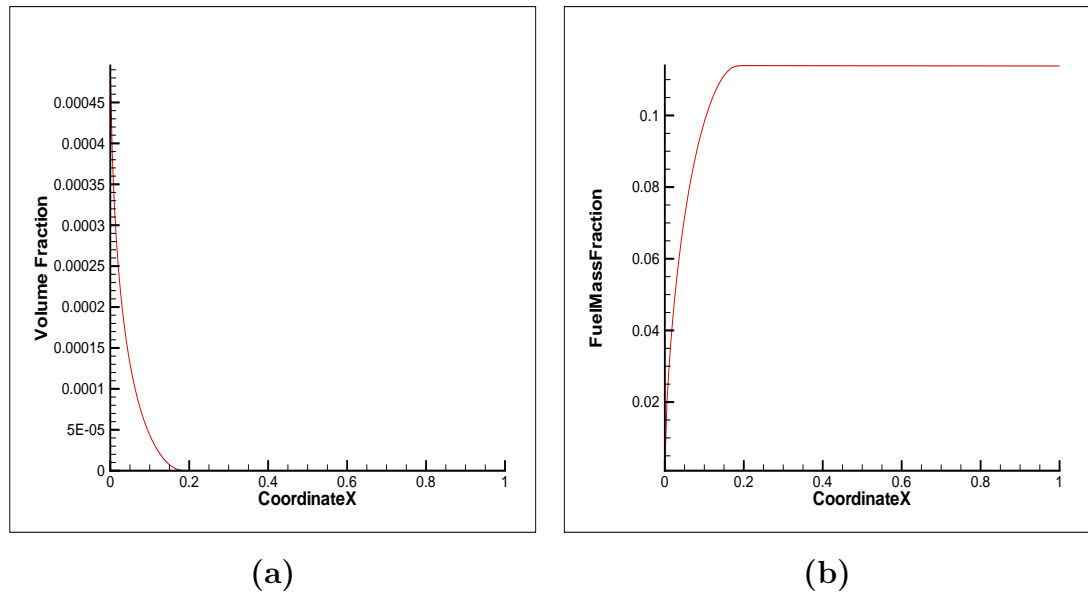


Figure 4.14: Case 2: Gas-droplet channel flow with $u_{gi} = 2.0$ and $u_{di} = 1.0$. (a) Variation of droplet-phase volume fraction, ϑ_d along the channel (b) Variation of evaporated fuel mass fraction, M_F along the channel

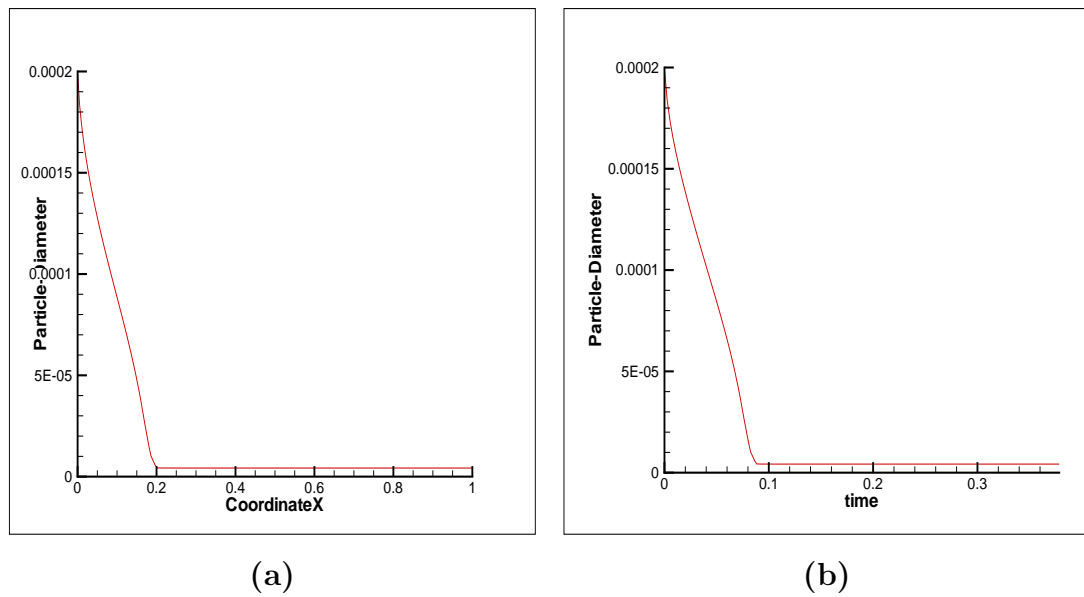


Figure 4.15: Case 1: Gas-droplet channel flow with $u_{gi} = 2.0$ and $u_{di} = 1.0$. (a) Variation of droplet-diameter, d_d along the channel (b) Variation of droplet-diameter, d_d , with time

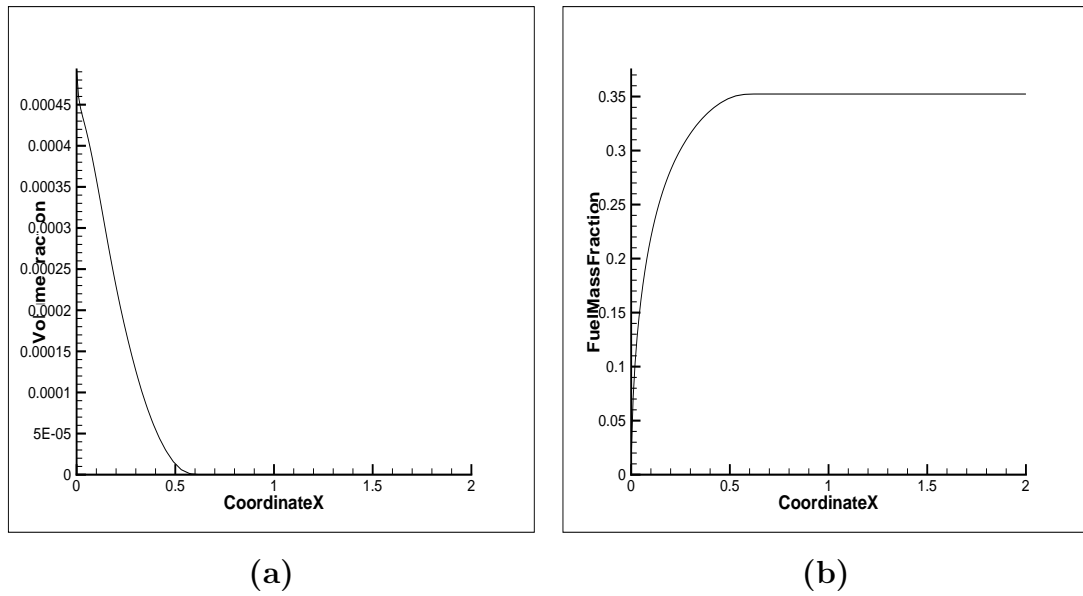


Figure 4.16: Case 2: Gas-droplet channel flow with $u_{gi} = 1.0$ and $u_{di} = 2.0$. (a) Variation of droplet-phase volume fraction, ϑ_d along the channel (b) Variation of evaporated fuel mass fraction, M_F along the channel

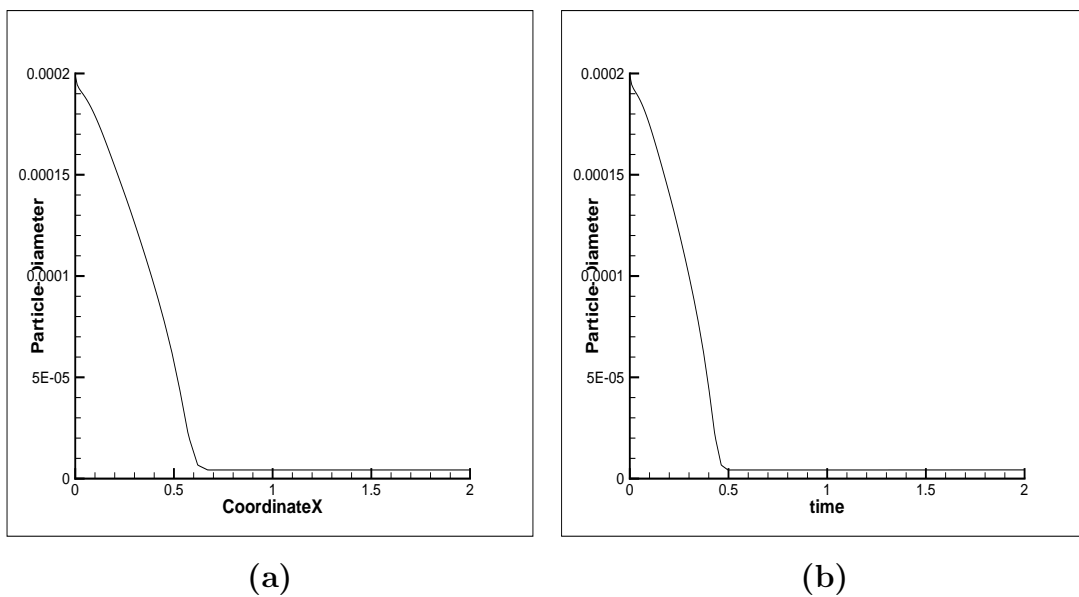


Figure 4.17: Case 2: Gas-droplet channel flow with $u_{gi} = 1.0$ and $u_{di} = 2.0$. (a) Variation of droplet-diameter, d_d along the channel (b) Variation of droplet-diameter, d_d , with time

4.1.4 Gas-droplet channel flow with dummy $Re = 100$ and $Ja = 0.5$

The inlet non-dimensionalized droplet temperature equal to 0 (= 300K). The non-dimensionalized saturation temperature of n-heptane, T_{sat} , is 1 (= 371.4 K) at atmospheric pressure. The inlet properties are given in Table. 4.4. At the wall, the homogeneous Neumann boundary condition is applied for gas-phase velocity and the gas-phase temperature. The latter condition means an insulated boundary condition is applied for temperature while the former implies friction-less ('slip') walls (to avoid friction-work) and ensures a uniform flow profile in the channel. Since we have applied constant (Ja), therefore, we are forced to apply non-dimensionalized Dirichlet boundary condition of 1 (= 371.4K) at both the walls for droplet-phase temperature. Since, the droplet inlet temperature is lower than the saturation temperature, transient heating of the droplets takes place. It is observed from the plots that evaporation length is nearly similar to as of first case.

Table 4.4: Case 3: Inlet conditions

Inlet non dimensionlized conditions	
Gas-phase inlet temperature, T_{gi}	6.625(=773.0 K)
Droplet-phase inlet temperature, T_{di}	0(=300.0 K)
Inlet fuel mass fraction, M_{Fo}	0.0
Gas-phase inlet density, ρ_{gi}	1(=1.225 kg/m ³)
Droplet-phase inlet volume fraction, ϑ_{do}	0.0005
Droplet inlet diameter, d_{do}	200

Gas-droplet channel flow with $u_{gi} = 2.0$ and $u_{di} = 2.0$

It is observed that evaporation length is more compared to previous cases as the droplet inlet temperature is less compared to the saturation temperature, so transient heating of the droplets is taking place.

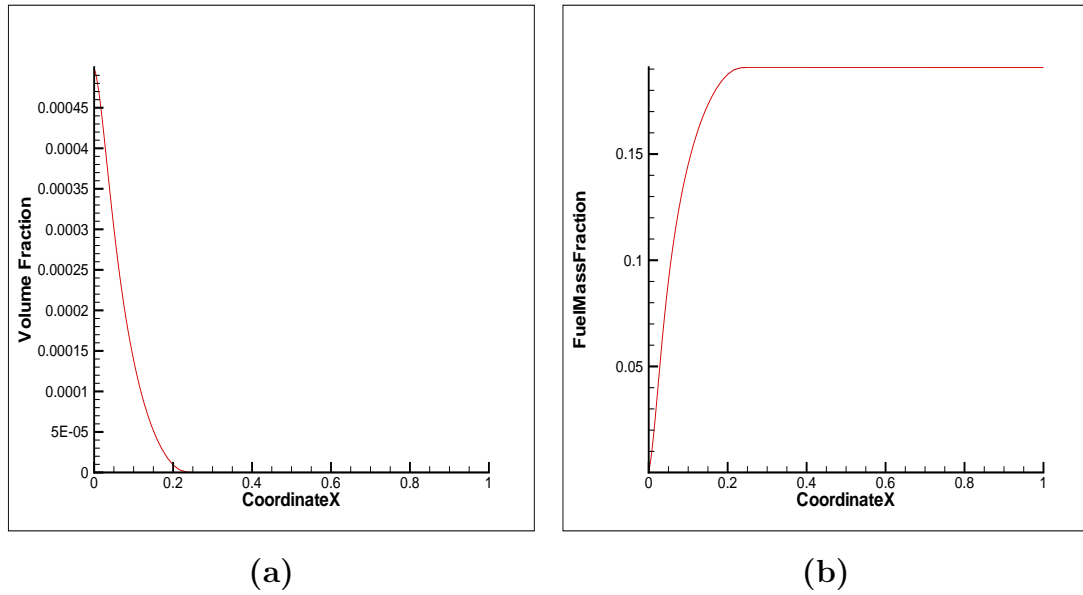


Figure 4.18: Case 3: Gas-droplet channel flow with $u_{gi} = 1.0$ and $u_{di} = 1.0$. (a) Variation of droplet-phase volume fraction, ϑ_d along the channel (b) Variation of evaporated fuel mass fraction, M_F along the channel

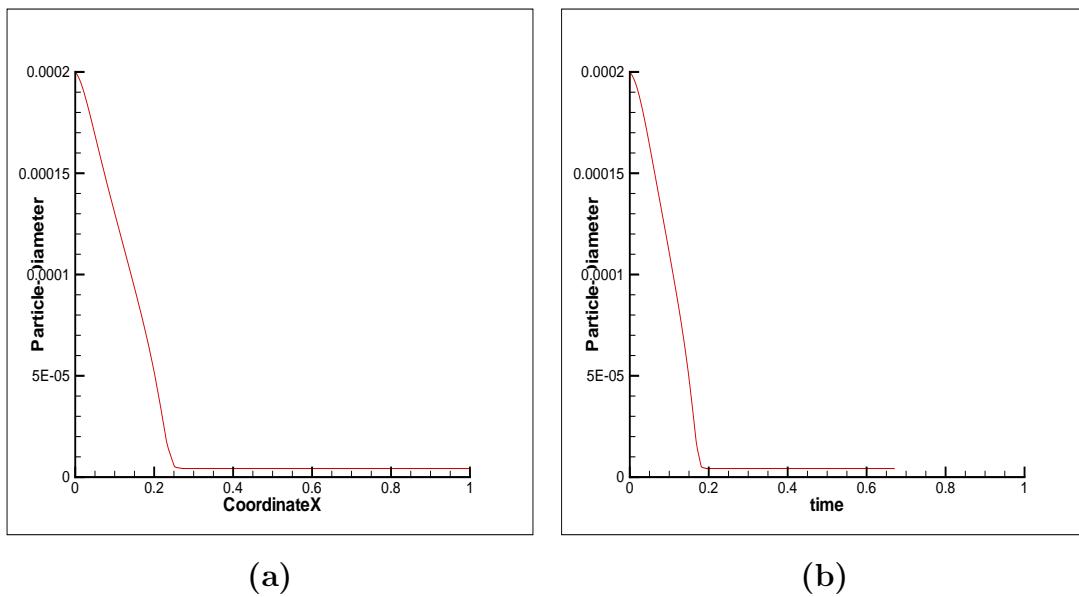


Figure 4.19: Case 3: Gas-droplet channel flow with $u_{gi} = 1.0$ and $u_{di} = 1.0$. (a) Variation of droplet-diameter, d_d along the channel (b) Variation of droplet-diameter, d_d , with time

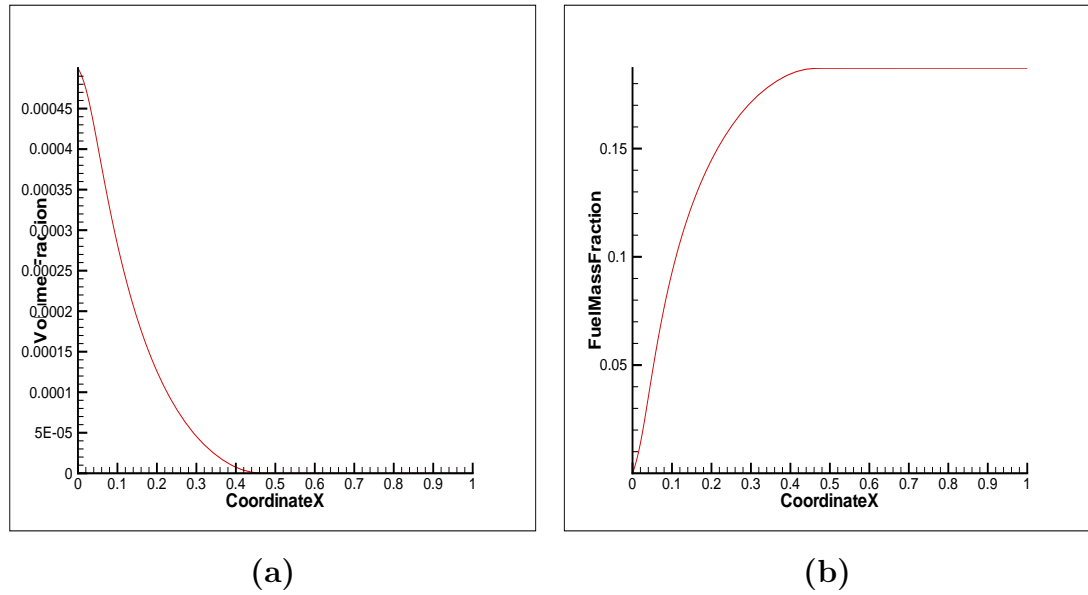


Figure 4.20: Case 3: Gas-droplet channel flow with $u_{gi} = 2.0$ and $u_{di} = 2.0$. (a) Variation of droplet-phase volume fraction, ϑ_d along the channel (b) Variation of evaporated fuel mass fraction, M_F along the channel

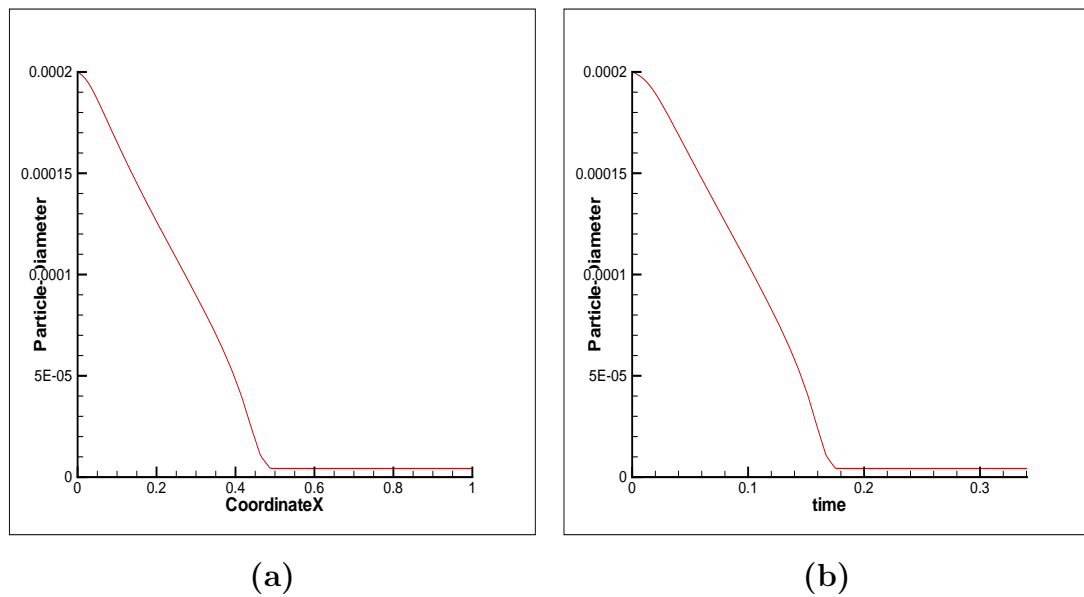


Figure 4.21: Case 3: Gas-droplet channel flow with $u_{gi} = 2.0$ and $u_{di} = 2.0$. (a) Variation of droplet-diameter, d_d along the channel (b) Variation of droplet-diameter, d_d , with time

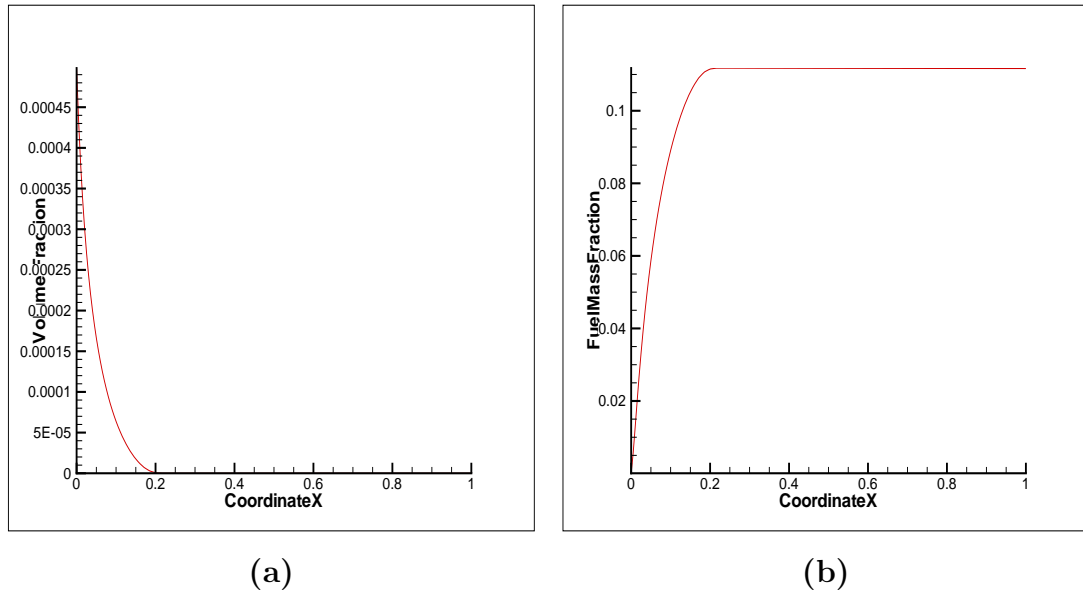


Figure 4.22: Case 3: Gas-droplet channel flow with $u_{gi} = 2.0$ and $u_{di} = 1.0$. (a) Variation of droplet-phase volume fraction, ϑ_d along the channel (b) Variation of evaporated fuel mass fraction, M_F along the channel

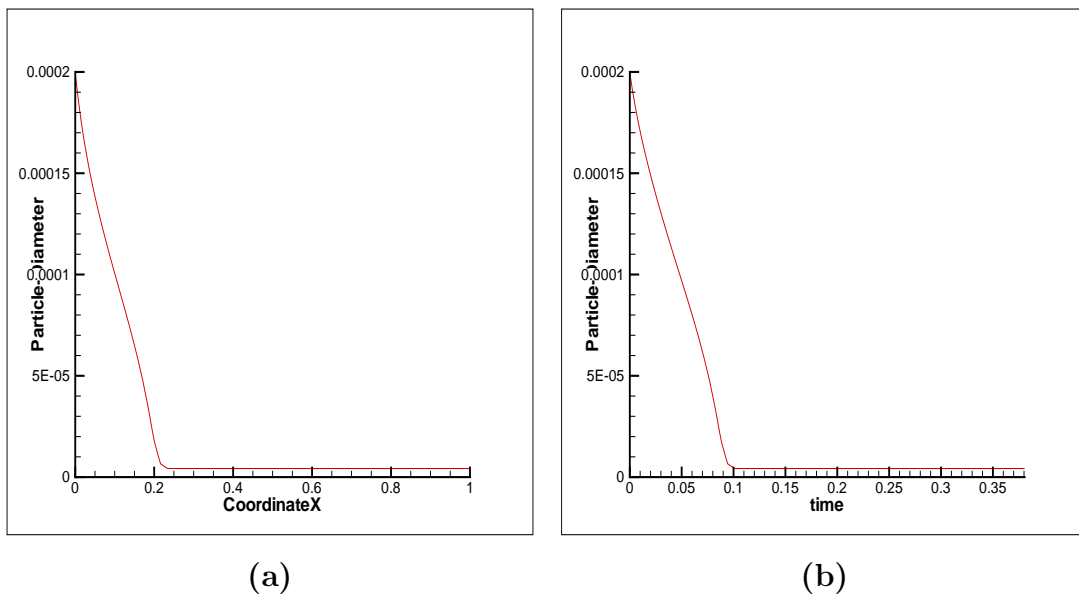


Figure 4.23: Case 3: Gas-droplet channel flow with $u_{gi} = 2.0$ and $u_{di} = 1.0$. (a) Variation of droplet-diameter, d_d along the channel (b) Variation of droplet-diameter, d_d , with time

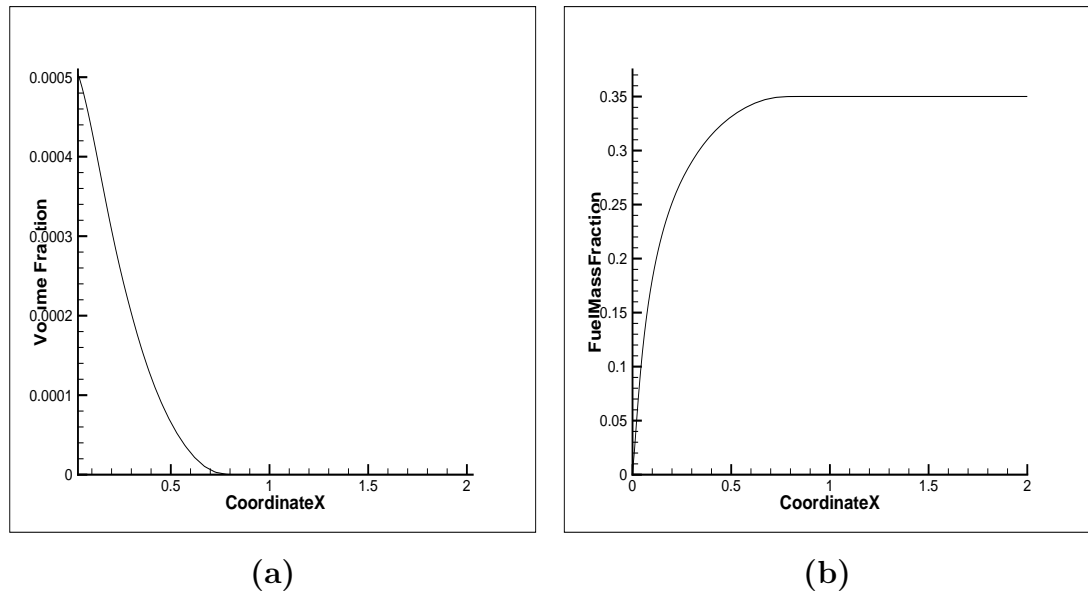


Figure 4.24: Case 3: Gas-droplet channel flow with $u_{gi} = 1.0$ and $u_{di} = 2.0$. (a) Variation of droplet-phase volume fraction, ϑ_d along the channel (b) Variation of evaporated fuel mass fraction, M_F along the channel

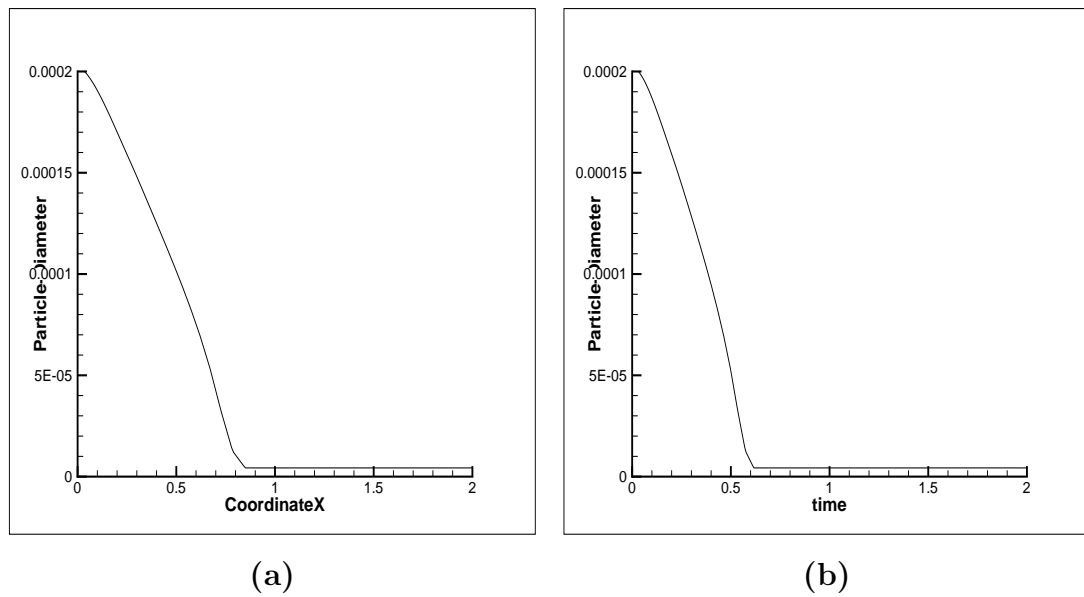


Figure 4.25: Case 3: Gas-droplet channel flow with $u_{gi} = 1.0$ and $u_{di} = 2.0$. (a) Variation of droplet-diameter, d_d along the channel (b) Variation of droplet-diameter, d_d , with time

4.1.5 Gas-droplet channel flow with dummy $Re = 100$ and $Ja = 3.071$

The inlet non-dimensionalized droplet temperature equal to 0 ($= 371.4\text{K}$). The non-dimensionalized saturation temperature of n-heptane, (T_{sat} , is 0 ($= 371.4\text{ K}$) at atmospheric pressure. The inlet properties are given in Table. 4.2. At the wall, the homogeneous Neumann boundary condition is applied for gas-phase velocity and the gas-phase temperature. The latter condition means an insulated boundary condition is applied for temperature while the former implies friction-less ('slip') walls (to avoid friction-work) and ensures a uniform flow profile in the channel. Since we have applied constant (Ja), therefore, we are forced to apply non-dimensionalized Dirichlet boundary condition of 1 ($= 773.0\text{K}$) at both the walls for droplet-phase temperature. Since, the droplet inlet temperature is equal to the saturation temperature, no transient heating of the droplets takes place and the droplet temperature remains constant at its inlet value while the droplets evaporate due to heating. The conditions are such that the droplets evaporate totally by the end of the channel.

Table 4.5: Case 4: Inlet conditions

Inlet non dimensionlized conditions	
Gas-phase inlet temperature, T_{gi}	1($=773.0\text{ K}$)
Droplet-phase inlet temperature, T_{di}	0($=300.0\text{ K}$)
Inlet fuel mass fraction, M_{Fo}	0.0
Gas-phase inlet density, ρ_{gi}	1($=1.225\text{ kg/m}^3$)
Droplet-phase inlet volume fraction, ϑ_{do}	0.0005
Droplet inlet diameter, d_{do}	100

It is also observed from the plots that evaporation length is very less compared to the previous cases as the residence time of droplets is very less due to the decreased inlet diameter.

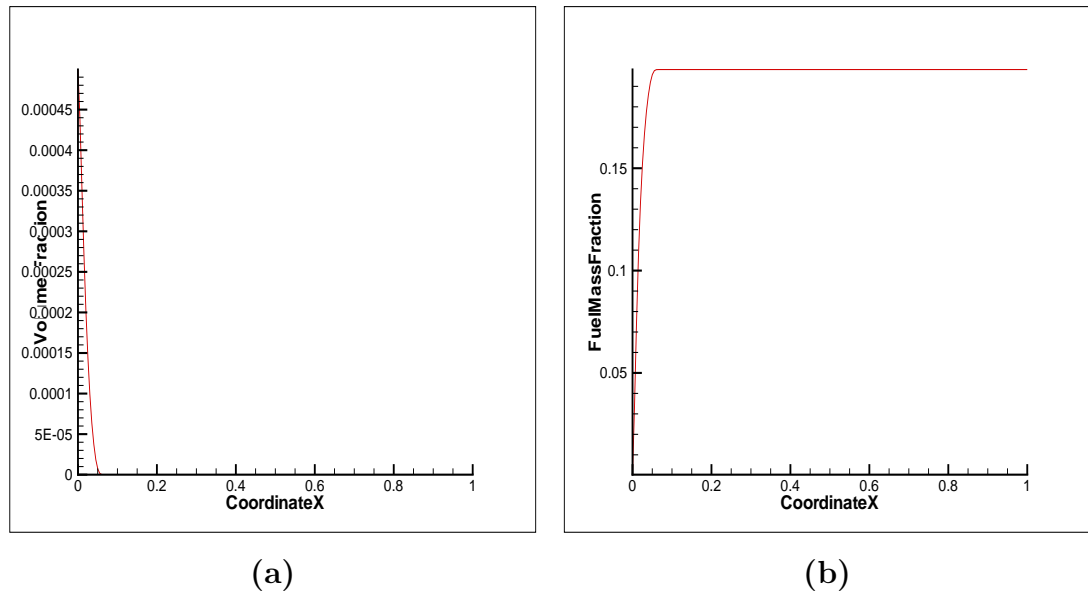


Figure 4.26: Case 4: Gas-droplet channel flow with $u_{gi} = 1.0$ and $u_{di} = 1.0$. (a) Variation of droplet-phase volume fraction, ϑ_d along the channel (b) Variation of evaporated fuel mass fraction, M_F along the channel

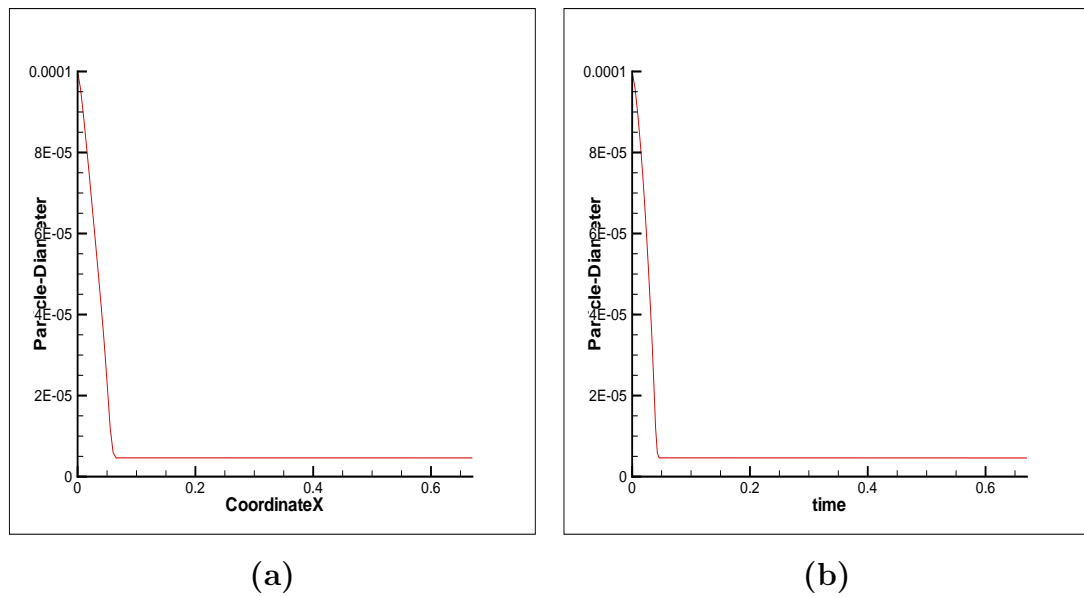


Figure 4.27: Case 4: Gas-droplet channel flow with $u_{gi} = 1.0$ and $u_{di} = 1.0$. (a) Variation of droplet-diameter, d_d along the channel (b) Variation of droplet-diameter, d_d , with time

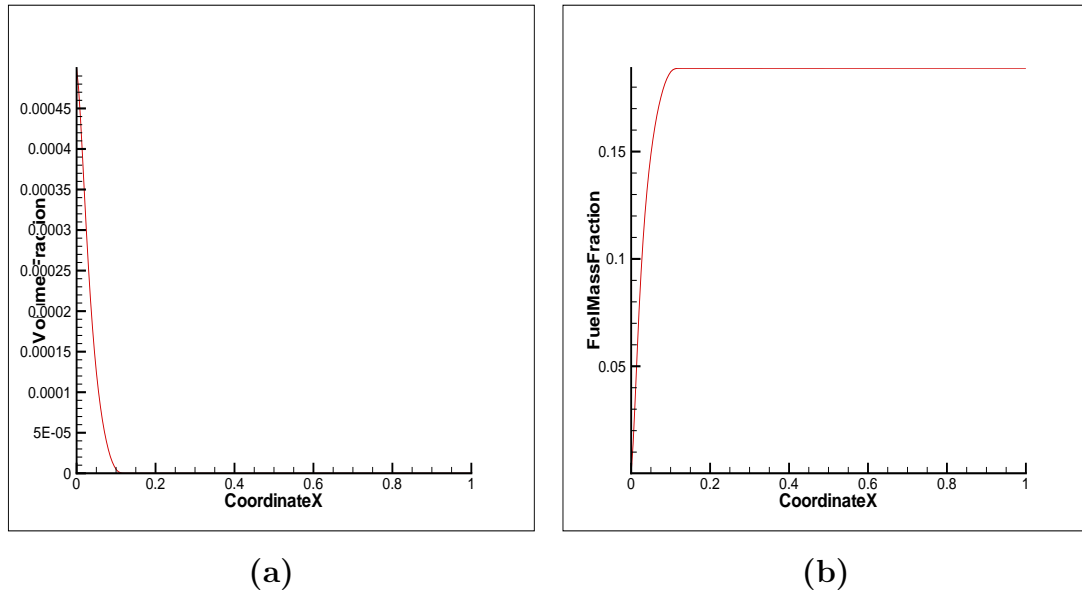


Figure 4.28: Case 4: Gas-droplet channel flow with $u_{gi} = 2.0$ and $u_{di} = 1.0$. (a) Variation of droplet-phase volume fraction, ϑ_d along the channel (b) Variation of evaporated fuel mass fraction, M_F along the channel

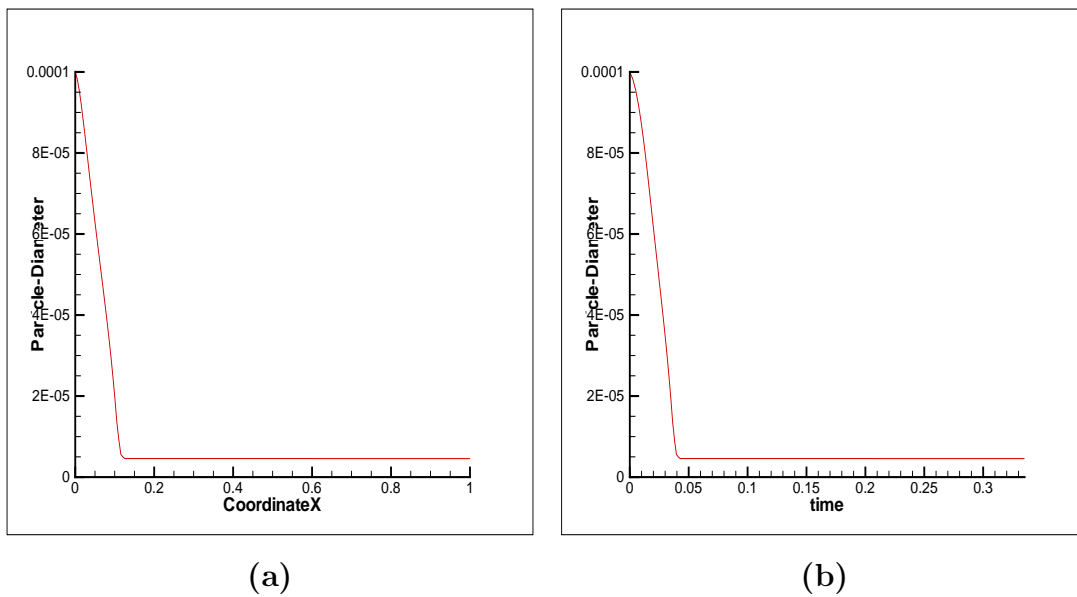


Figure 4.29: Case 4: Gas-droplet channel flow with $u_{gi} = 2.0$ and $u_{di} = 1.0$. (a) Variation of droplet-diameter, d_d along the channel (b) Variation of droplet-diameter, d_d , with time

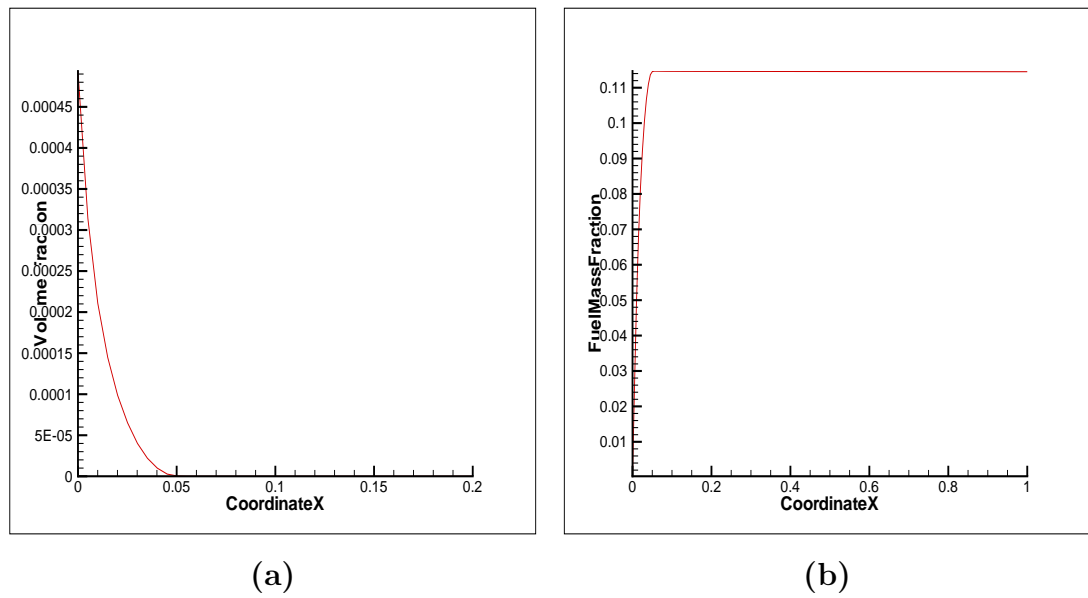


Figure 4.30: Case 4: Gas-droplet channel flow with $u_{gi} = 2.0$ and $u_{di} = 1.0$. (a) Variation of droplet-phase volume fraction, ϑ_d along the channel (b) Variation of evaporated fuel mass fraction, M_F along the channel

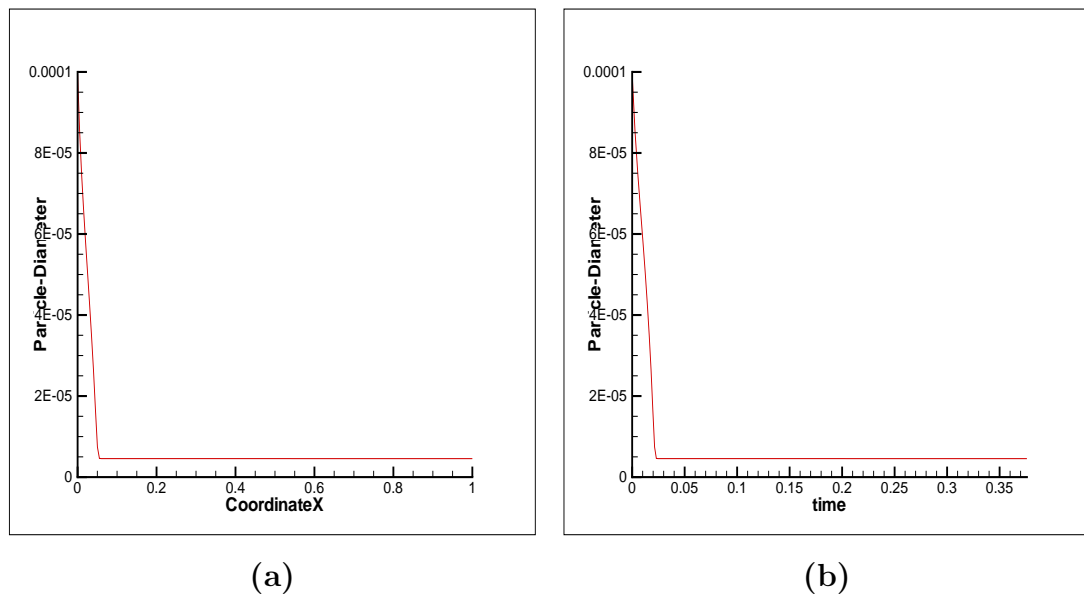


Figure 4.31: Case 4: Gas-droplet channel flow with $u_{gi} = 2.0$ and $u_{di} = 1.0$. (a) Variation of droplet-diameter, d_d along the channel (b) Variation of droplet-diameter, d_d , with time

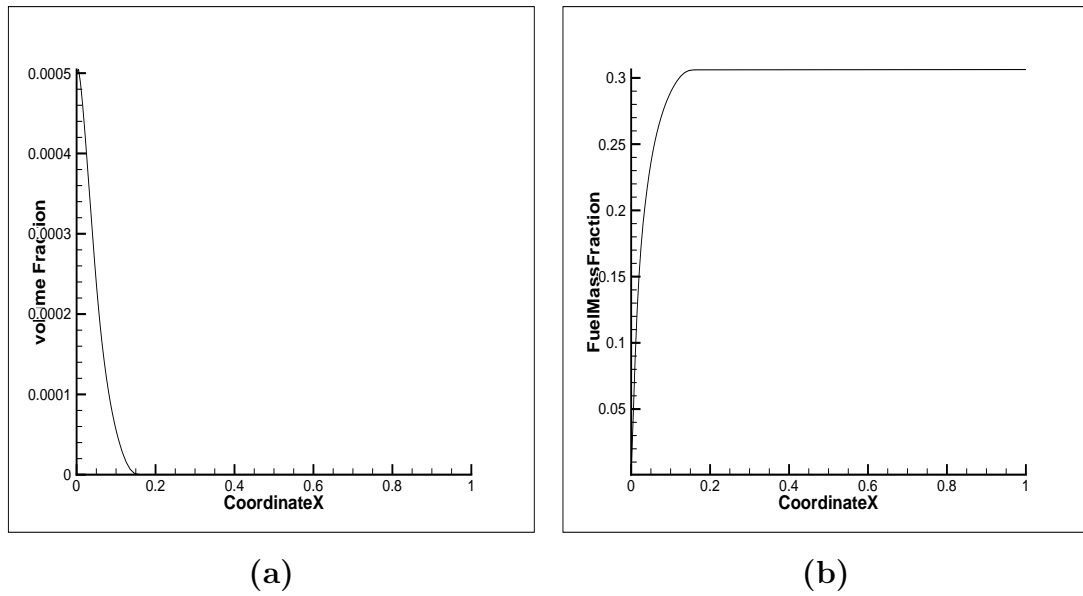


Figure 4.32: Case 4: Gas-droplet channel flow with $u_{gi} = 1.0$ and $u_{di} = 2.0$. (a) Variation of droplet-phase volume fraction, ϑ_d along the channel (b) Variation of evaporated fuel mass fraction, M_F along the channel

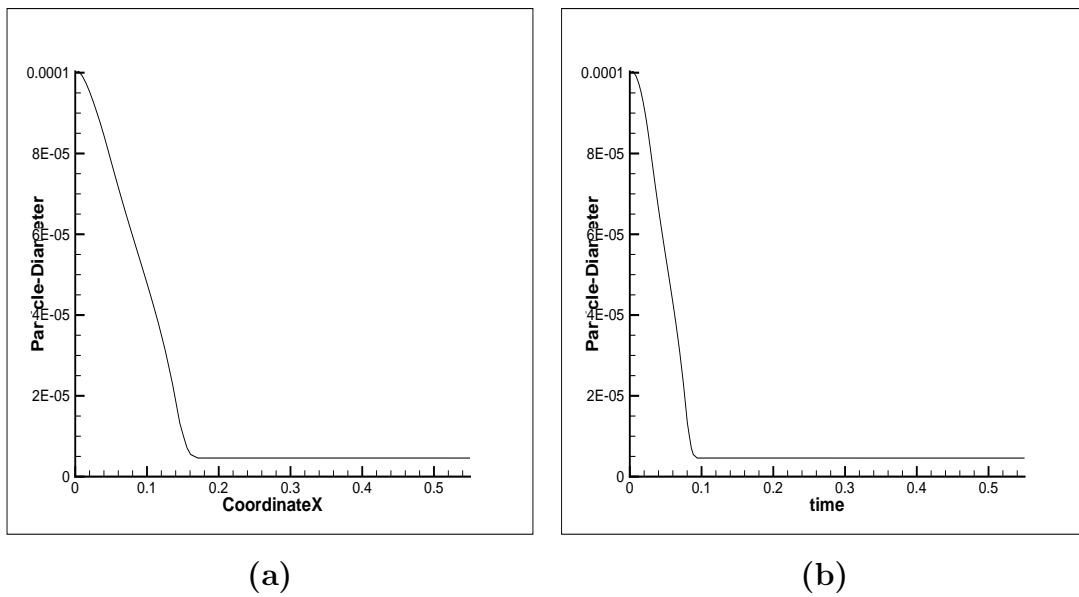


Figure 4.33: Case 4: Gas-droplet channel flow with $u_{gi} = 2.0$ and $u_{di} = 1.0$. (a) Variation of droplet-diameter, d_d along the channel (b) Variation of droplet-diameter, d_d , with time

4.1.6 Gas-droplet channel flow with dummy $Re = 100$ and $Ja = 2.784$

The inlet non-dimensionlized droplet temperature equal to 0 ($= 371.4K$).The non-dimensionlized saturation temperature of n-heptane, (T_{sat} , is 0 ($= 371.4 K$) at atmospheric pressure. The inlet properties are given in Table. 4.2. At the wall, the homogeneous Neumann boundary condition is applied for gas-phase velocity and the gas-phase temperature. The latter condition means an insulated boundary condition is applied for temperature while the former implies friction-less ('slip') walls (to avoid friction-work) and ensures a uniform flow profile in the channel. Since we have applied constant (Ja), therefore, we are forced to apply non-dimensionlized Dirichlett boundary condition of 1 ($= 773.0K$) at both the walls for droplet-phase temperature. Since, the droplet inlet temperature is equal to the saturation temperature, no transient heating of the droplets takes place and the droplet temperature remains constant at its inlet value while the droplets evaporate due to heating. The conditions are such that the droplets evaporate totally by the end of the channel.

Table 4.6: Case 5: Inlet conditions

Inlet non dimensionlized conditions	
Gas-phase inlet temperature, T_{gi}	1($=773.0 K$)
Droplet-phase inlet temperature, T_{di}	0($=371.4 K$)
Inlet fuel mass fraction, M_{Fo}	0.0
Gas-phase inlet density, ρ_{gi}	1($=1.225 kg/m^3$)
Droplet-phase inlet volume fraction, ϑ_{do}	0.0005
Droplet inlet diameter, d_{do}	100

It is observed that evaporation length is less compared to previous case as the droplet inlet temperature is equal to the saturation temperature, no transient heating of the droplets is taking place.

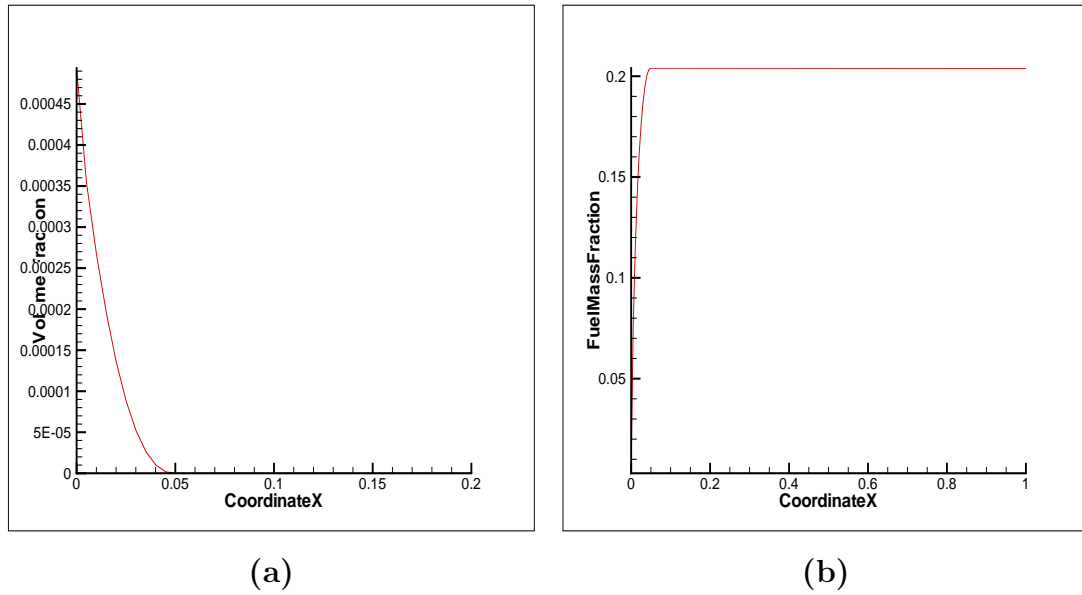


Figure 4.34: Case 5: Gas-droplet channel flow with $u_{gi} = 1.0$ and $u_{di} = 1.0$. (a) Variation of droplet-phase volume fraction, ϑ_d along the channel (b) Variation of evaporated fuel mass fraction, M_F along the channel

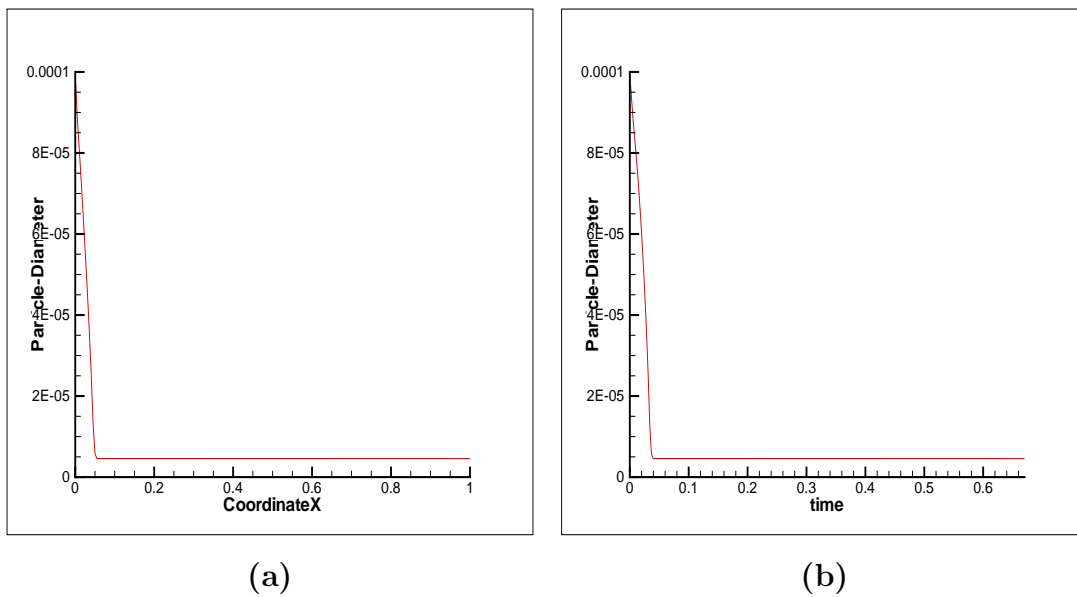


Figure 4.35: Case 5: Gas-droplet channel flow with $u_{gi} = 1.0$ and $u_{di} = 1.0$. (a) Variation of droplet-diameter, d_d along the channel (b) Variation of droplet-diameter, d_d , with time

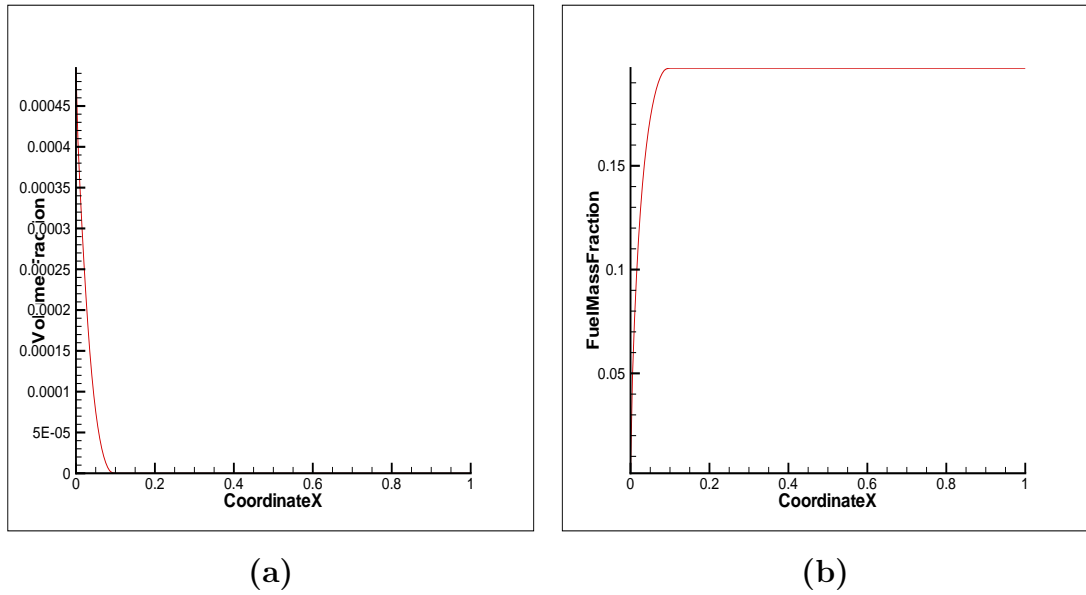


Figure 4.36: Case 5: Gas-droplet channel flow with $u_{gi} = 2.0$ and $u_{di} = 2.0$. (a) Variation of droplet-phase volume fraction, ϑ_d along the channel (b) Variation of evaporated fuel mass fraction, M_F along the channel

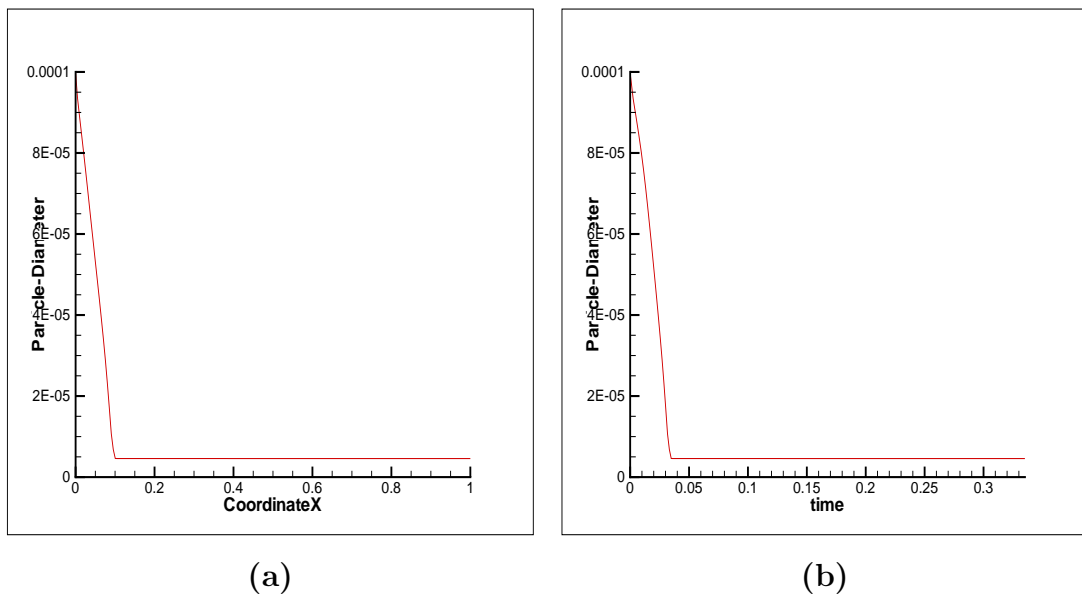


Figure 4.37: Case 5: Gas-droplet channel flow with $u_{gi} = 2.0$ and $u_{di} = 2.0$. (a) Variation of droplet-diameter, d_d along the channel (b) Variation of droplet-diameter, d_d , with time

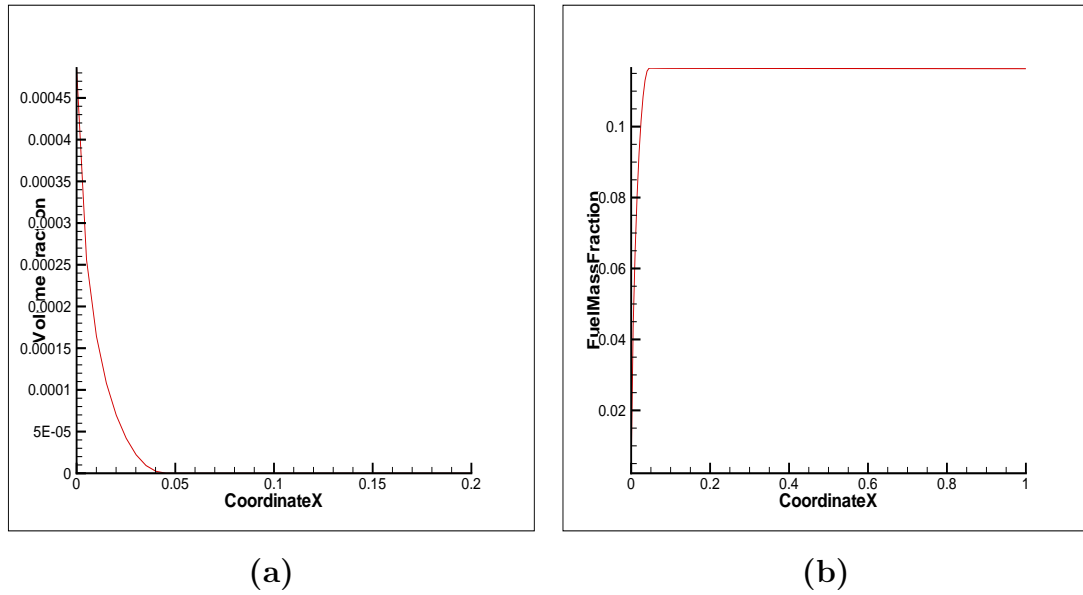


Figure 4.38: Case 5: Gas-droplet channel flow with $u_{gi} = 2.0$ and $u_{di} = 1.0$. (a) Variation of droplet-phase volume fraction, ϑ_d along the channel (b) Variation of evaporated fuel mass fraction, M_F along the channel

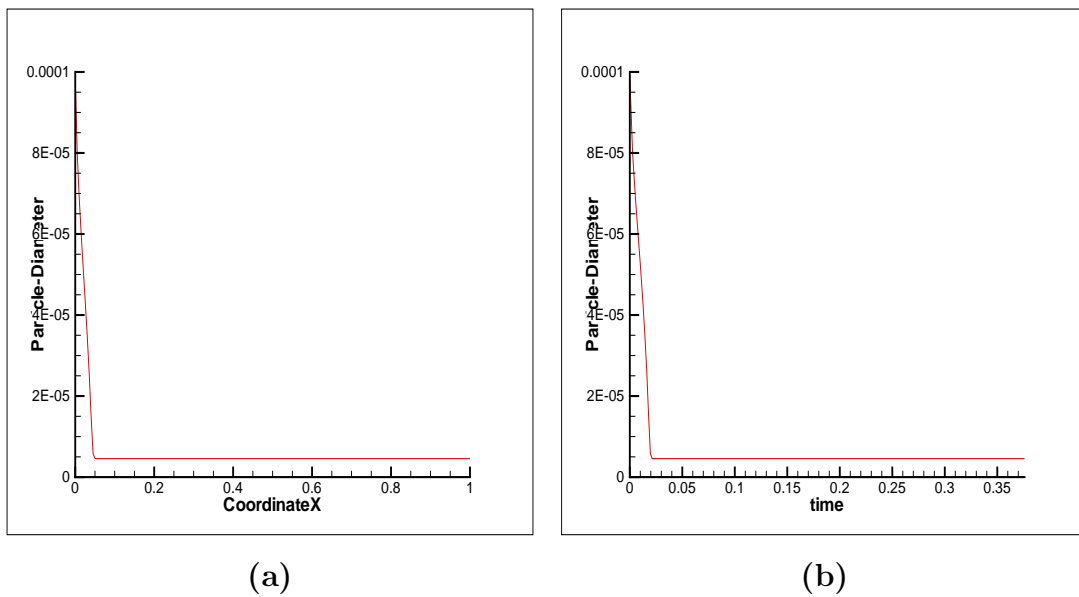


Figure 4.39: Case 5: Gas-droplet channel flow with $u_{gi} = 2.0$ and $u_{di} = 1.0$. (a) Variation of droplet-diameter, d_d along the channel (b) Variation of droplet-diameter, d_d , with time

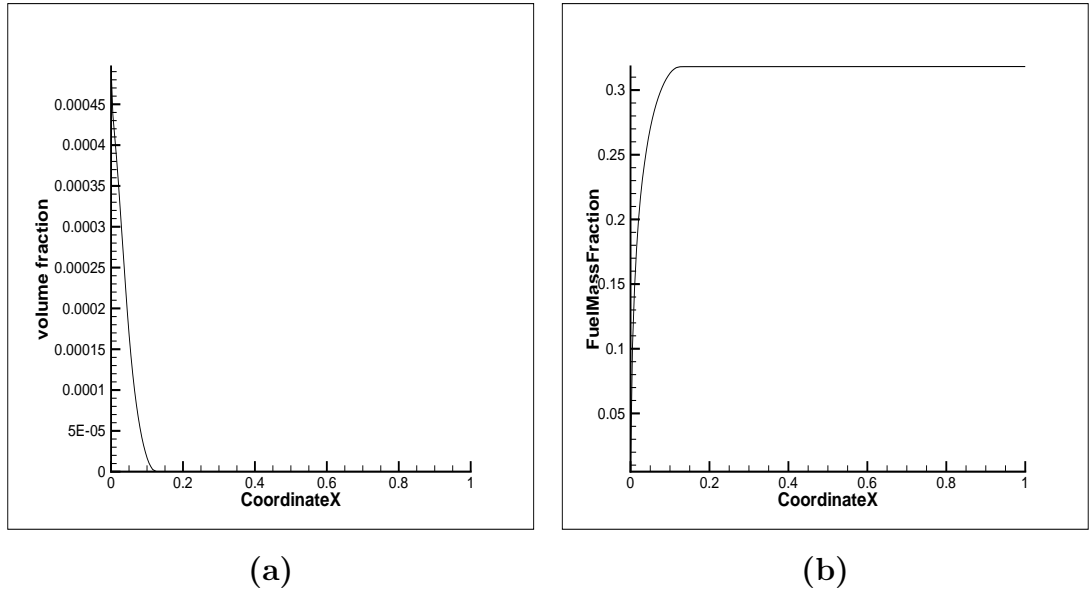


Figure 4.40: Case 5: Gas-droplet channel flow with $u_{gi} = 1.0$ and $u_{di} = 2.0$. (a) Variation of droplet-phase volume fraction, ϑ_d along the channel (b) Variation of evaporated fuel mass fraction, M_F along the channel

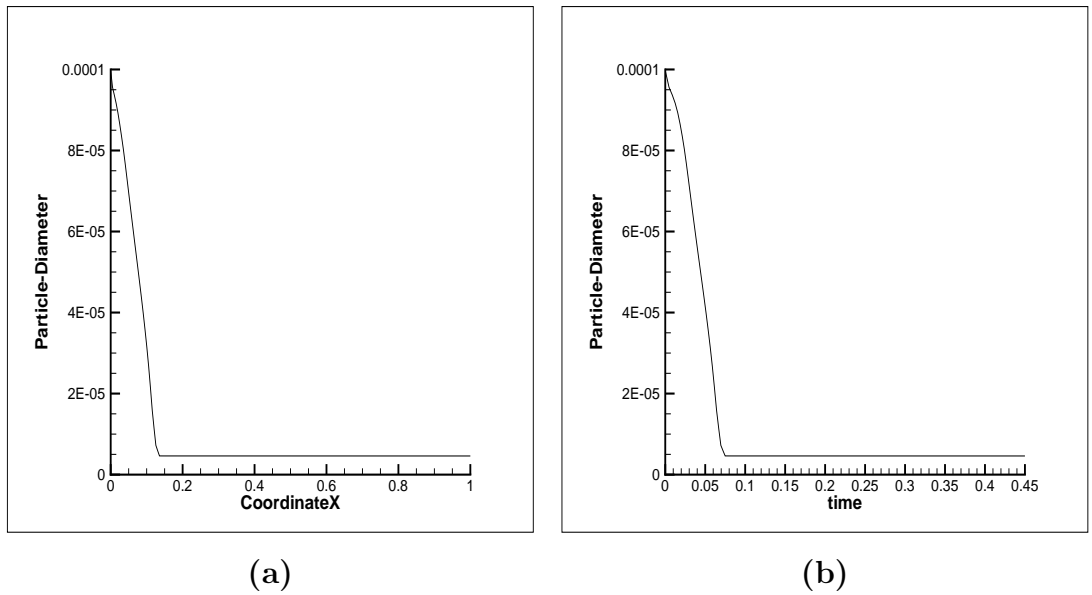


Figure 4.41: Case 5: Gas-droplet channel flow with $u_{gi} = 1.0$ and $u_{di} = 2.0$. (a) Variation of droplet-diameter, d_d along the channel (b) Variation of droplet-diameter, d_d , with time

4.1.7 Gas-droplet channel flow with dummy $Re = 100$ and $Ja = 0.5$

The inlet non-dimensionlized droplet temperature equal to 0 ($= 300\text{K}$).The non-dimensionlized saturation temperature of n-heptane, (T_{sat} , is 1 ($= 371.4 \text{ K}$) at atmospheric pressure. The inlet properties are given in Table. 4.2. At the wall, the homogeneous Neumann boundary condition is applied for gas-phase velocity and the gas-phase temperature .The latter condition means an insulated boundary condition is applied for temperature while the former implies friction-less ('slip') walls (to avoid friction-work) and ensures a uniform flow profile in the channel.Since we have applied constant (Ja), therefore, we apply non-dimensionlizedDirichlett boundary condition of 1($= 371.4\text{K}$) at both the walls for droplet-phase temperature. Since, the droplet inlet temperature is lower than the saturation temperature, transient heating of the droplets takes place.The conditions are such that the droplets evaporate totally by the end of the channel

Table 4.7: Case 6: Inlet conditions

Inlet non dimenstionlized conditions	
Gas-phase inlet temperature, T_{gi}	1($=773.0 \text{ K}$)
Droplet-phase inlet temperature, T_{di}	0($=300.0 \text{ K}$)
Inlet fuel mass fraction, M_{Fo}	0.0
Gas-phase inlet density, ρ_{gi}	1($=1.225 \text{ kg/m}^3$)
Droplet-phase inlet volume fraction, ϑ_{do}	0.0005
Droplet inlet diameter, d_{do}	100

It is observed that evaporation length is more compared to previous cases as the droplet inlet temperature is less compared to the saturation temperature,so transient heating of the droplets is taking place.

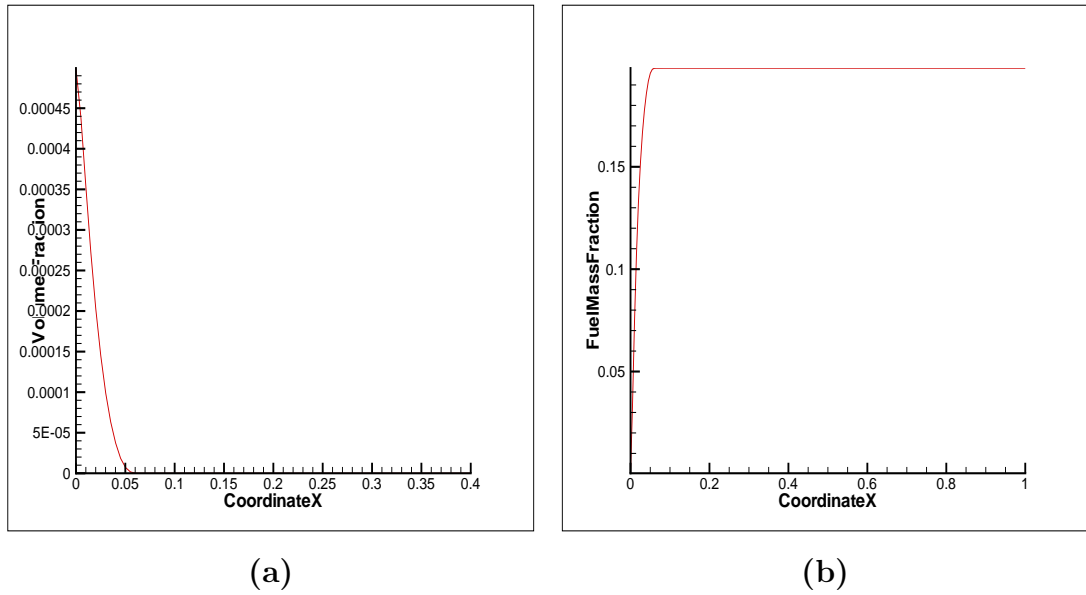


Figure 4.42: Case 6: Gas-droplet channel flow with $u_{gi} = 1.0$ and $u_{di} = 1.0$. (a) Variation of droplet-phase volume fraction, ϑ_d along the channel (b) Variation of evaporated fuel mass fraction, M_F along the channel

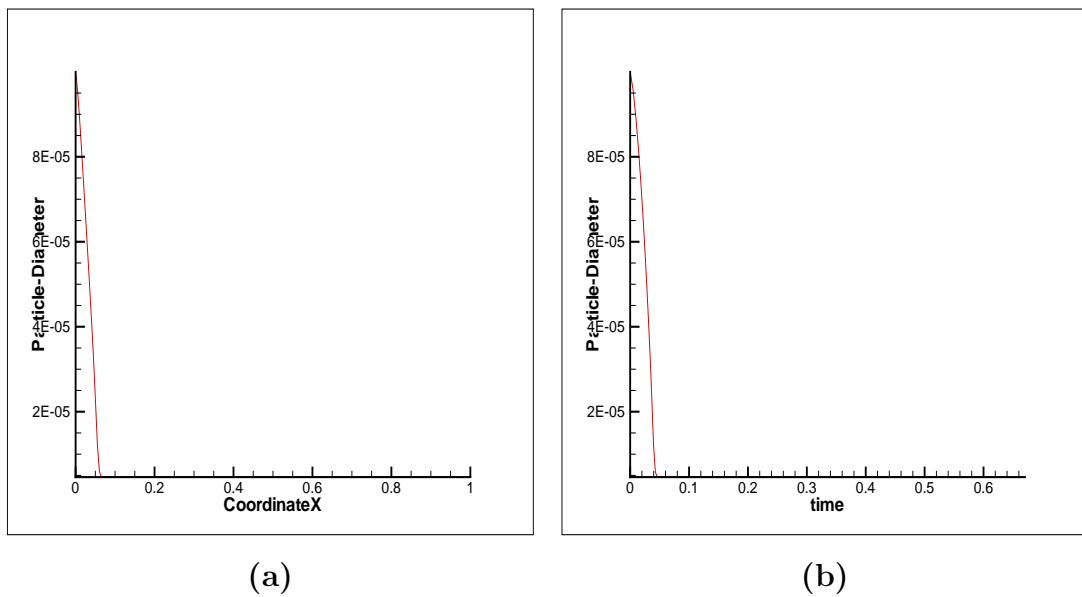


Figure 4.43: Case 6: Gas-droplet channel flow with $u_{gi} = 1.0$ and $u_{di} = 1.0$. (a) Variation of droplet-diameter, d_d along the channel (b) Variation of droplet-diameter, d_d , with time

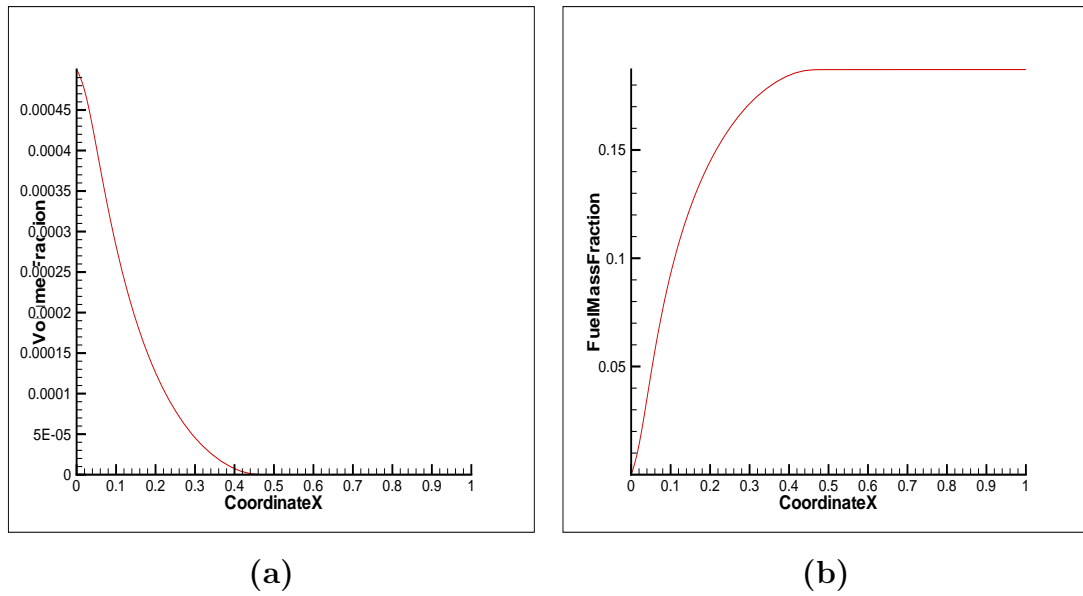


Figure 4.44: Case 6: Gas-droplet channel flow with $u_{gi} = 2.0$ and $u_{di} = 2.0$. (a) Variation of droplet-phase volume fraction, ϑ_d along the channel (b) Variation of evaporated fuel mass fraction, M_F along the channel

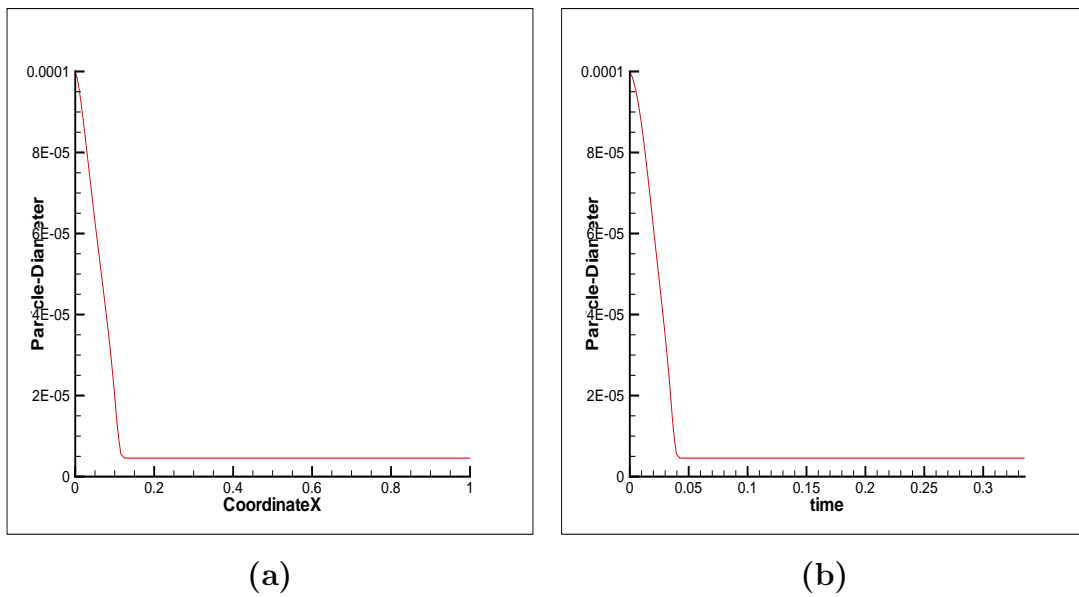


Figure 4.45: Case 6: Gas-droplet channel flow with $u_{gi} = 2.0$ and $u_{di} = 2.0$. (a) Variation of droplet-diameter, d_d along the channel (b) Variation of droplet-diameter, d_d , with time

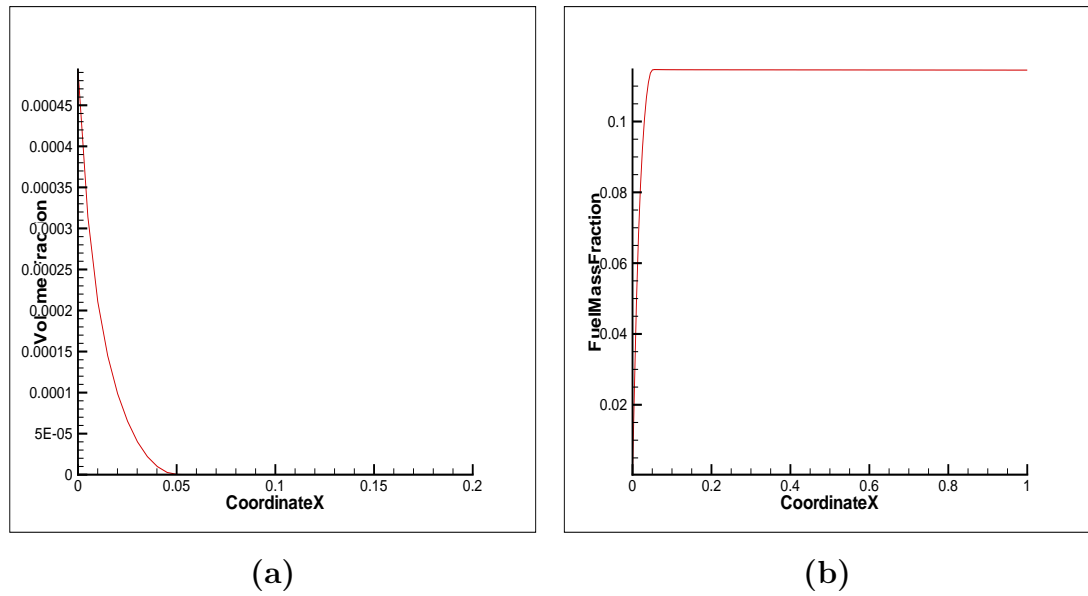


Figure 4.46: Case 6: Gas-droplet channel flow with $u_{gi} = 2.0$ and $u_{di} = 1.0$. (a) Variation of droplet-phase volume fraction, ϑ_d along the channel (b) Variation of evaporated fuel mass fraction, M_F along the channel

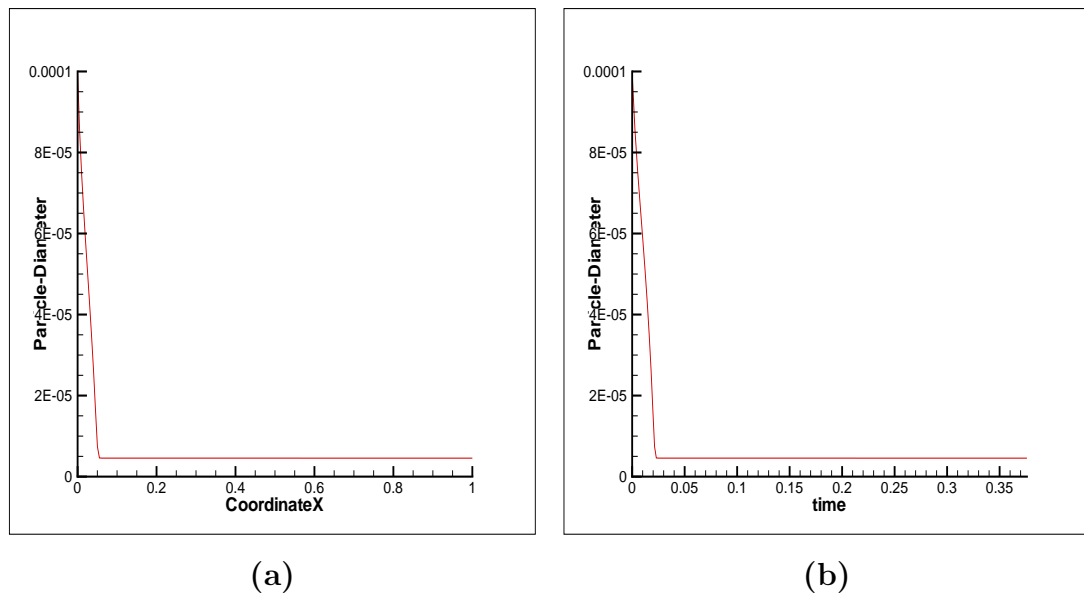


Figure 4.47: Case 6: Gas-droplet channel flow with $u_{gi} = 2.0$ and $u_{di} = 1.0$. (a) Variation of droplet-diameter, d_d along the channel (b) Variation of droplet-diameter, d_d , with time

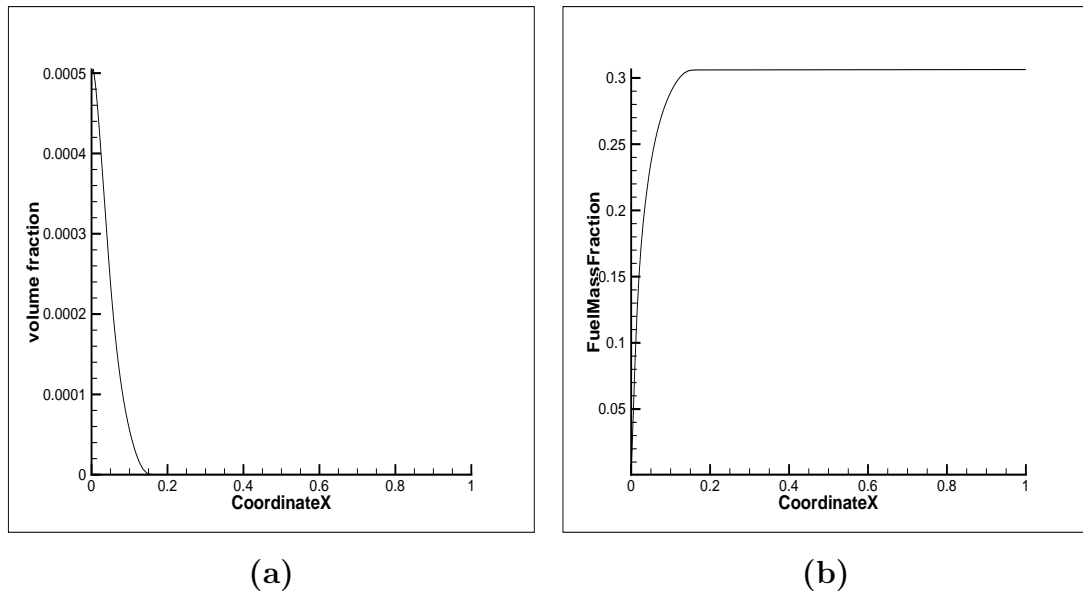


Figure 4.48: Case 6: Gas-droplet channel flow with $u_{gi} = 1.0$ and $u_{di} = 2.0$. (a) Variation of droplet-phase volume fraction, ϑ_d along the channel (b) Variation of evaporated fuel mass fraction, M_F along the channel

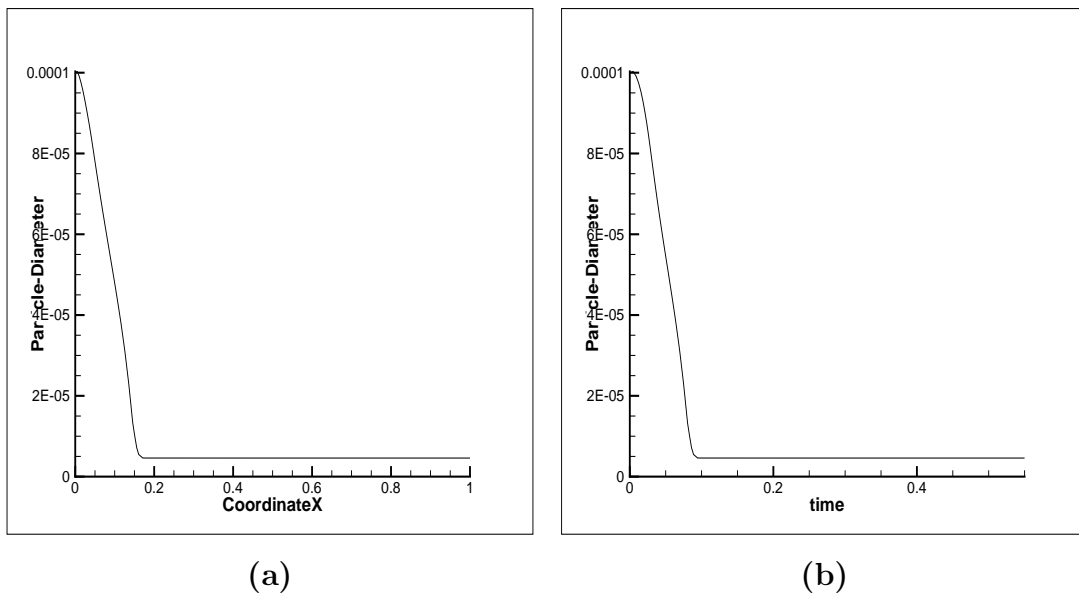


Figure 4.49: Case 6: Gas-droplet channel flow with $u_{gi} = 1.0$ and $u_{di} = 2.0$. (a) Variation of droplet-diameter, d_d along the channel (b) Variation of droplet-diameter, d_d , with time

4.1.8 Gas-droplet channel flow with dummy $Re = 200$ and $Ja = 3.071$

The inlet non-dimensionalized droplet temperature equal to 0 ($= 300\text{K}$). The non-dimensionalized saturation temperature of n-heptane, T_{sat} , is 0.16117 ($= 371.4\text{ K}$) at atmospheric pressure. The inlet properties are given in Table. 4.8. At the wall, the homogeneous Neumann boundary condition is applied for gas-phase velocity. This condition means friction-less ('slip') walls (to avoid friction-work) and ensures a uniform flow profile in the channel. Since we have applied constant (Ja) therefore we apply Dirichlet boundary condition at both the walls for gas-phase temperature and droplet-phase temperature. Since, the droplet inlet temperature is lower than the saturation temperature, transient heating of the droplets takes place. The conditions are such that the droplets evaporate totally by the end of the channel.

Table 4.8: Case 7: Inlet conditions

Inlet non dimensionstionlized conditions	
Gas-phase inlet temperature, T_{gi}	1($=773.0\text{ K}$)
Droplet-phase inlet temperature, T_{di}	0($=300.0\text{ K}$)
Inlet fuel mass fraction, M_{Fo}	0.0
Gas-phase inlet density, ρ_{gi}	1($=1.225\text{ kg/m}^3$)
Droplet-phase inlet volume fraction, ϑ_{do}	0.0005
Droplet inlet diameter, d_{do}	100

Gas-droplet channel flow with $u_{gi} = 1.0$ and $u_{di} = 1.0$

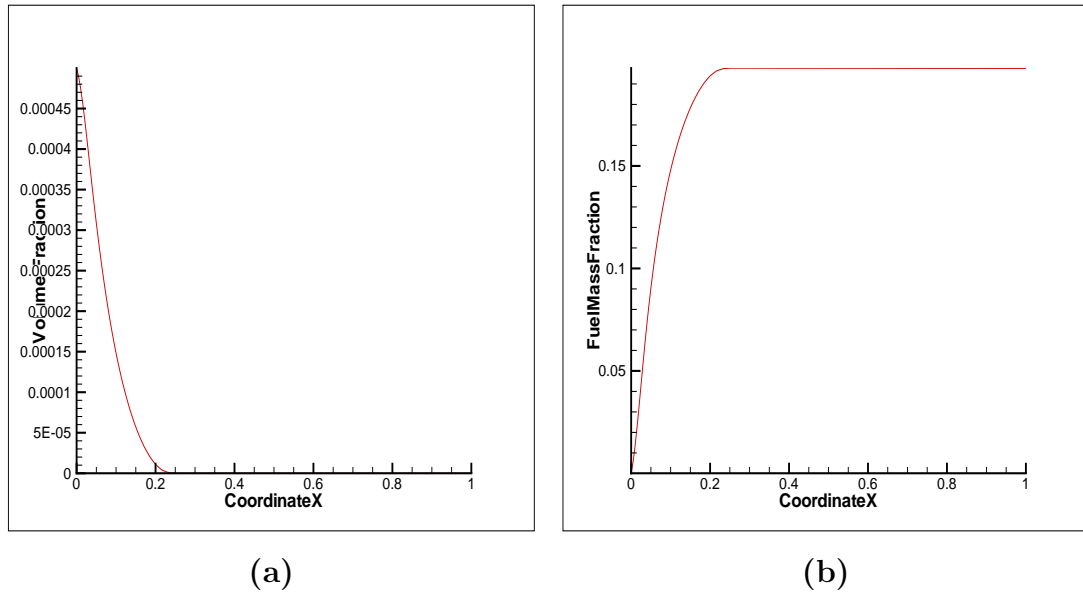


Figure 4.50: Case 7: Gas-droplet channel flow with $u_{gi} = 1.0$ and $u_{di} = 1.0$. (a) Variation of droplet-phase volume fraction, ϑ_d along the channel (b) Variation of evaporated fuel mass fraction, M_F along the channel

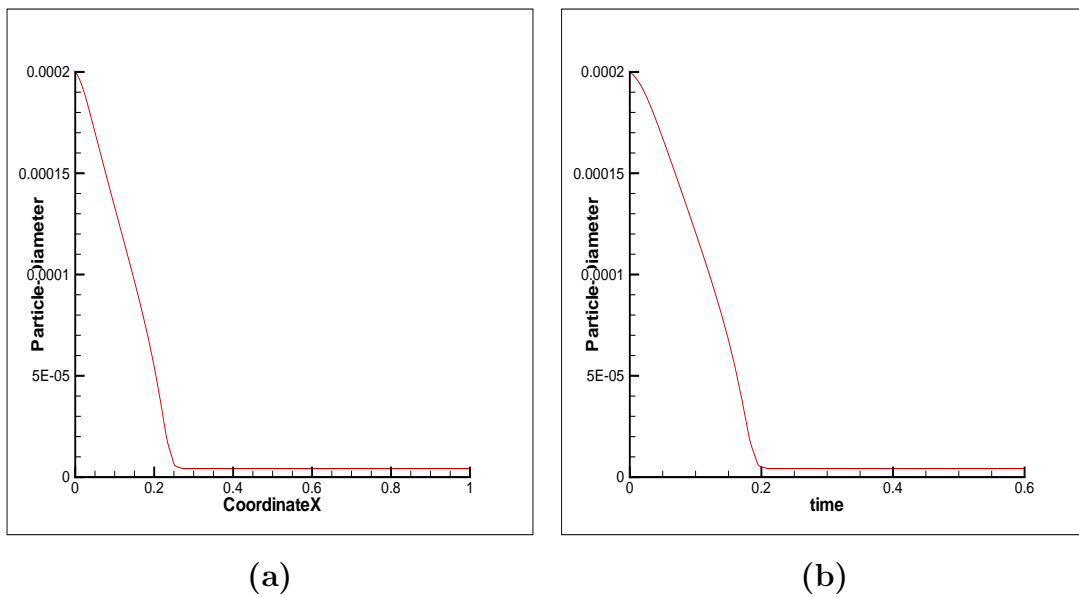


Figure 4.51: Case 7: Gas-droplet channel flow with $u_{gi} = 1.0$ and $u_{di} = 1.0$.(a) Variation of droplet-diameter, d_d along the channel (b) Variation of droplet-diameter, d_d , with time

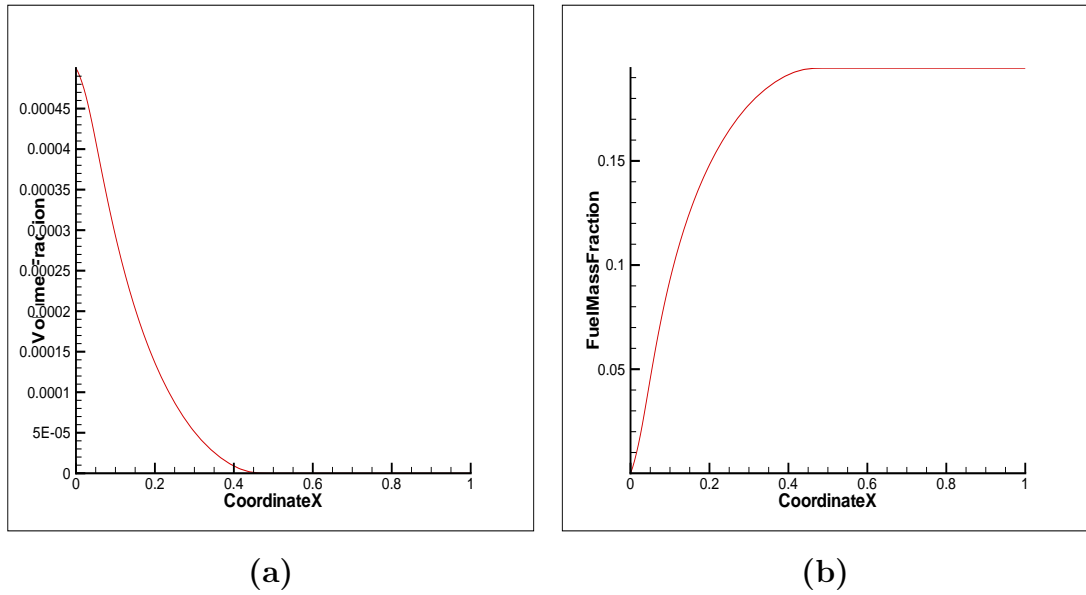


Figure 4.52: Case 7: Gas-droplet channel flow with $u_{gi} = 2.0$ and $u_{di} = 2.0$. (a) Variation of droplet-phase volume fraction, ϑ_d along the channel (b) Variation of evaporated fuel mass fraction, M_F along the channel

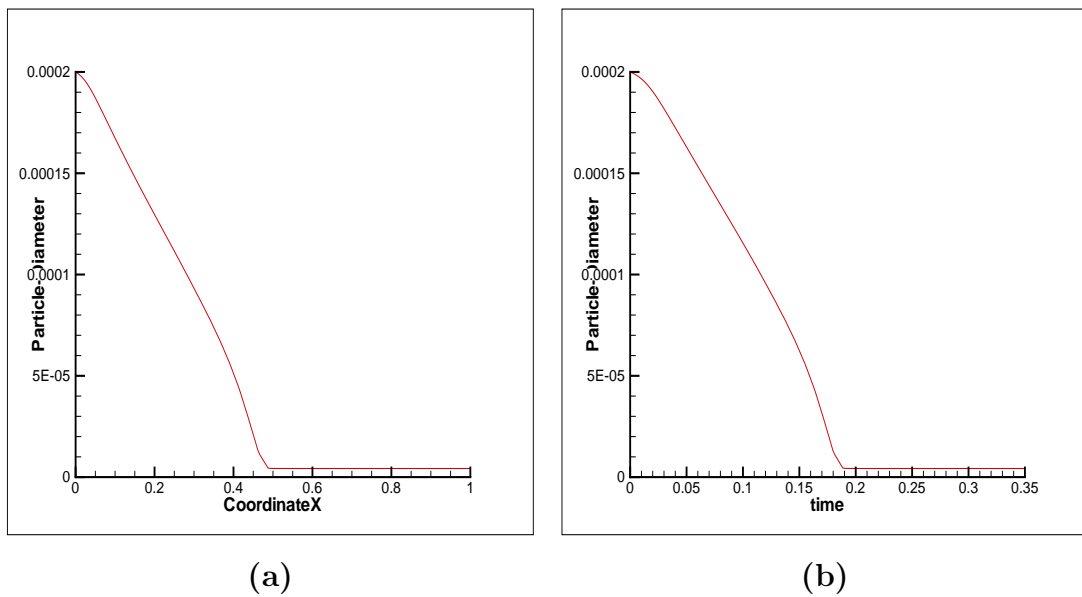


Figure 4.53: Case 7: Gas-droplet channel flow with $u_{gi} = 2.0$ and $u_{di} = 2.0$. (a) Variation of droplet-diameter, d_d along the channel (b) Variation of droplet-diameter, d_d , with time

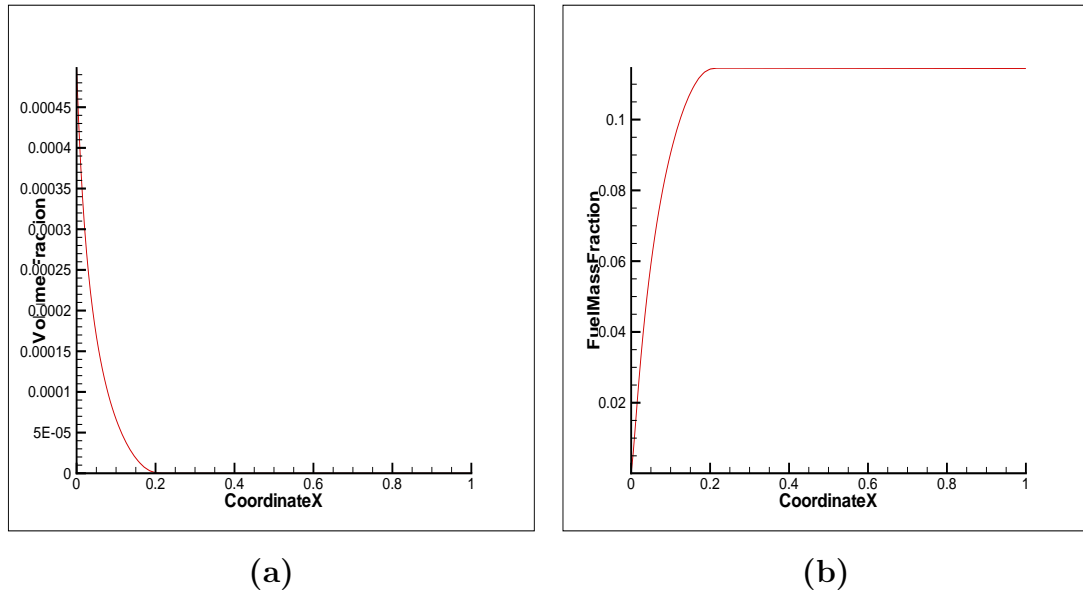


Figure 4.54: Case 7: Gas-droplet channel flow with $u_{gi} = 2.0$ and $u_{di} = 1.0$. (a) Variation of droplet-phase volume fraction, ϑ_d along the channel (b) Variation of evaporated fuel mass fraction, M_F along the channel

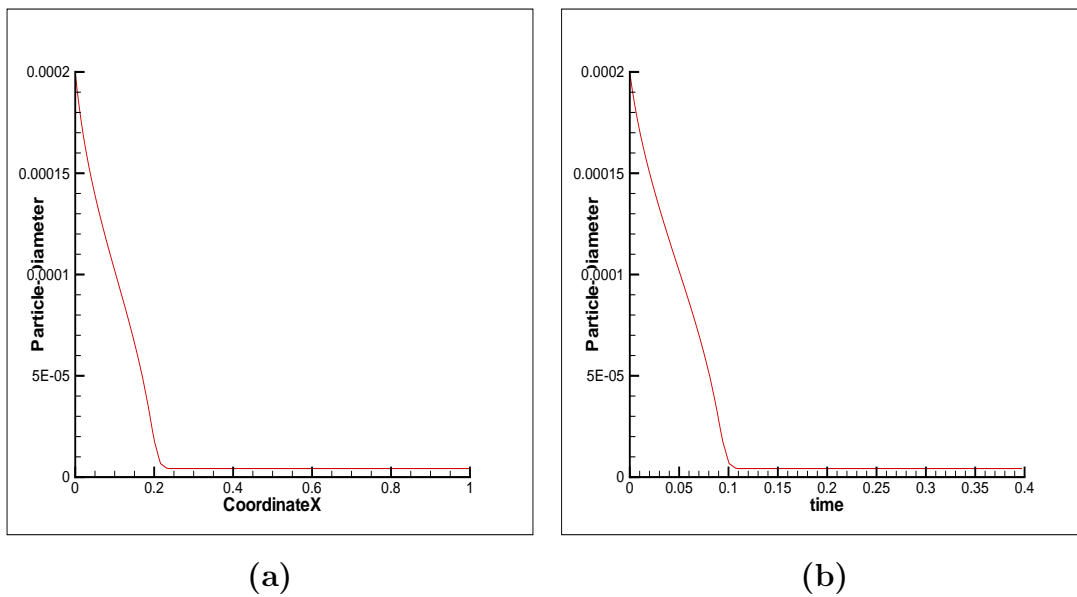


Figure 4.55: Case 7: Gas-droplet channel flow with $u_{gi} = 2.0$ and $u_{di} = 1.0$. (a) Variation of droplet-diameter, d_d along the channel (b) Variation of droplet-diameter, d_d , with time

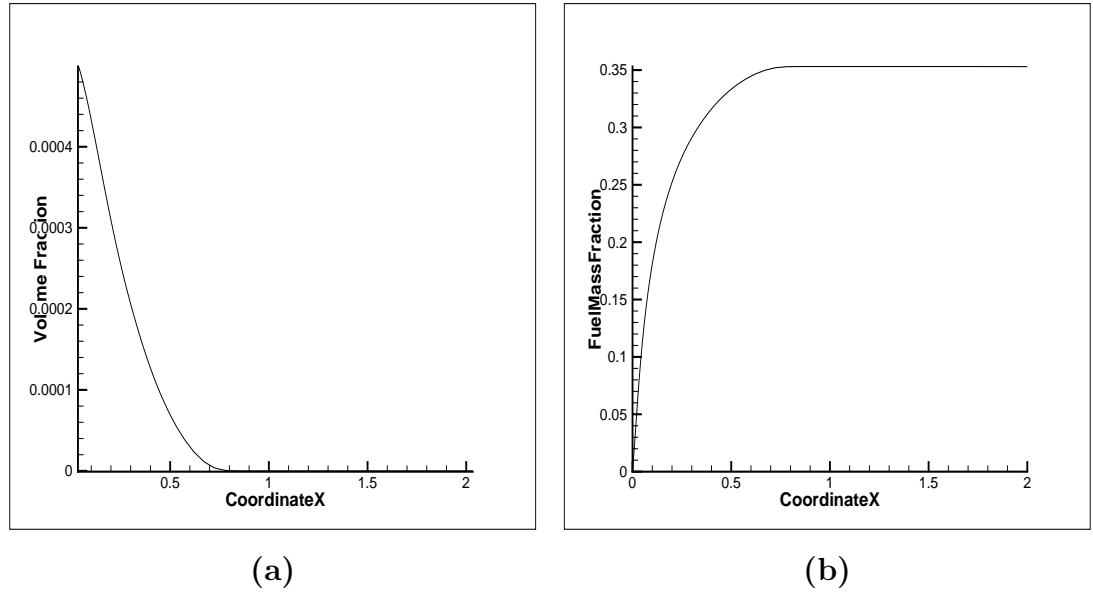


Figure 4.56: Case 7: Gas-droplet channel flow with $u_{gi} = 1.0$ and $u_{di} = 2.0$. (a) Variation of droplet-phase volume fraction, ϑ_d along the channel (b) Variation of evaporated fuel mass fraction, M_F along the channel

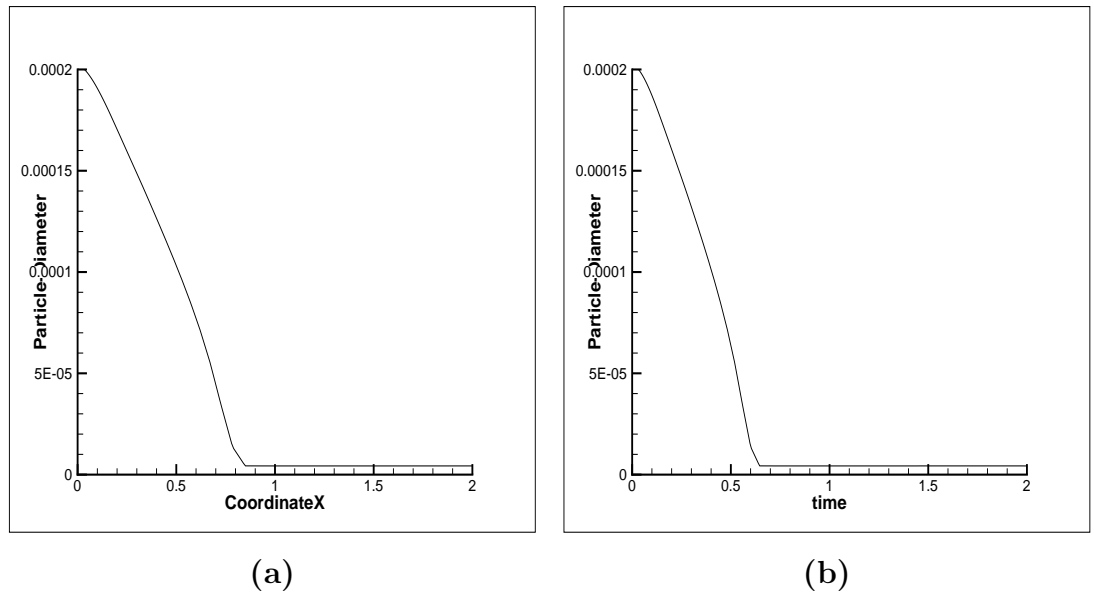


Figure 4.57: Case 7: Gas-droplet channel flow with $u_{gi} = 1.0$ and $u_{di} = 2.0$. (a) Variation of droplet-diameter, d_d along the channel (b) Variation of droplet-diameter, d_d , with time

4.1.9 Gas-droplet channel flow with dummy $Re = 200$ and $Ja = 2.784$

The inlet non-dimensionalized droplet temperature equal to 0 ($= 371.4\text{K}$). The non-dimensionalized saturation temperature of n-heptane, T_{sat} , is 0 ($= 371.4\text{ K}$) at atmospheric pressure. The inlet properties are given in Table. 4.9. At the wall, the homogeneous Neumann boundary condition is applied for gas-phase velocity and the gas-phase temperature. The latter condition means an insulated boundary condition is applied for temperature while the former implies friction-less ('slip') walls (to avoid friction-work) and ensures a uniform flow profile in the channel. Since we have applied constant (Ja), therefore, we apply non-dimensionalized Dirichlet boundary condition of 1 ($= 773.0\text{K}$) at both the walls for droplet-phase temperature. Since, the droplet inlet temperature is equal to the saturation temperature, no transient heating of the droplets takes place and the droplet temperature remains constant at its inlet value while the droplets evaporate due to heating. The conditions are such that the droplets evaporate totally by the end of the channel.

Table 4.9: Case 8: Inlet conditions

Inlet non dimensionlized conditions	
Gas-phase inlet temperature, T_{gi}	1($=773.0\text{ K}$)
Droplet-phase inlet temperature, T_{di}	0($=371.4\text{ K}$)
Inlet fuel mass fraction, M_{Fo}	0.0
Gas-phase inlet density, ρ_{gi}	1($=1.225\text{ kg/m}^3$)
Droplet-phase inlet volume fraction, ϑ_{do}	0.0005
Droplet inlet diameter, d_{do}	200

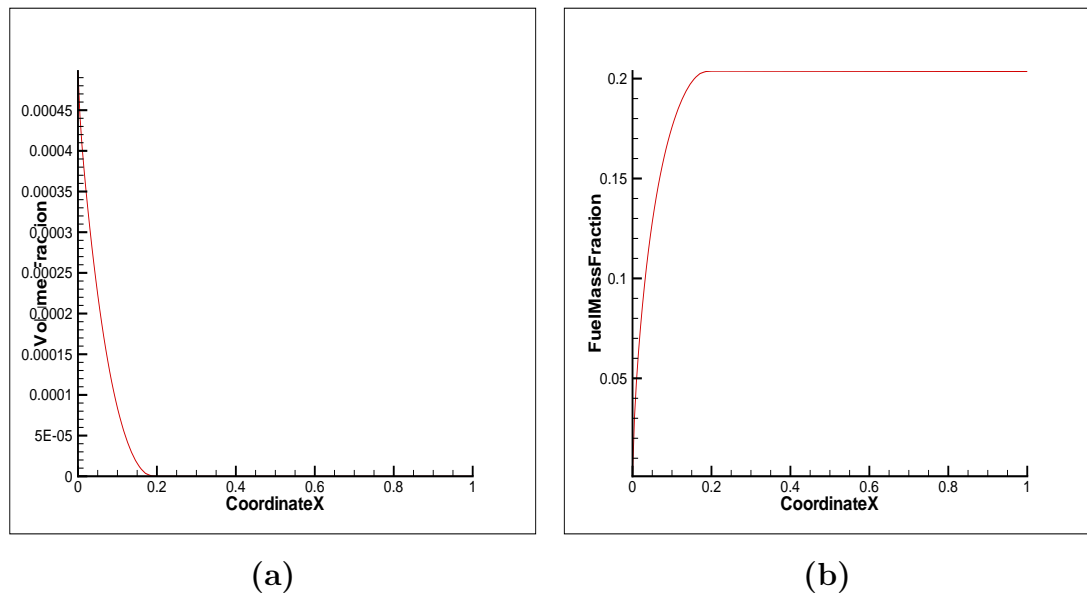


Figure 4.58: Case 8: Gas-droplet channel flow with $u_{gi} = 1.0$ and $u_{di} = 1.0$. (a) Variation of droplet-phase volume fraction, ϑ_d along the channel (b) Variation of evaporated fuel mass fraction, M_F along the channel

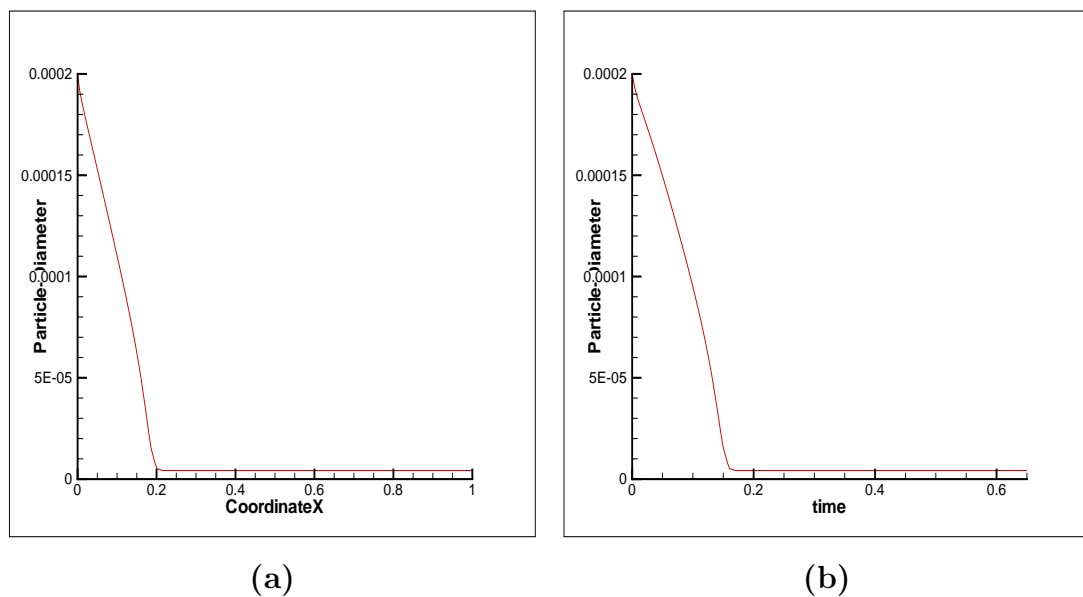


Figure 4.59: Case 8: Gas-droplet channel flow with $u_{gi} = 1.0$ and $u_{di} = 1.0$. (a) Variation of droplet-diameter, d_d along the channel (b) Variation of droplet-diameter, d_d , with time

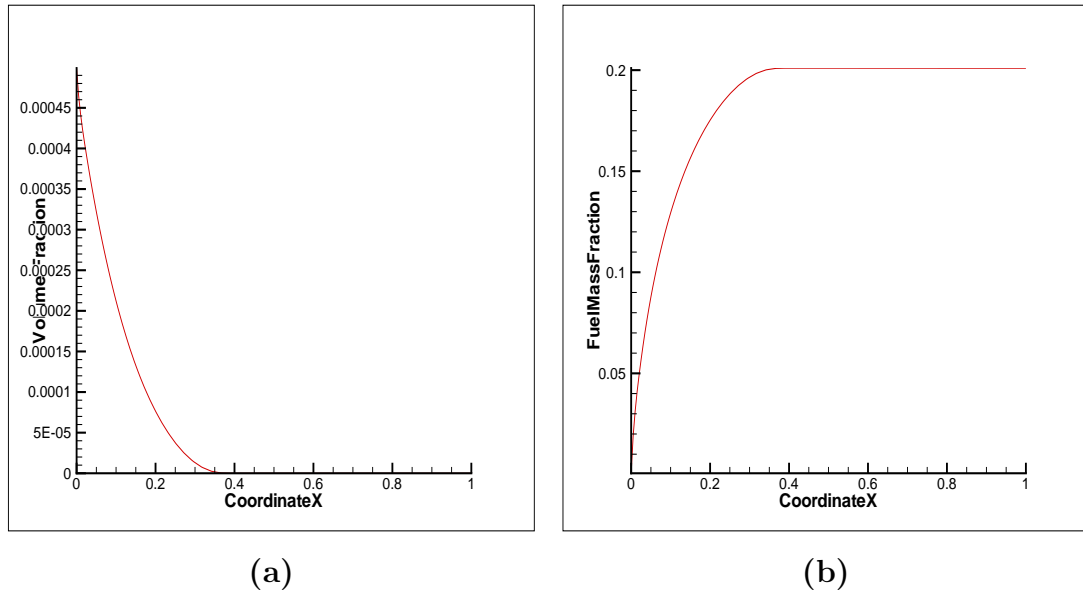


Figure 4.60: Case 8: Gas-droplet channel flow with $u_{gi} = 2.0$ and $u_{di} = 2.0$. (a) Variation of droplet-phase volume fraction, ϑ_d along the channel (b) Variation of evaporated fuel mass fraction, M_F along the channel

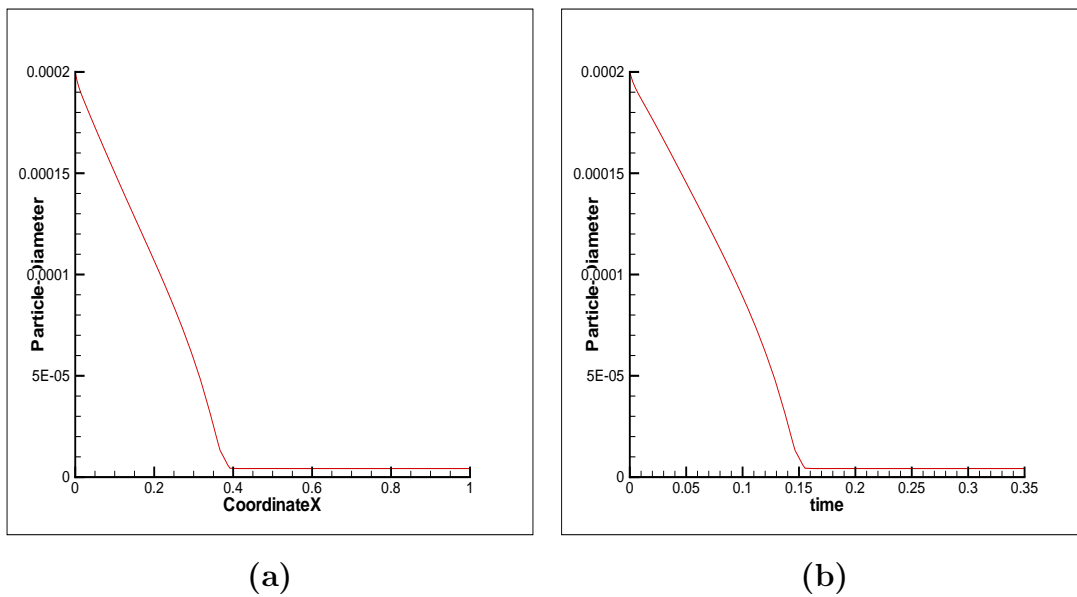


Figure 4.61: Case 8: Gas-droplet channel flow with $u_{gi} = 2.0$ and $u_{di} = 2.0$. (a) Variation of droplet-diameter, d_d along the channel (b) Variation of droplet-diameter, d_d , with time

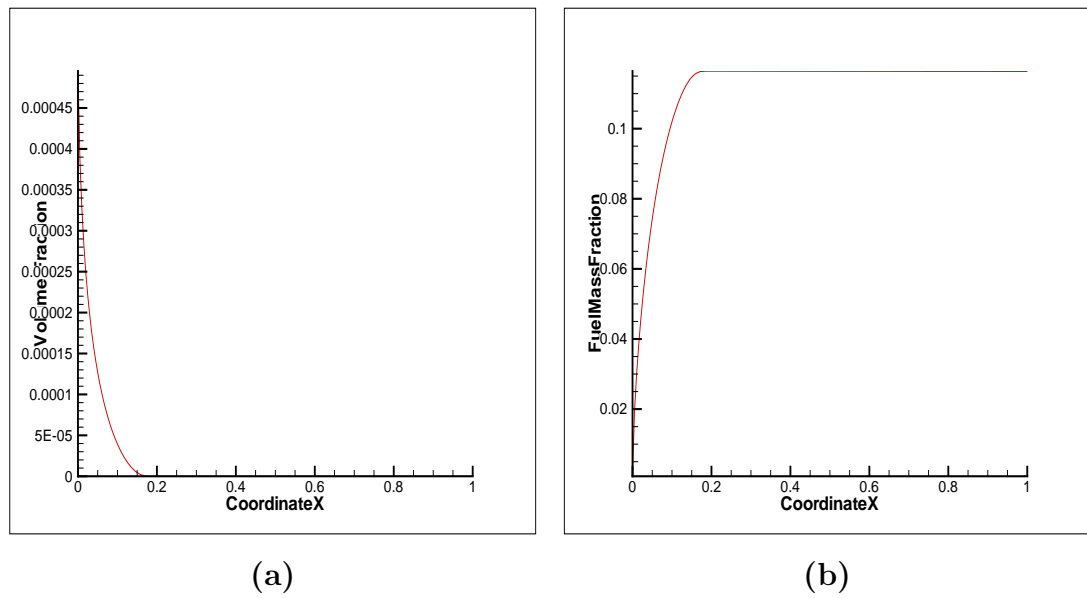


Figure 4.62: Case 8: Gas-droplet channel flow with $u_{gi} = 2.0$ and $u_{di} = 1.0$. (a) Variation of droplet-phase volume fraction, ϑ_d along the channel (b) Variation of evaporated fuel mass fraction, M_F along the channel

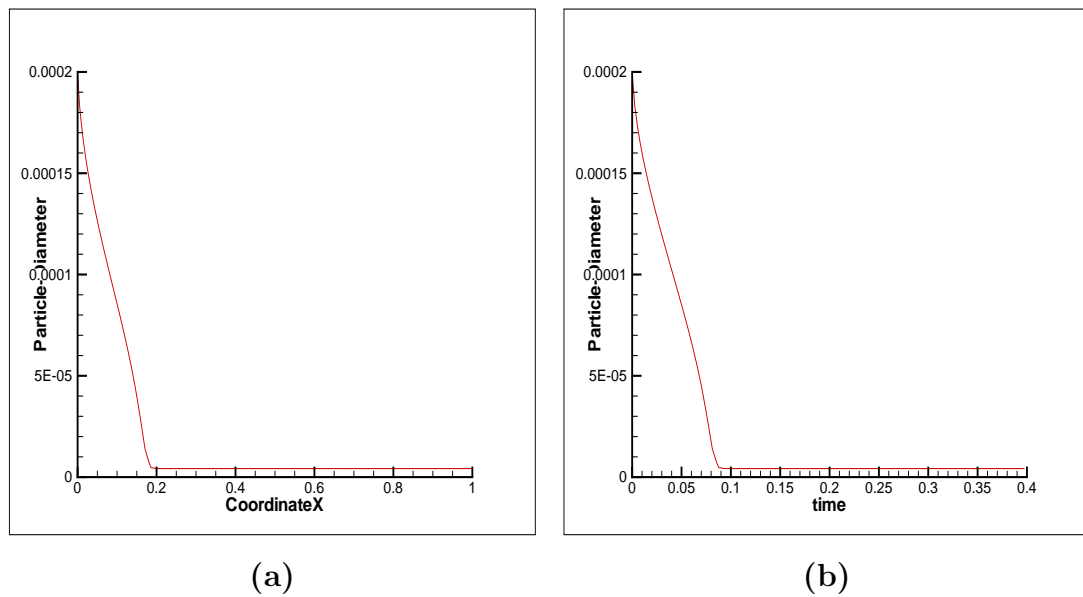


Figure 4.63: Case 8: Gas-droplet channel flow with $u_{gi} = 2.0$ and $u_{di} = 1.0$. (a) Variation of droplet-diameter, d_d along the channel (b) Variation of droplet-diameter, d_d , with time

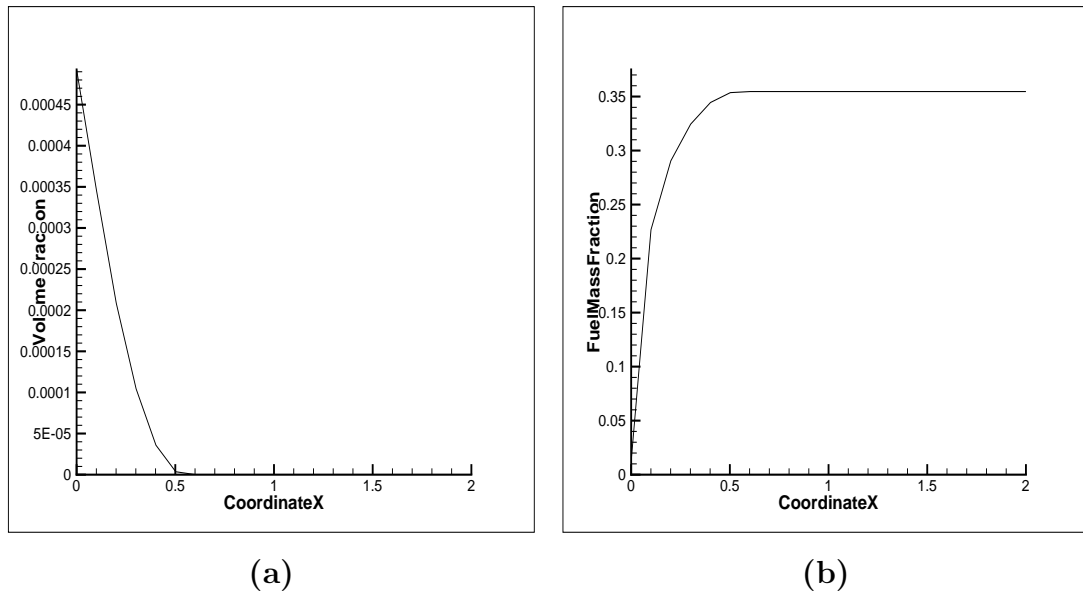


Figure 4.64: Case 8: Gas-droplet channel flow with $u_{gi} = 1.0$ and $u_{di} = 2.0$. (a) Variation of droplet-phase volume fraction, ϑ_d along the channel (b) Variation of evaporated fuel mass fraction, M_F along the channel

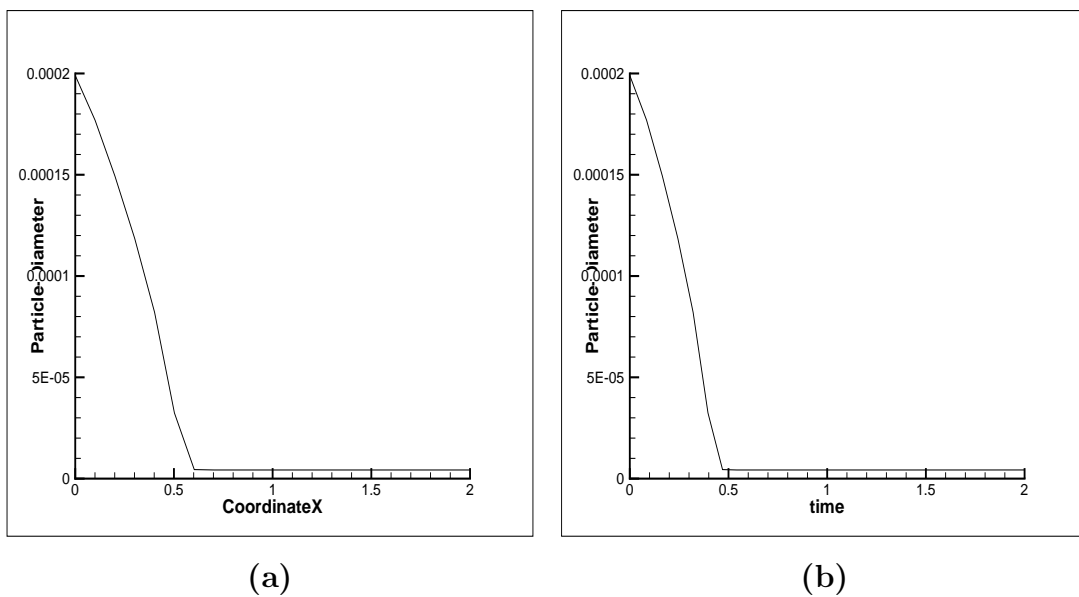


Figure 4.65: Case 8: Gas-droplet channel flow with $u_{gi} = 1.0$ and $u_{di} = 2.0$. (a) Variation of droplet-diameter, d_d along the channel (b) Variation of droplet-diameter, d_d , with time

4.1.10 Gas-droplet channel flow with dummy $Re = 200$ and $Ja = 0.5$

The inlet non-dimensionalized droplet temperature equal to 0 (= 300K). The non-dimensionalized saturation temperature of n-heptane, T_{sat} , is 1 (= 371.4 K) at atmospheric pressure. The inlet properties are given in Table. 4.10. At the wall, the homogeneous Neumann boundary condition is applied for gas-phase velocity and the gas-phase temperature. The latter condition means an insulated boundary condition is applied for temperature while the former implies friction-less ('slip') walls (to avoid friction-work) and ensures a uniform flow profile in the channel. Since we have applied constant (Ja), therefore, we apply non-dimensionalized Dirichlet boundary condition of 1 (= 371.4K) at both the walls for droplet-phase temperature. Since, the droplet inlet temperature is lower than the saturation temperature, transient heating of the droplets takes place.

Table 4.10: Case 9: Inlet conditions

Inlet non dimensionionized conditions	
Gas-phase inlet temperature, T_{gi}	1(=773.0 K)
Droplet-phase inlet temperature, T_{di}	0(=300.0 K)
Inlet fuel mass fraction, M_{Fo}	0.0
Gas-phase inlet density, ρ_{gi}	1(=1.225 kg/m ³)
Droplet-phase inlet volume fraction, ϑ_{do}	0.0005
Droplet inlet diameter, d_{do}	200

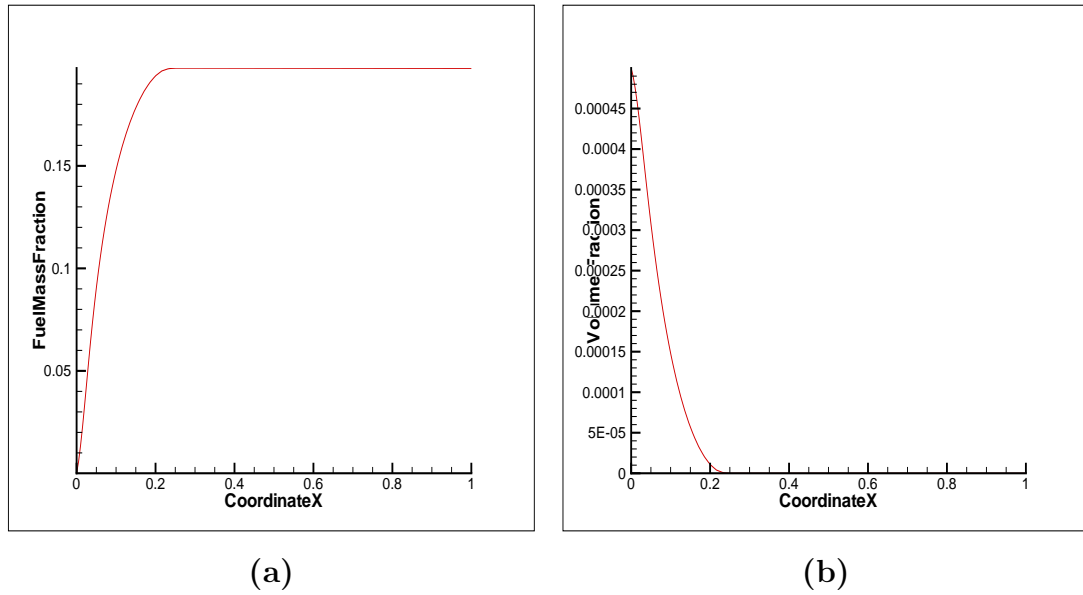


Figure 4.66: Case 9: Gas-droplet channel flow with $u_{gi} = 1.0$ and $u_{di} = 1.0$. (a) Variation of droplet-phase volume fraction, ϑ_d along the channel (b) Variation of evaporated fuel mass fraction, M_F along the channel

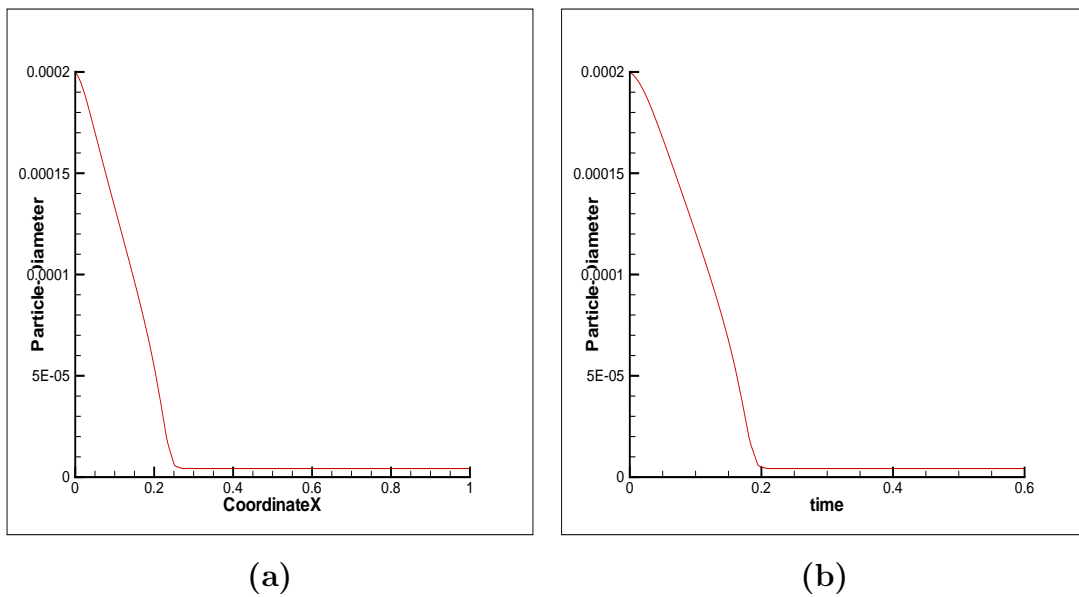


Figure 4.67: Case 9: Gas-droplet channel flow with $u_{gi} = 1.0$ and $u_{di} = 1.0$.(a) Variation of droplet-diameter, d_d along the channel (b) Variation of droplet-diameter, d_d , with time

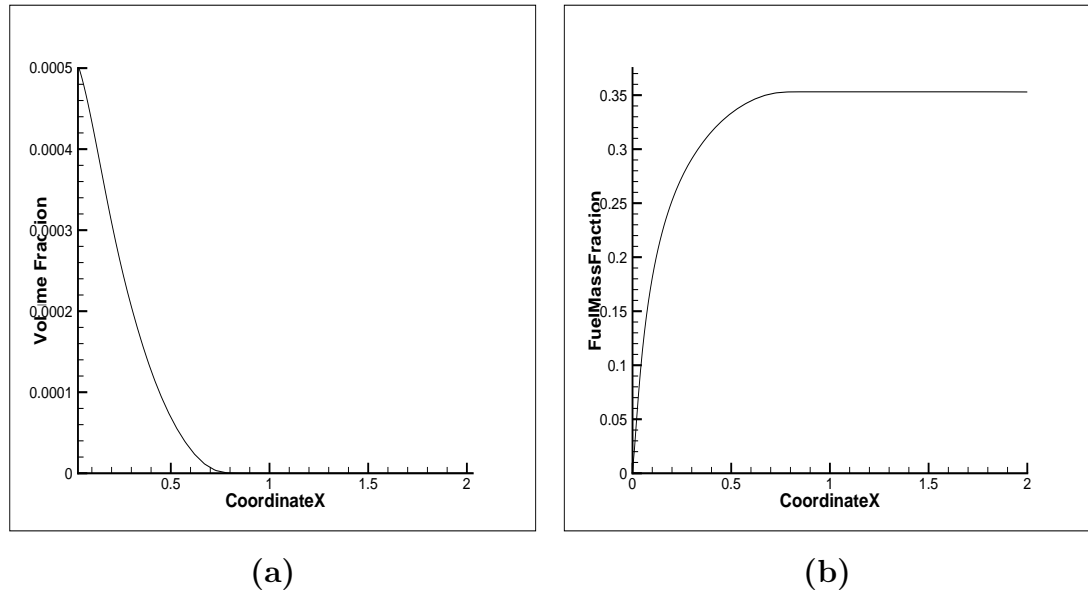


Figure 4.68: Case 9: Gas-droplet channel flow with $u_{gi} = 2.0$ and $u_{di} = 2.0$. (a) Variation of droplet-phase volume fraction, ϑ_d along the channel (b) Variation of evaporated fuel mass fraction, M_F along the channel

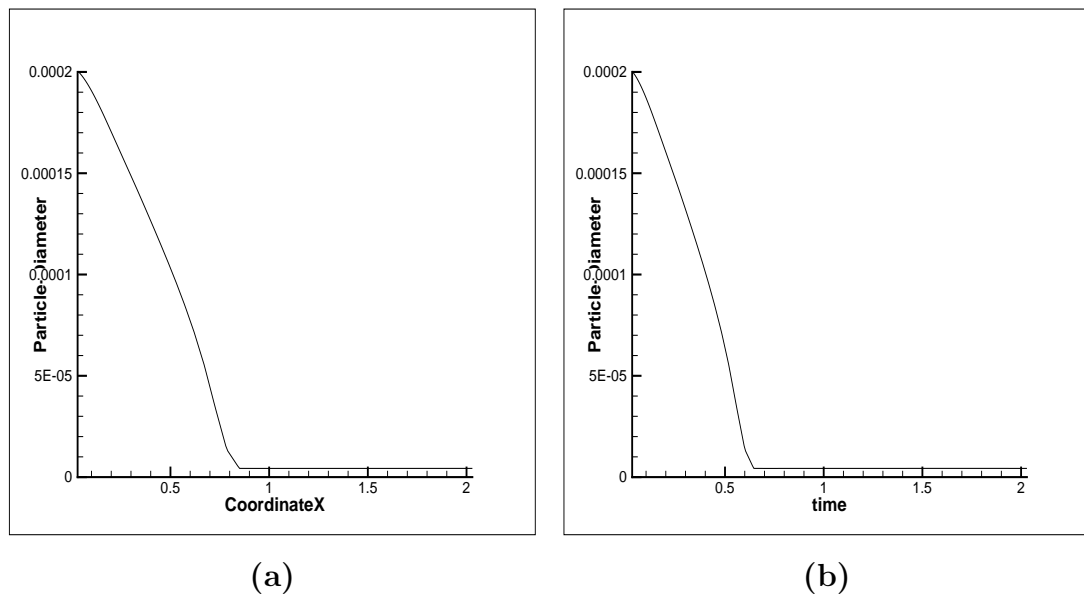


Figure 4.69: Case 9: Gas-droplet channel flow with $u_{gi} = 2.0$ and $u_{di} = 2.0$. (a) Variation of droplet-diameter, d_d along the channel (b) Variation of droplet-diameter, d_d , with time

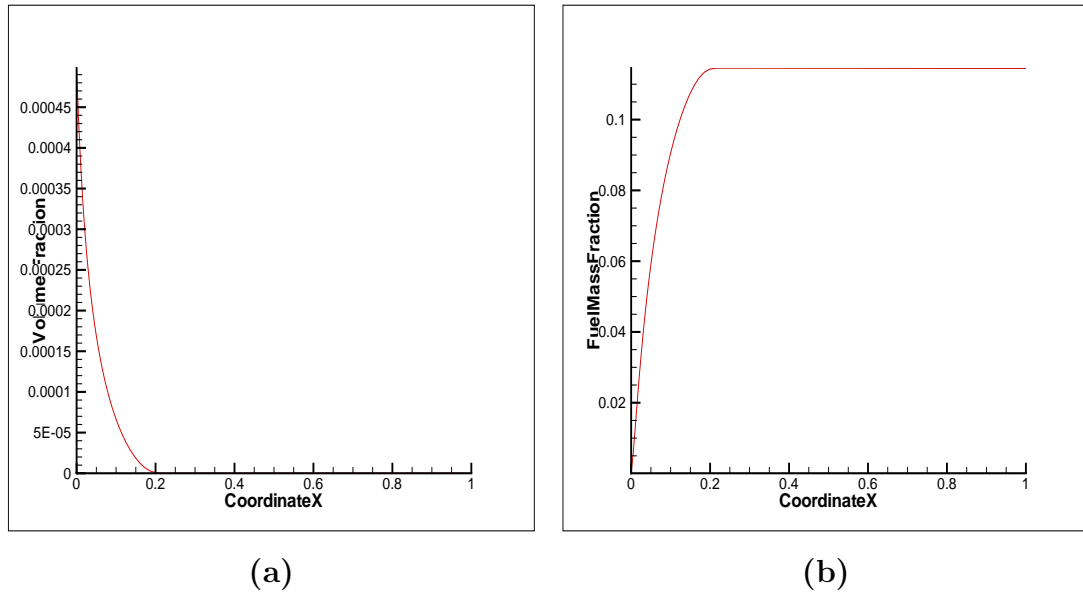


Figure 4.70: Case 9: Gas-droplet channel flow with $u_{gi} = 2.0$ and $u_{di} = 1.0$. (a) Variation of droplet-phase volume fraction, ϑ_d along the channel (b) Variation of evaporated fuel mass fraction, M_F along the channel

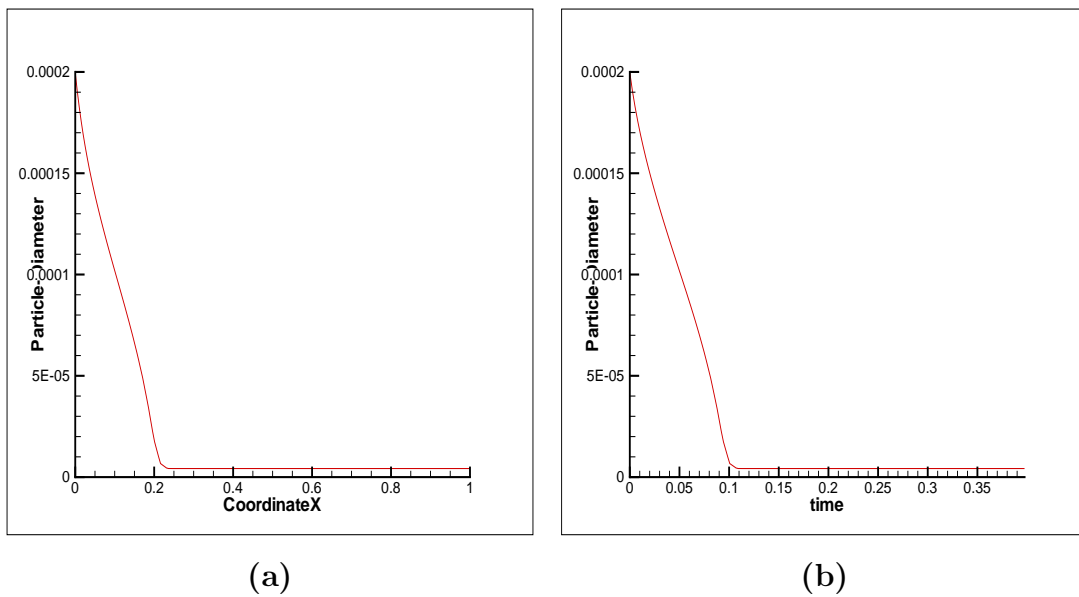


Figure 4.71: Case 9: Gas-droplet channel flow with $u_{gi} = 2.0$ and $u_{di} = 1.0$. (a) Variation of droplet-diameter, d_d along the channel (b) Variation of droplet-diameter, d_d , with time

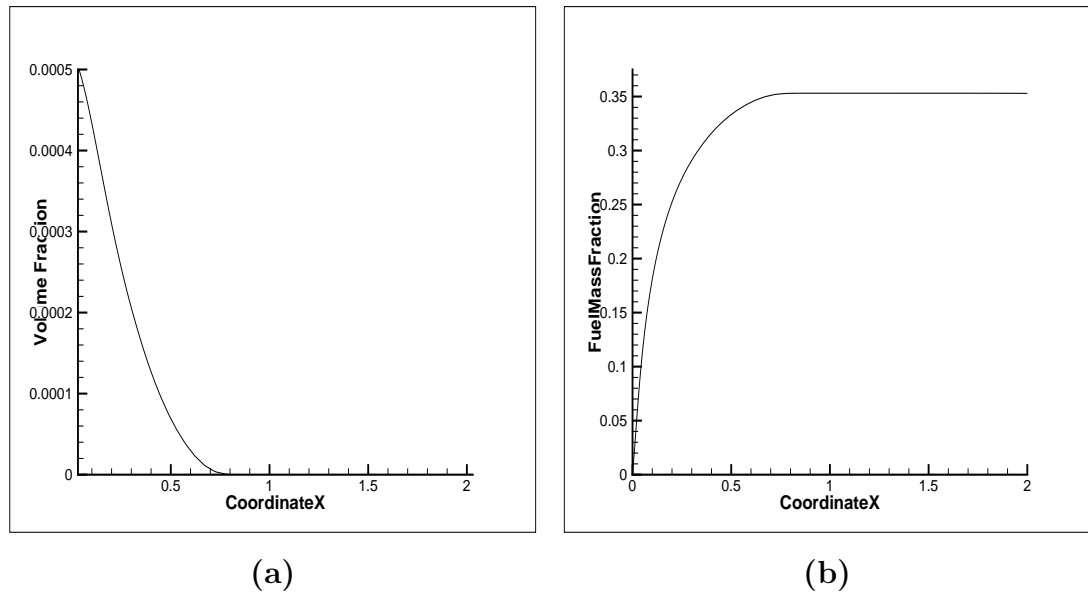


Figure 4.72: Case 9: Gas-droplet channel flow with $u_{gi} = 1.0$ and $u_{di} = 2.0$. (a) Variation of droplet-phase volume fraction, ϑ_d along the channel (b) Variation of evaporated fuel mass fraction, M_F along the channel

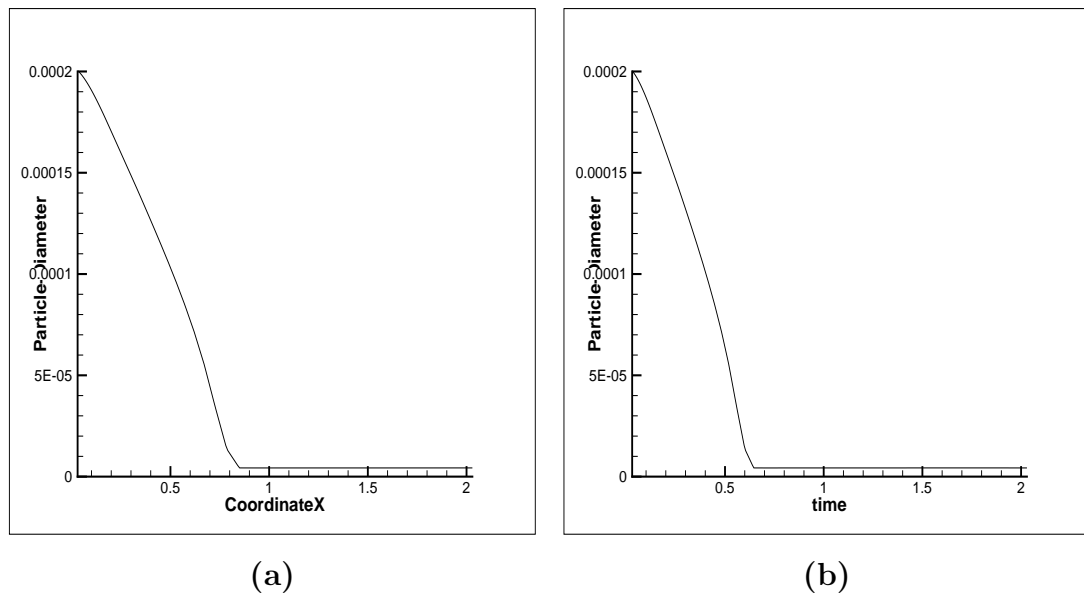


Figure 4.73: Case 9: Gas-droplet channel flow with $u_{gi} = 1.0$ and $u_{di} = 2.0$. (a) Variation of droplet-diameter, d_d along the channel (b) Variation of droplet-diameter, d_d , with time

4.1.11 Gas-droplet channel flow with dummy $Re = 100$ and $Ja = 3.071$

The inlet non-dimensionalized droplet temperature equal to 0 ($= 300\text{K}$).The non-dimensionalized saturation temperature of n-heptane, T_{sat} , is 0.16117 ($= 371.4 \text{ K}$) at atmospheric pressure. The inlet properties are given in Table. 4.11. At the wall, the homogeneous Neumann boundary condition is applied for gas-phase velocity .This condition means friction-less ('slip') walls (to avoid friction-work) and ensures a uniform flow profile in the channel.Since we have applied constant (Ja) therefore we apply non-dimensionalized Dirichlett boundary condition of 1 ($= 773.0\text{K}$) at both the walls for gas-phase temperature and droplet-phase temperature. Since, the droplet inlet temperature is lower than the saturation temperature, transient heating of the droplets takes place. The conditions are such that the droplets evaporate totally by the end of the channel.

Table 4.11: Case 10: Inlet conditions

Inlet non dimenstionlized conditions	
Gas-phase inlet temperature, T_{gi}	1($=773.0 \text{ K}$)
Droplet-phase inlet temperature, T_{di}	0($=300.0 \text{ K}$)
Inlet fuel mass fraction, M_{F_o}	0.0
Gas-phase inlet density, ρ_{gi}	1($=1.225 \text{ kg/m}^3$)
Droplet-phase inlet volume fraction, ϑ_{do}	0.0005
Droplet inlet diameter, d_{do}	100

4.1.12 Gas-droplet channel flow with dummy $Re = 100$ and $Ja = 2.784$

The inlet non-dimensionalized droplet temperature equal to 0 ($= 371.4\text{K}$).The non-dimensionalized saturation temperature of n-heptane, T_{sat} , is 0 ($= 371.4 \text{ K}$) at atmospheric pressure. The inlet properties are given in Table. 4.12. At the wall, the homogeneous Neumann boundary condition is applied for gas-phase velocity and the gas-phase temperature .The latter condition means an insulated boundary condition is applied for temperature while the former implies friction-less ('slip') walls (to avoid

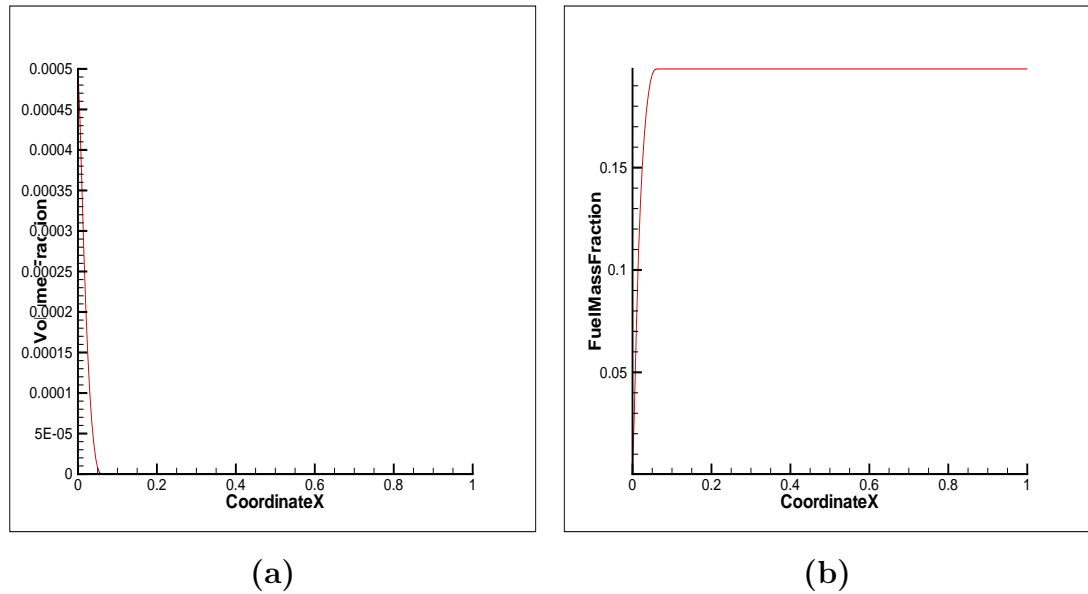


Figure 4.74: Case 10: Gas-droplet channel flow with $u_{gi} = 1.0$ and $u_{di} = 1.0$. (a) Variation of droplet-phase volume fraction, ϑ_d along the channel (b) Variation of evaporated fuel mass fraction, M_F along the channel

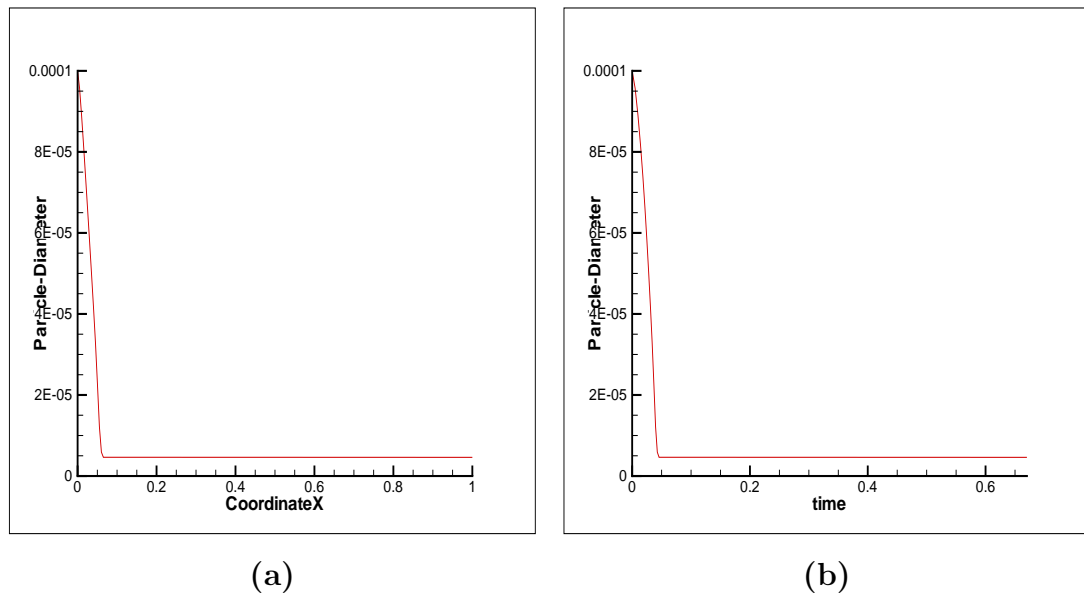


Figure 4.75: Case 10: Gas-droplet channel flow with $u_{gi} = 1.0$ and $u_{di} = 1.0$. (a) Variation of droplet-diameter, d_d along the channel (b) Variation of droplet-diameter, d_d , with time

friction-work) and ensures a uniform flow profile in the channel. Since we have applied

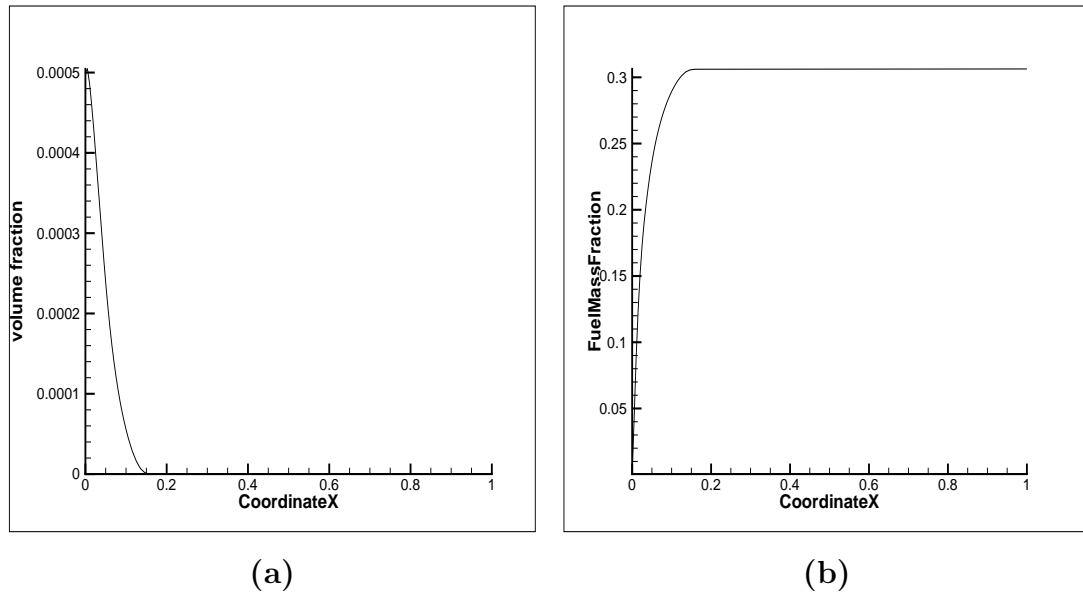


Figure 4.76: Case 10: Gas-droplet channel flow with $u_{gi} = 1.0$ and $u_{di} = 2.0$. (a) Variation of droplet-phase volume fraction, ϑ_d along the channel (b) Variation of evaporated fuel mass fraction, M_F along the channel

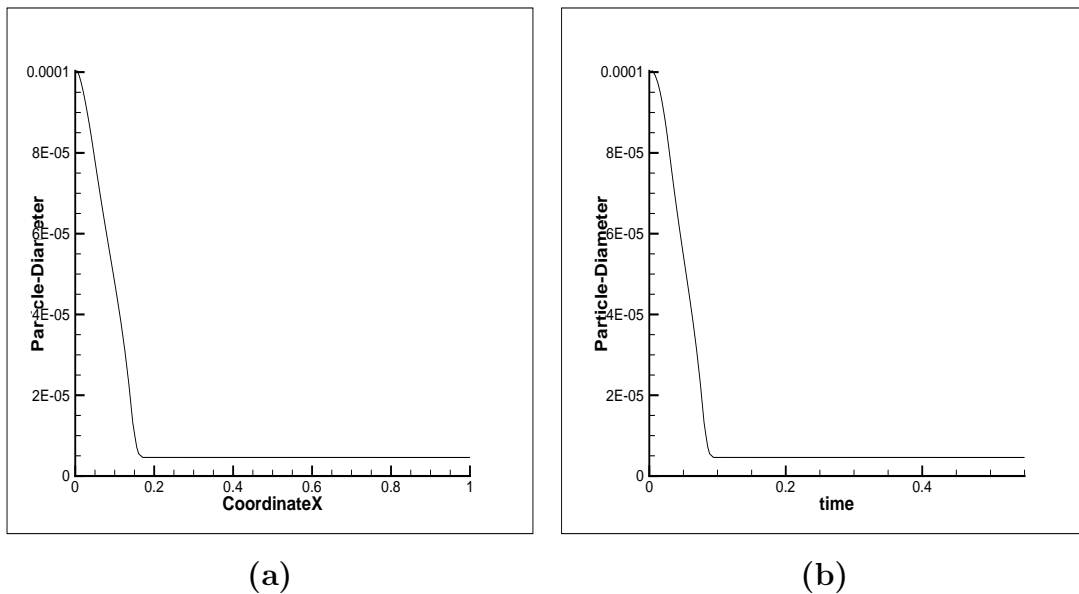


Figure 4.77: Case 10: Gas-droplet channel flow with $u_{gi} = 1.0$ and $u_{di} = 2.0$. (a) Variation of droplet-diameter, d_d along the channel (b) Variation of droplet-diameter, d_d , with time

constant (Ja), therefore, we apply non-dimensionalized Dirichlet boundary condition

of 1(= 773.0K) at both the walls for droplet-phase temperature. Since, the droplet inlet temperature is equal to the saturation temperature, no transient heating of the droplets takes place and the droplet temperature remains constant at its inlet value while the droplets evaporate due to heating. The conditions are such that the droplets evaporate totally by the end of the channel.

Table 4.12: Case 11: Inlet conditions

Inlet non dimensionstionized conditions	
Gas-phase inlet temperature, T_{gi}	1(=773.0 K)
Droplet-phase inlet temperature, T_{di}	0(=371.4 K)
Inlet fuel mass fraction, M_{Fo}	0.0
Gas-phase inlet density, ρ_{gi}	1(=1.225 kg/m ³)
Droplet-phase inlet volume fraction, ϑ_{do}	0.0005
Droplet inlet diameter, d_{do}	100

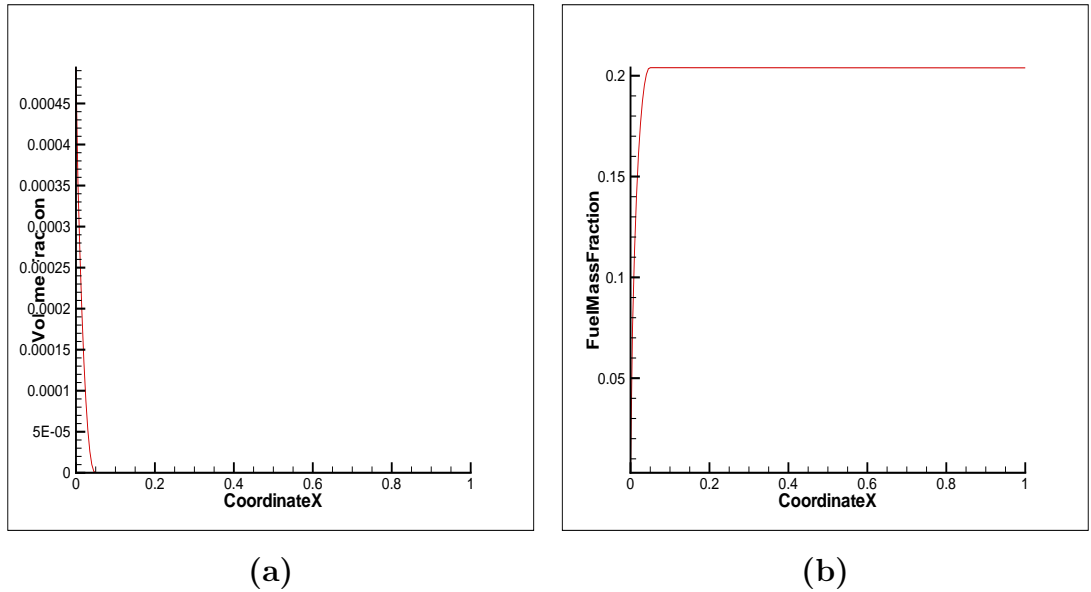


Figure 4.78: Case 11: Gas-droplet channel flow with $u_{gi} = 1.0$ and $u_{di} = 1.0$. (a) Variation of droplet-phase volume fraction, ϑ_d along the channel (b)Variation of evaporated fuel mass fraction, M_F along the channel

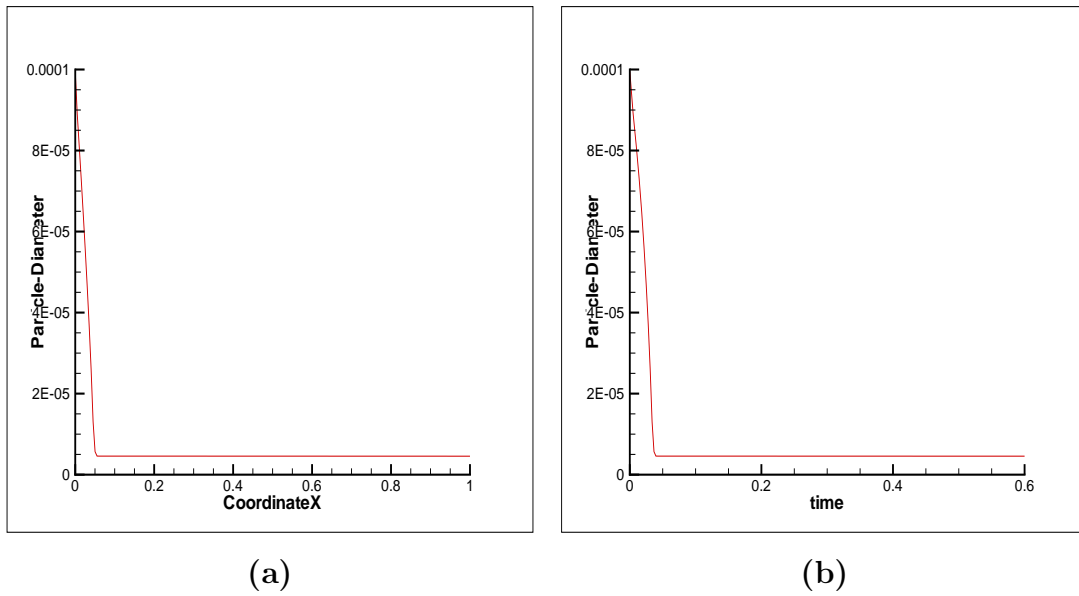


Figure 4.79: Case 11: Gas-droplet channel flow with $u_{gi} = 1.0$ and $u_{di} = 1.0$. (a) Variation of droplet-diameter, d_d along the channel (b) Variation of droplet-diameter, d_d , with time

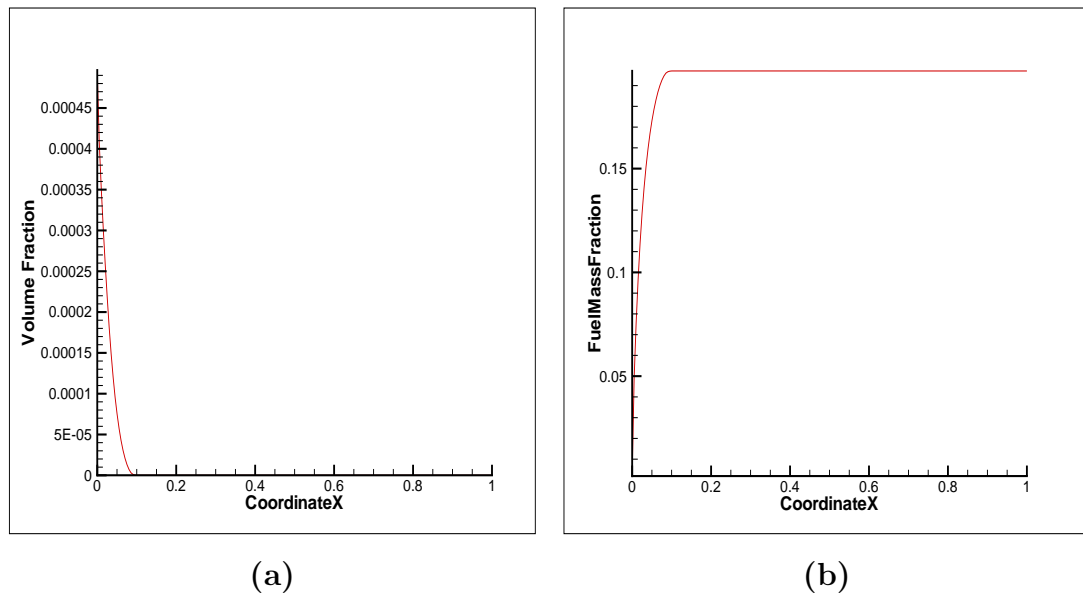


Figure 4.80: Case 11: Gas-droplet channel flow with $u_{gi} = 2.0$ and $u_{di} = 2.0$. (a) Variation of droplet-phase volume fraction, ϑ_d along the channel (b) Variation of evaporated fuel mass fraction, M_F along the channel

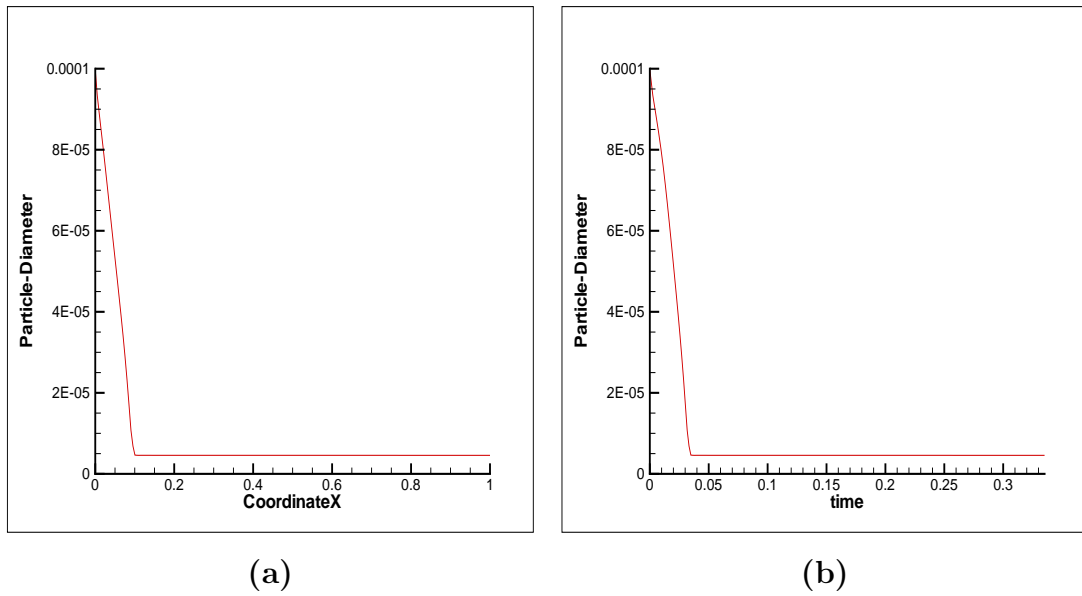


Figure 4.81: Case 11: Gas-droplet channel flow with $u_{gi} = 2.0$ and $u_{di} = 2.0$. (a) Variation of droplet-diameter, d_d along the channel (b) Variation of droplet-diameter, d_d , with time

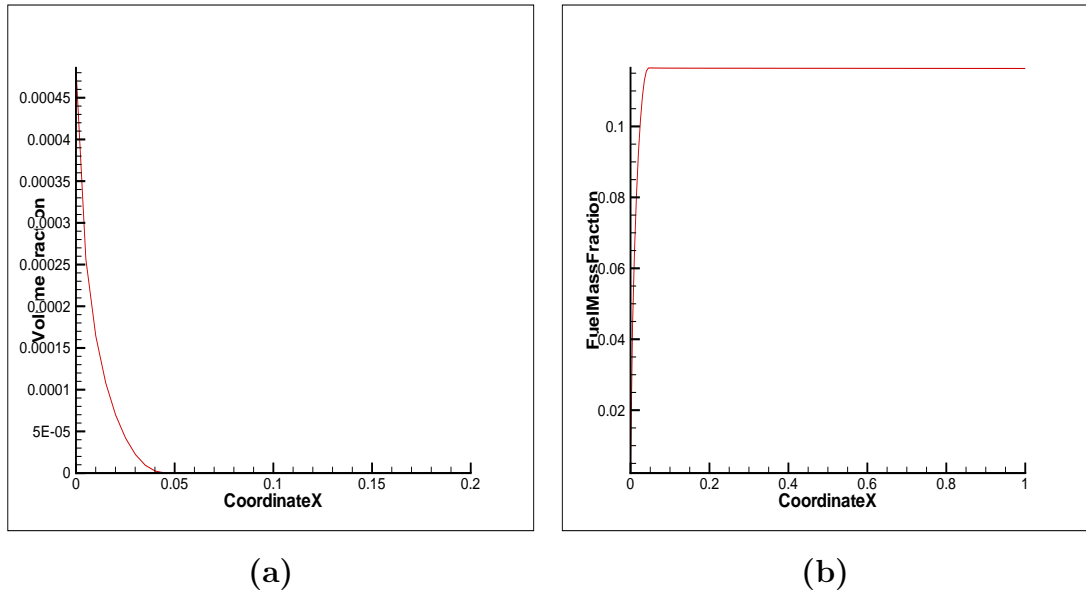


Figure 4.82: Case 11: Gas-droplet channel flow with $u_{gi} = 2.0$ and $u_{di} = 1.0$. (a) Variation of droplet-phase volume fraction, ϑ_d along the channel (b) Variation of evaporated fuel mass fraction, M_F along the channel

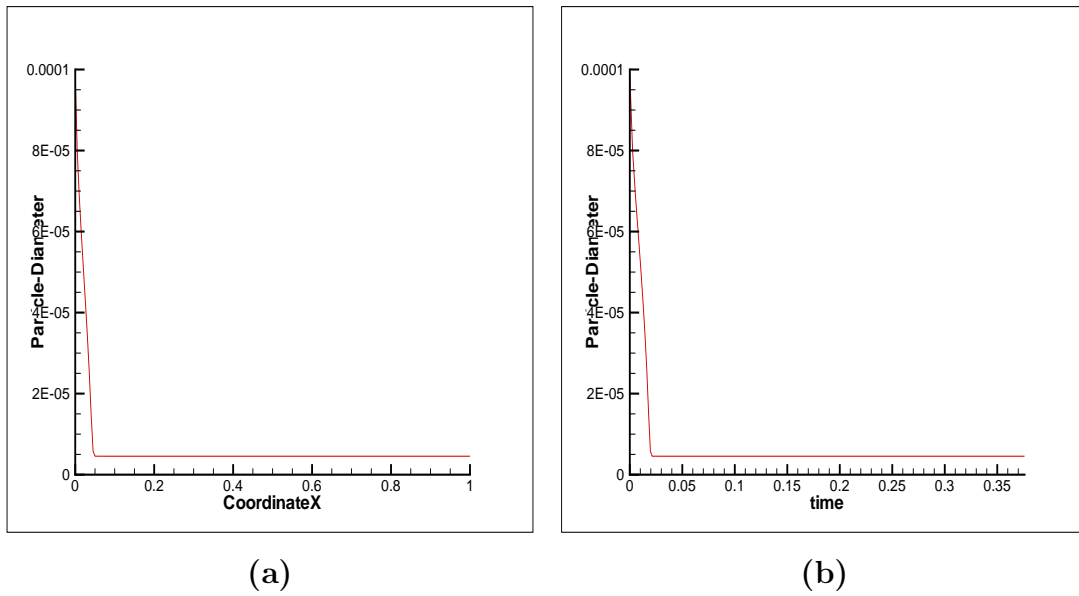


Figure 4.83: Case 11: Gas-droplet channel flow with $u_{gi} = 2.0$ and $u_{di} = 1.0$. (a) Variation of droplet-diameter, d_d along the channel (b) Variation of droplet-diameter, d_d , with time

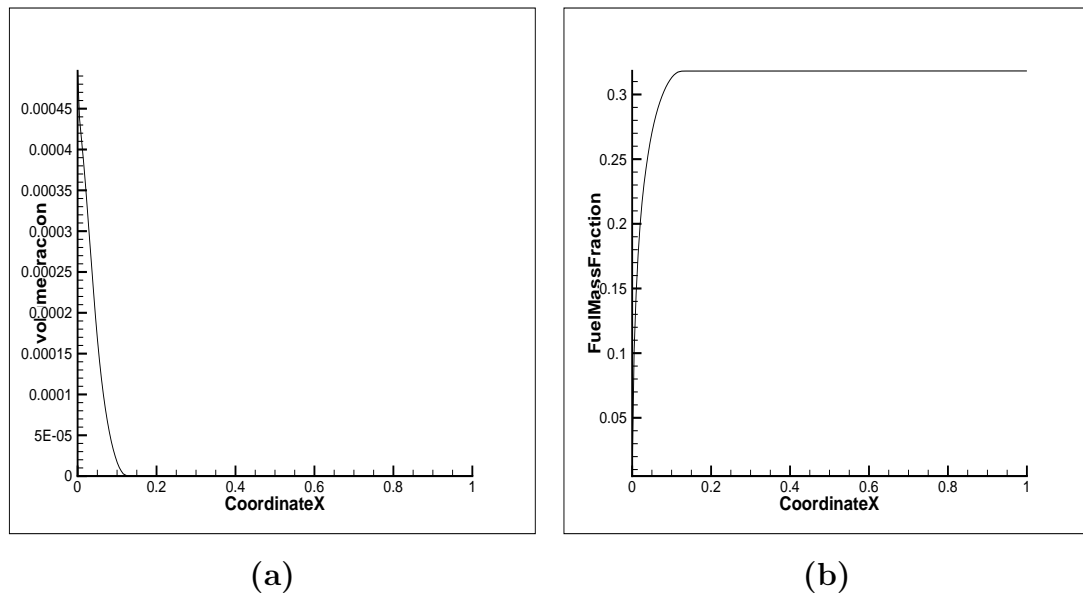


Figure 4.84: Case 11: Gas-droplet channel flow with $u_{gi} = 1.0$ and $u_{di} = 2.0$. (a) Variation of droplet-phase volume fraction, ϑ_d along the channel (b) Variation of evaporated fuel mass fraction, M_F along the channel

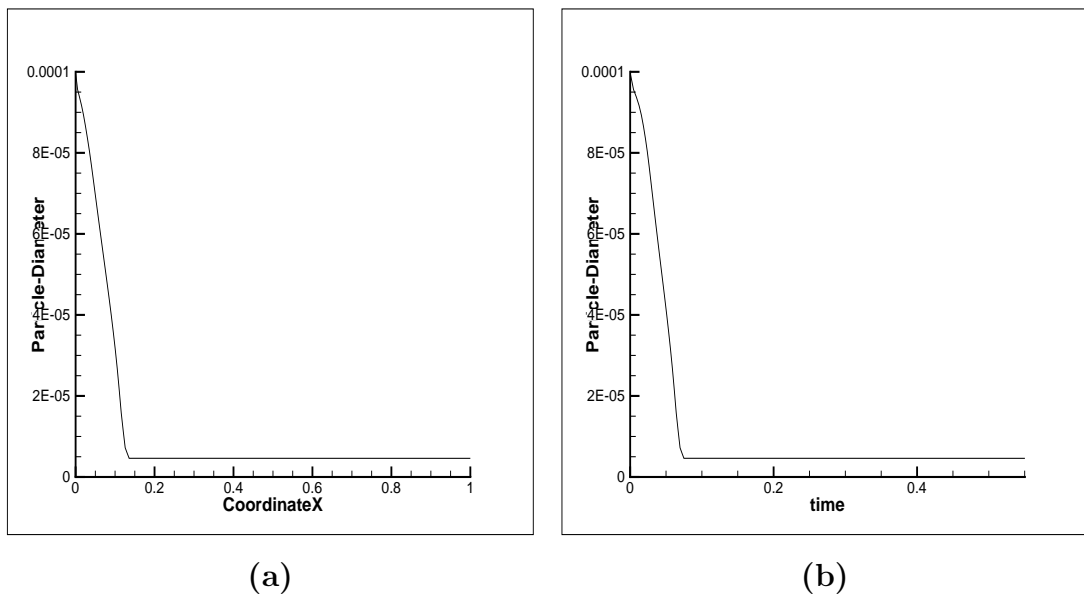


Figure 4.85: Case 11: Gas-droplet channel flow with $u_{gi} = 1.0$ and $u_{di} = 2.0$. (a) Variation of droplet-diameter, d_d along the channel (b) Variation of droplet-diameter, d_d , with time

4.1.13 Gas-droplet channel flow with dummy $Re = 100$ and $Ja = 0.5$

The inlet droplet non-dimensionalized temperature equal to 0 (= 300K). The non-dimensionalized saturation temperature of n-heptane, T_{sat} , is 1 (= 371.4 K) at atmospheric pressure. The inlet properties are given in Table 4.13. At the wall, the homogeneous Neumann boundary condition is applied for gas-phase velocity and the gas-phase temperature. The latter condition means an insulated boundary condition is applied for temperature while the former implies friction-less ('slip') walls (to avoid friction-work) and ensures a uniform flow profile in the channel. Since we have applied constant (Ja), therefore, we apply non-dimensionalized Dirichlet boundary condition of 1 (= 371.4K) at both the walls for droplet-phase temperature. Since, the droplet inlet temperature is lower than the saturation temperature, transient heating of the droplets takes place.

Table 4.13: Case 12: Inlet conditions

Inlet non dimensionlized conditions	
Gas-phase inlet temperature, T_{gi}	1(=773.0 K)
Droplet-phase inlet temperature, T_{di}	0(=300.0 K)
Inlet fuel mass fraction, M_{F_o}	0.0
Gas-phase inlet density, ρ_{gi}	1(=1.225 kg/m ³)
Droplet-phase inlet volume fraction, ϑ_{do}	0.0005
Droplet inlet diameter, d_{do}	100

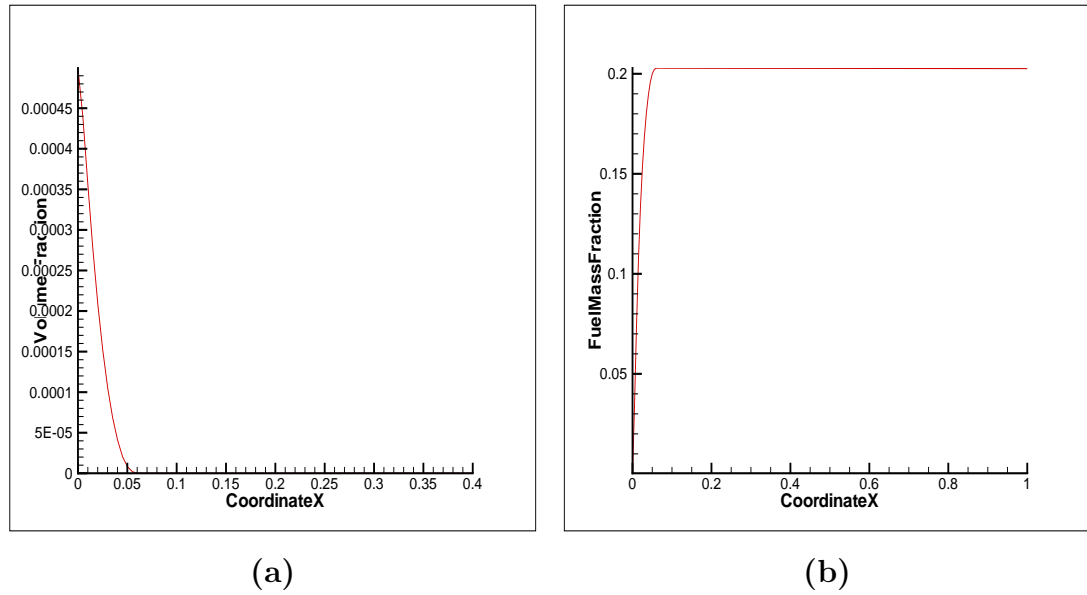


Figure 4.86: Case 12:Gas-droplet channel flow with $u_{gi} = 1.0$ and $u_{di} = 1.0$. (a) Variation of droplet-phase volume fraction, ϑ_d along the channel (b) Variation of evaporated fuel mass fraction, M_F along the channel

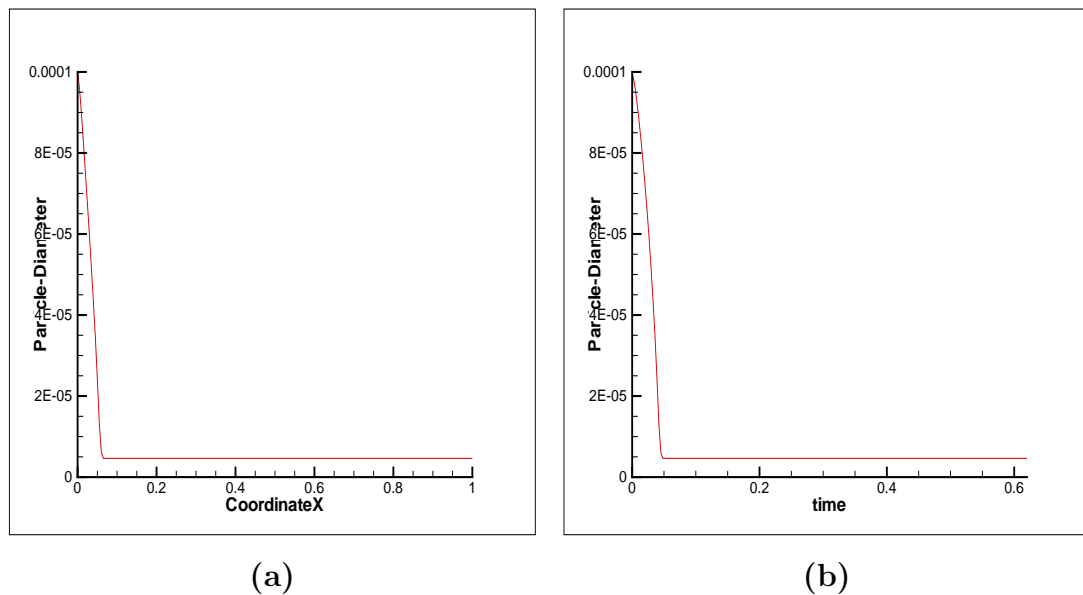


Figure 4.87: Case 12:Gas-droplet channel flow with $u_{gi} = 1.0$ and $u_{di} = 1.0$.(a) Variation of droplet-diameter, d_d along the channel (b) Variation of droplet-diameter, d_d , with time

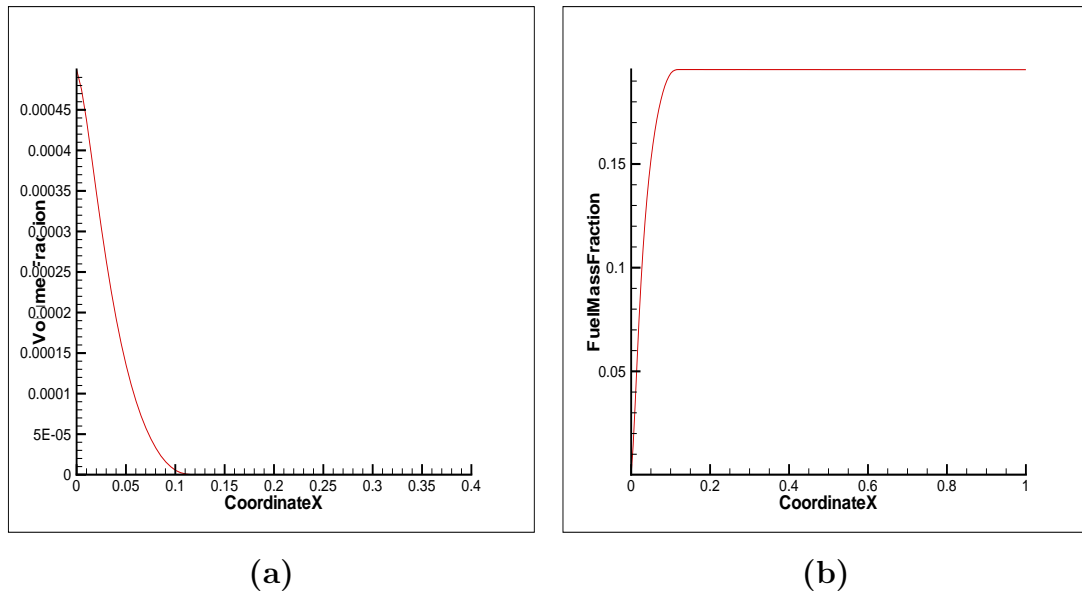


Figure 4.88: Case 12: Gas-droplet channel flow with $u_{gi} = 2.0$ and $u_{di} = 2.0$. (a) Variation of droplet-phase volume fraction, ϑ_d along the channel (b) Variation of evaporated fuel mass fraction, M_F along the channel

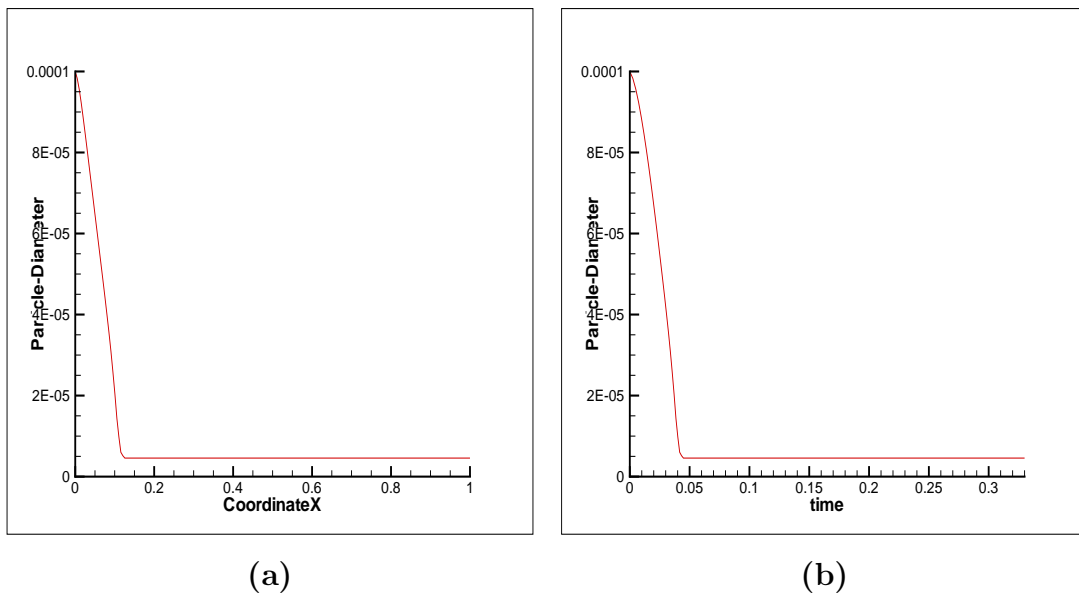


Figure 4.89: Case 12: Gas-droplet channel flow with $u_{gi} = 2.0$ and $u_{di} = 2.0$. (a) Variation of droplet-diameter, d_d along the channel (b) Variation of droplet-diameter, d_d , with time

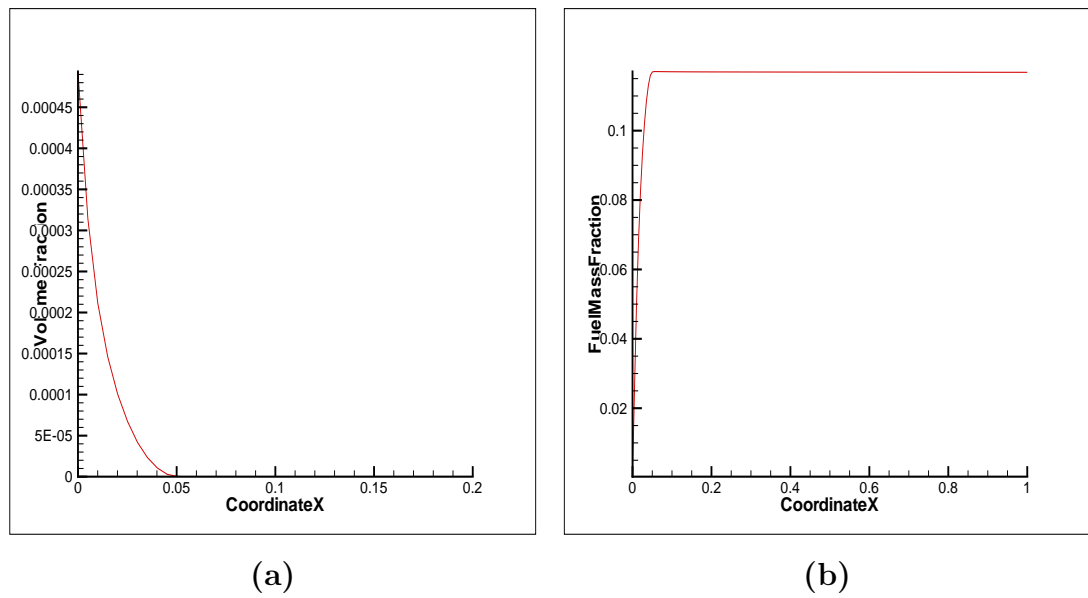


Figure 4.90: Case 12: Gas-droplet channel flow with $u_{gi} = 2.0$ and $u_{di} = 1.0$. (a) Variation of droplet-phase volume fraction, ϑ_d along the channel (b) Variation of evaporated fuel mass fraction, M_F along the channel

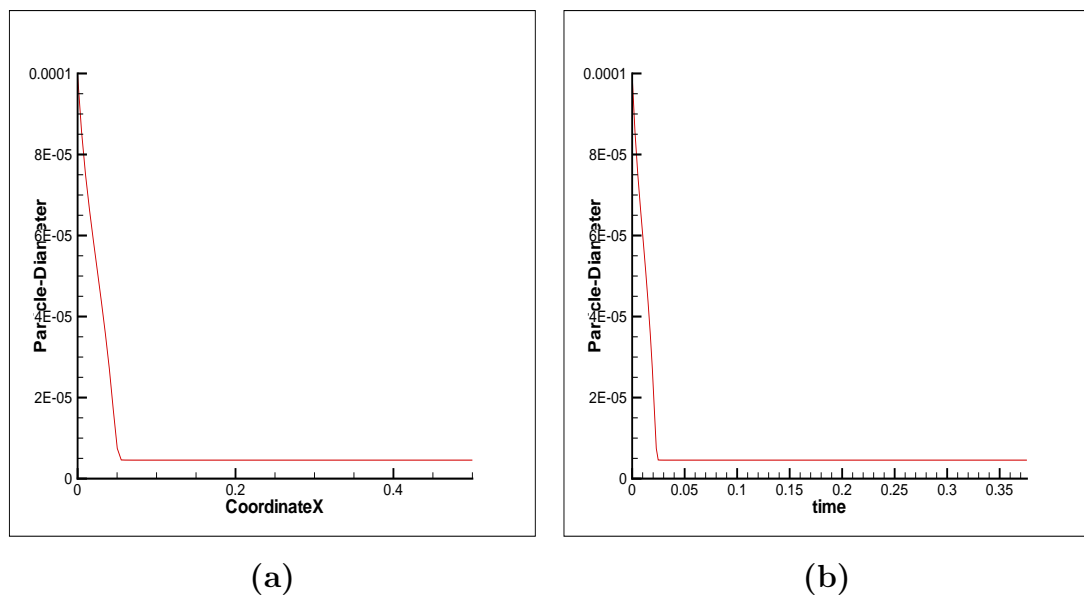


Figure 4.91: Case 12 : Gas-droplet channel flow with $u_{gi} = 2.0$ and $u_{di} = 1.0$. (a) Variation of droplet-diameter, d_d along the channel (b) Variation of droplet-diameter, d_d , with time

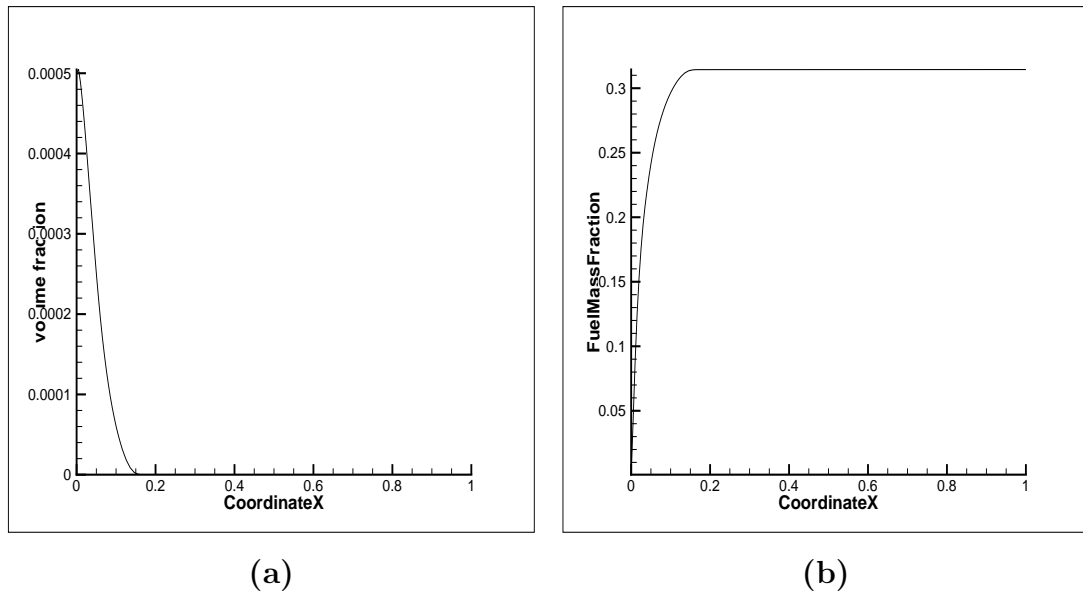


Figure 4.92: Case 12: Gas-droplet channel flow with $u_{gi} = 1.0$ and $u_{di} = 2.0$. (a) Variation of droplet-phase volume fraction, ϑ_d along the channel (b) Variation of evaporated fuel mass fraction, M_F along the channel

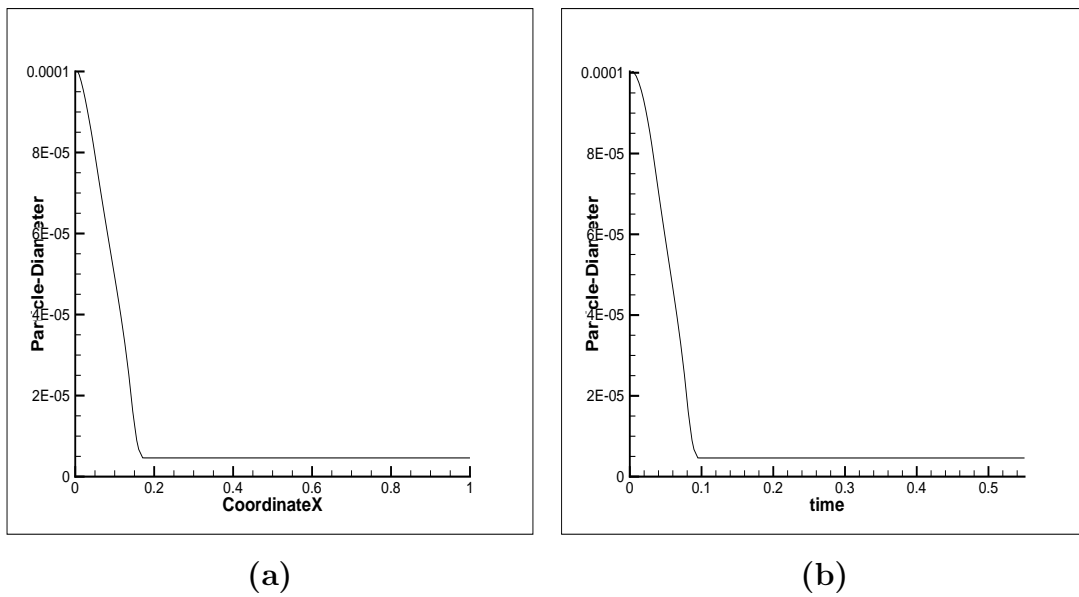


Figure 4.93: Case 12: Gas-droplet channel flow with $u_{gi} = 1.0$ and $u_{di} = 2.0$. (a) Variation of droplet-diameter, d_d along the channel (b) Variation of droplet-diameter, d_d , with time

4.1.14 Closure

Since the the parameters infuencing the problem are the gas Reynolds number Re_g , the droplet Reynolds number Re_d , and the Jacob number Ja . The Re_g in most practical flows is too high for laminar computations so here was fixed at a dummy value of 100 and 200 (it has been found that the results are quite insensitive to these value).

Initially only the value of droplet Reynolds Re_d is varied keeping Jacob number Ja constant and evaporation length x was measured & it was found that the evaporation length increases with droplet Reynolds number. Further simulations were done by varying Jacob number Ja keeping droplet Reynolds number Re_d constant & it was found that when the Jacob number number is less than unity, evaporation length decreases with increase in Jacob number Ja and when the Jacob number number is greater than unity, evaporation length increases with increase in Jacob number Ja .

Chapter 5

Conclusion and Scope of the Future Work

Conclusion

An Eulerian-Eulerian model for simulating gas-droplet flows had been previously implemented (Mrunalini 2012) as a separate module in a general purpose CFD solver, *IITK-DAE Anupravaha*. The classical model for droplet evaporation developed by Spalding with simplifying assumptions was implemented in the module and was found to give satisfactory results for low and moderate evaporation rates. The evaporation model was thoroughly tested in this thesis and the results obtained were compared with existing literature. Results showed a very good match between the model predictions and published results.

Since the parameters influencing the problem are the gas Reynolds number Re_g , the droplet Reynolds number Re_d , and the Jacob number Ja . The Re_g in most practical flows is too high for laminar computations so here was fixed at a dummy value of 100 and 200 (it has been found that the results are quite insensitive to these values).

Initially only the value of droplet Reynolds Re_d is varied keeping Jacob number Ja constant and evaporation length x was measured & it was found that the evaporation length increases with droplet Reynolds number. Further simulations were done by varying Jacob number Ja keeping droplet Reynolds number Re_d constant & it was found that when the Jacob number is less than unity, evaporation length decreases with increase in Jacob number Ja and when the Jacob number is greater than unity, evaporation length increases with increase in Jacob number Ja .

Scope of the Future work

The module is implemented in a general purpose CFD solver for both 2-D and 3-D problems on structured grid but has been tested only for 2-D problems. The implementation has to be further verified against 3-D test cases and for unstructured grid too. The module has been implemented only for laminar gas-droplet flows, but many problems which are of practical importance are turbulent. So the next phase of work in future may be the implementation of turbulence both for the gas-phase and the droplet-phase; which may also lead a way for the solver to simulate problems involving droplet combustion.

Sophisticated evaporation models which take into account the non-equilibrium effects and are suitable for high evaporation rate conditions may also need to be implemented. These models are able to simulate complex problems like turbulent evaporating sprays involving high droplet Reynolds number and evaporation rate. Detailed analysis and comparison of such models are found in Faeth [11], Miller [24] and Sirignano [35]. The present evaporation model assumes uniform temperature within the droplet which may prove inaccurate for high evaporation rate conditions. Non-uniformity of the droplet temperature can be modeled by adding extra heat transfer terms in the droplet phase energy equation, as done by Miller [24]. Convergence difficulties were observed for gas-droplet flows with very small values of volume fraction ($\leq 5 \times 10^{-6}$) in the domain. Further investigation is needed in this regard.

The solver considers mono-sized droplets. For problems of practical importance continuous size distribution can be represented by droplets with different sizes which correspond to classes of droplets with each class having its separate set of equations as done by Guo [18]. The present solver deals with flows in the laminar -flow regime only. This can be extended to incorporate turbulence effects on evaporating jet-flows as Elghobashi [10].

The solver considers single component droplets, while many practical applications involving blended fuels require simulation of multi-component droplets. Daif et al.[6] have presented experimental results of vaporization of multi-component droplets in a convective flow. Further development of the present solver to address the vaporization characteristics of multi-component fuel droplets may also be taken up in the future.

Appendix A

Appendix

A.1 Properties of fluids used

For validation of the evaporation model, n-heptane and hexane are used as droplet-phase and air is considered as the carrier-phase. The properties of these fluids used for validation have been given below

A.1.1 Properties of Air

The following relations have been used for calculating the thermodynamic properties of air:

- Specific heat at constant pressure for air

$$C_{pa} = c1 + c2 \left(\frac{c3/T_r}{\sinh(c3/T_r)} \right)^2 + c4 \left(\frac{c5/T_r}{\cosh(c5/T_r)} \right)^2 \quad (\text{A.1})$$

where $c1 = 0.2896 \times 10^5$, $c2 = 0.09390 \times 10^5$, $c3 = 3.0120 \times 10^3$, $c4 = 0.0758 \times 10^5$, $c5 = 1484$

In the above expression C_{pa} is in $J/kmol K$

- Thermal conductivity for air in $(W/m K)$

$$k_a = 1.5207 \times 10^{-11} T_r^3 - 4.8574 \times 10^{-8} T_r^2 + 1.0184 \times 10^{-4} T_r - 3.9333 \times 10^{-4} \quad (\text{A.2})$$

A.1.2 Properties of n-heptane

The following physical properties of n-heptane have been used ([28],[23]).

- Normal boiling Temperature $T_{bn} = 371.6 K$, Molecular weight $M_F = 100.204$, Critical temperature $T_{cri} = 540.17 K$, Critical pressure $P_{cri} = 2631.633 kPa$

- Vapour pressure is obtained by the Clausius-Clapeyron equation as

$$P_{Fs} = \exp \left(14.2146 - \frac{3151.68}{T_d - 43} \right) \text{ for } T_d \geq T_{bn} \text{ (kPa)} \quad (\text{A.3})$$

$$P_{Fs} = \exp \left(14.3896 - \frac{3209.45}{T_d - 43} \right) \text{ for } T_d = T_{bn} \text{ (kPa)} \quad (\text{A.4})$$

where T_d is the droplet temperature in K and T_{bn} is the saturation temperature at atmospheric pressure.

- Latent heat of vaporization as a function of droplet temperature is

$$L = 317.8 \times 1000.0 \left(\frac{540.17 - T_d}{540.17 - 371.4} \right)^{0.38} \text{ (J/kg)} \quad (\text{A.5})$$

- Specific heat at constant pressure for fuel vapour

$$C_{vd} = (0.363 + 0.000467 T_r) \times (5 - 0.001 \rho_d) \text{ (J/kg K)} \quad (\text{A.6})$$

where $\rho_d = 684.0 kg/m^3$

- Thermal conductivity of vapour in $(W/m K)$

$$k_v = 10^{-7} \times (14.52 T_{ref} - 5.14)^{2/3} \times (C_{vd} M_F / \lambda) \quad (\text{A.7})$$

where

$$\lambda = T_{cri}^{1/6} \times M_F^{0.5} \left(\frac{P_{atm}}{P_{cri}} \right)^{2/3} \quad (\text{A.8})$$

where $T_{ref} = T_r / T_{cri}$

- Density of liquid fuel, ρ_d in (kg/m^3)

For $T_d \leq 538.0$

$$\rho_d = -941.03 + 19.96181 T_d - 0.08612051 T_d^2 + 1.579494 \times 10^{-4} T_d^3 - 1.089345 \times 10^{-7} T_d^4 \quad (\text{A.9})$$

Otherwise

$$\rho_d = 4.19528 \times 10^7 - 2.360524 \times 10^5 T_d + 442.7316 T_d^2 - 0.2767921 T_d \quad (\text{A.10})$$

where T_r is the reference temperature obtained by the '1/3' rule.

A.1.3 Physical properties of Hexane ([24])

- Normal boiling temperature $T_{bn} = 344.6 K$, Molecular weight $M_F = 86.178$, Critical temperature $T_{cri} = 507.6 K$ and Critical pressure $P_{cri} = 3.04 \times 10^6 Pa$
- Specific heat of liquid droplet $C_{ld} = 2302.0 (J/kg K)$
- Vapour pressure is obtained by the Clausius-Clapeyron equation as

$$P_{FS} = \exp \left(14.0932 - \frac{2834.61}{T_d - 43} \right) \text{ for } T_d \geq T_{bn} \text{ (kPa)} \quad (\text{A.11})$$

$$P_{FS} = \exp \left(14.3896 - \frac{3209.45}{T_d - 43} \right) \text{ for } T_d = T_{bn} \text{ (kPa)} \quad (\text{A.12})$$

where T_d is the droplet temperature in K and T_{bn} is the saturation temperature at atmospheric pressure.

- Latent heat of vaporization

$$L = 5.1478 \times 10^5 \left(1 - \frac{T_d}{512} \right)^{0.3861} (J/kg) \quad (\text{A.13})$$

- Specific heat of vapour

$$C_{vd} = -51.31 + 6.767 T_r - 3.626 \times 10^{-3} T_r^2 (J/kg K) \quad (\text{A.14})$$

- Thermal conductivity of vapour in $(W/m K)$

$$k_{vd} = 1.112 \times 10^{-2} + 3.837 \times 10^{-5} T_r + 3.778 \times 10^{-8} T_r^2 \quad (\text{A.15})$$

- Density of liquid, $\rho_d = 664.0 (kg/m^3)$.

- Viscosity of vapour

$$\mu_{vd} = 5.592 \times 10^{-6} + 5.622 \times 10^{-9} T_r (kg/m s) \quad (\text{A.16})$$

where T_r is the reference temperature obtained by the '1/3' rule.

References

- [1] ABRAMZON, B., AND SIRIGNANO, W.A., “Droplet vaporization model for spray combustion calculation”, *Int. J. of Heat and Mass Transfer*, Vol. 32, pp. 1605-1618, 1989.
- [2] ADHIRAJ KISHORE DASGUPTA, “Numerical Simulation of Dilute Gas-Particle flows using Eulerian-Eulerian approach in a General Purpose CFD Solver”, Thesis for the Degree of Master of Technology, *Department of Mechanical Engineering*, Indian Institute of Technology Kanpur, 2008.
- [3] ASANO, K., “Mass Transfer from Fundamentals to Modern Industrial Applications” *Wiley publications*, 2006.
- [4] CHIN, J.S., AND LEFEBVRE, A.H., “The Role of Heat-up Period in Fuel Drop Evaporation”, *Int. J. Turbo Jet Engines*, Vol. 2, pp. 315-325, 1985.
- [5] CROWE, C.T., SOMMERFELD, M. AND TSUJI, Y., “Multiphase flows with droplets and particles”, *CRC Press: Boca Raton*, 1998.
- [6] DAIF, A., BOUAZIZ, M., CHESNEAU, X. AND CHERIF, A.A., “Comparison of multicomponent fuel droplet vaporization experiments in forced convection with the Sirignano model”, *Exp. Thermal Fluid Sci.*, Vol. 18, pp. 282-290, 1999.
- [7] DARWISH, M., MOUKALLED, F. AND SEKAR, B., “A unified formulation of the segregated class of algorithms for multifluid flow at all speeds”, *Numerical Heat Transfer, Part B: Fundamentals*, Vol. 40:2, pp. 99-137, 2001.
- [8] DOWNING, C.G., “The evaporation of drops of pure liquids at elevated temperatures: rates of evaporation and wet-bulb temperatures”, *AIChE Journal*, Vol. 12, pp. 760-766, 1966.

-
- [9] ESWARAN V. ET AL., "Development of a General Purpose Robust CFD Solver", Project Report No. 1, *Department of Mechanical Engineering*, Indian Institute of Technology Kanpur, December, 2005.
- [10] ELGHOBASHI, S. E. AND MOSTAFA, A. A., "A two-equation turbulence model for jet flows laden with vaporizing droplets", *Int. J. Multiphase flow*, Vol. 11, pp. 515-533, 1985.
- [11] FAETH, G.M., "Current Status of Droplet and Liquid Combustion", *Prog. Energy Combust. Sci.*, Vol. 3, pp. 191-224, 1977.
- [12] FLUENT MULTIPHASE FLOWS DOCUMENTATION, *Fluent Inc. Lebanon, NH*
- [13] FROLOV, S.M., FROLOV, F.S., BASARA B., "Simple Model of Transient Drop Vaporization", *Journal of Russian Laser Research*, Vol. 27, No. 6, pp. 562-574, 2006.
- [14] FROSSLING, N., "On the Evaporation of Falling Droplets", *Gerlands Beitr. Geophys.*, Vol. 52, pp. 170-216, 1938.
- [15] LOTH, E., "Numerical approaches for motion of dispersed particles, droplets and bubbles", *Progress in Energy and Combustion Science*, Vol. 26, pp. 161-223, 2000.
- [16] FUCHS, N.A., "Evaporation and droplet growth in gaseous media", *London: Pergamon Press*, 1959.
- [17] GODSAVE, G.A.E., "Studies of the Combustion of Drops in a Fuel Spray-the Burning of Single Drops of Fuel", *Fourth Symposium (International) on the Combustion*, Williams and Wilkins, Baltimore, pp. 818-830, 1953.
- [18] GUO, Y.C., CHAN, C.K., AND LAU, K.S., "A pure Eulerian model for simulating dilute spray combustion", *Fuel*, Vol. 81, pp. 2131-2144, 2002.
- [19] HUBBARD, G.L., DENNY, V. E. AND MILLS, A.F., *Int. J. Heat Mass Transfer*, Vol. 16, pp. 1003-1008, 1973.
- [20] KOLAITIS, D.I., FOUNTI, M. A., "A comparative study of numerical models for Eulerian-Lagrangian simulations of turbulent evaporating sprays", *International Journal of Heat and Fluid Flow*, Vol. 27, pp. 424-435, 2006.

-
- [21] KOLEV, N.I., "Multiphase flow dynamics", *Springer-Verlag*, Vol. 2, 2005.
- [22] ISHII, M. AND HIBIKI, T., "Thermo-Fluid Dynamics of Two-Phase Flow", *Springer Science+Business Media, Inc.*, 1990.
- [23] LEFEBVRE, A.H., "Atomization and sprays", *Taylor and Francis*, 1989.
- [24] MILLER, R.S., HARSTAD, K. AND BELLAN, J., "Evaluation of equilibrium and non-equilibrium evaporation models for many-droplet gas-liquid flow simulations", *International Journal of Multiphase Flow*, Vol. 24, pp. 1025-1055, 1998.
- [25] MONGIA, H.C. AND MOSTAFA, A.A., "On the modeling of turbulent evaporating sprays: Eulerian versus Lagrangian approach", *Int. J. Heat Mass Transfer*, Vol. 30, pp. 2583-2593, 1987.
- [26] MRUNALINI B, "Development of finite volume solver for Dilute Gas-Particle flows with evaporation", Thesis for the Degree of Master of Technology, *Department of Mechanical Engineering*, Indian Institute of Technology Hyderabad, 2012
- [27] PATANKAR S.V., "Numerical Heat Transfer and Fluid Flow", *Taylor and Francis*, 2004.
- [28] PERRY, R H., GREEN, D.W., "Perry's chemical engineers' handbook", *McGraw Hill Publications*, 1997.
- [29] RHIE C.M. AND CHOW W.L., "Numerical Study of the Turbulent Flow Past an Airfoil with Trailing Edge Separation", *AIAA Journal*, Vol. 21, No. 11, pp. 1525-1532, 1983.
- [30] RANZ, W.E., AND MARSHALL, W. R., "Evaporation from Drops", *Chem. Eng. Prog.*, Vol. 48, Part I, pp. 141-146, Part II, pp. 173-180, 1952.
- [31] REID, R.C., PRAUSNITZ, J.M. AND POLING, B.E., "The properties of gases and liquids", *McGraw-Hill International Editions*, 1988.
- [32] HAYDER SALMAN, MARIOS SOTERIOU, "Lagrangian simulation of Evaporating Droplet sprays", *Physics of Fluids*, Vol.16, No.12, 4601-4621, 2004.

-
- [33] SAZHIN, S., MARTYNOV, S., SHISHKOVA, I., CRUVA, C., KARIMI, K., GOROKHOVSKI, M., SAZHINA E., HEIKAL, M., “Modelling of Droplet heating, Evaporation and Break-up: Recent Developments”, *International Journal of Multiphase*, 2006.
- [34] SHASHWAT SWAMI JAISWAL, “Numerical Simulation of Dilute Gas-Droplet flows”, Thesis for the Degree of Master of Technology, *Department of Mechanical Engineering*, Indian Institute of Technology Kanpur, 2008.
- [35] SIRIGNANO, W.A., “Fluid dynamics and Transport of Droplets and Sprays”, *Cambridge University Press*, 1999.
- [36] SPALDING, D.B., “The combustion of liquid fuels”, *Fourth Symposium (International) on the Combustion, Williams and Wilkins, Baltimore*, pp. 847-864, 1953.